

Reaction Mechanism for Pd-Catalyzed Decarboxylation of Carboxylic Acid

Fuli Deng

Vollständiger Abdruck von der TUM School of Natural Sciences der Technischen Universität München zur Erlangung des akademischen Grades einer

Doktorin der Naturwissenschaften (Dr. rer. nat.)

genehmigten Dissertation.

Vorsitz: Prof. Dr.-Ing. Kai-Olaf Hinrichsen

Prüfer*innen der Dissertation:

1. Prof. Dr. Johannes A. Lercher
2. Prof. Dr. Klaus Köhler

Die Dissertation wurde am 23.01.2023 bei der Technischen Universität München eingereicht und durch die TUM School of Natural Sciences am 06.03.2023 angenommen.

Preface

This dissertation is a publication-based doctoral thesis. It is based on independent articles that have been published in international peer-reviewed scientific journals. The first chapter of this dissertation primarily serves as an introduction to the motivation and related research background, followed by a detailed description of certain research works related to the decarboxylation of carboxylic acids. The presented work was carried out at the Chair of Technical Chemistry II of the Technical University of Munich (TUM) between October 2018 and February 2023 under the supervision of Prof. Dr. Johannes A. Lercher.

Acknowledgement

The thesis marks the end of a long and memorable journey that I could not have completed without the dedicated support of my supervisors and peer colleges. Looking back on the past and right into the future, I am deeply grateful.

First of all, I would like to give my heartfelt thanks to my supervisor, Prof. Dr. Johannes A. Lercher, for giving me this precious chance to have my doctoral study at TC2. Without your professional guidance and your continuous support, I could not have completed this thesis. Your kindness, illuminating guidance, and profound professional knowledge always inspired me to explore more about the magic catalysis world, and will certainly enlighten me throughout my future career.

My sincere thanks further go to my mentors: Dr. Erika Ember, Prof. Dr. Andreas Jentys, and especially Prof. Dr. Yue Liu. Although I have only worked with Erika for a few short months, I am very grateful for your patience and encouragement, you really helped me a lot for having a smooth adaptation part to my doctoral study. Andy, I am appreciating for your help and suggestion on my research work, I always remember your encouragement after my first group seminar presentation, which meant a lot to me. Then, I would like to express my sincere gratitude to Yue. You guided me along with my research topics and put forward numerous insightful suggestions, productive discussion and constant encouragement, which I am still benefiting from these. It is so lucky for me to have such great supervisor who always had such helpful guidance throughout my doctoral study, and therefore I will always bear this good memory in my mind.

Furthermore, I would like to thank all of our senior scientists in TCII at TUM. Dr. Maricruz Sanchez- Sanchez, Dr. Eszter Baráth and Dr. Rachit Khare. Thank all of your kind help in science as well as in consultation, especially Rachit, you had given me great patience and kindness when I ask for your help. And Dr. Hui Shi, thank you so much not only for your kindness scientific help, but also for you saved me from being homeless by leaving me the most pleasant apartment I ever had in Munich.

Our technical and administrative staffs in our group have been very kind and helpful, I would like to express my appreciate to Iqbal Muhammad for his help in catalysts sample measurements and other troublesome thing in the lab, to Franz-Xaver Hecht for saving me from the numerous GC problem at beginning of my research work; to Martin Neukamm for all his help in AAS measurement and signature, and also to Andreas Marx for solving all the electronic

problems. Bettina Federmann, Stefanie Seibold, Kateryna Kryvkoare and Verona Bekteshi Sylva are also sincerely acknowledged for their administrative helps in countless official paper-works. Thank all of you for your supports and inputs in my work.

I am most grateful to my biomass lab mates, Dr. Guanhua Cheng, Dr. Xi Chen, Dr. Iris Kaming Yu, Dr. Qiang Liu, Niklas Pfriem, Lara Milakovic and Florian Zahn for their companion in the past several years. Their diligence, humor, understanding, and support have allowed me to happily complete countless experiments. The lunchtime with Guanhua and Iris was also enjoyable and unforgettable, I am impressed by the special recipes they created.

Moreover, I warmly thanks my collaborator Dr. Juanjuan Huang for all the effort she put into XANES measurement. You are blessed to have a glorious future in America.

I also must express great thanks to my former and current colleagues: Dr. Ruixue Zhao, it has always been a lot of fun traveling with you and the great promotions you provide really 'saved' a lot. And Dr Wei Zhang (F), Dr. Lingli Ni, Dr. Lei Tao, Dr. Yong Wang, Dr. Wei Zhang (M), Hongwen Chen, Huidong Xu, Chuanlei Li, Siyuan Huang, Xiaomai Chen, Tao Ying, with whom we had such great time together making my life in Munich more interesting. And Dr. Insu Lee, Dr. Martina Aigner, Dr. Laura Löbbert, Dr. Roland Weindl, Alexander Wellmann with whom we had shared an impressive trip during the ULM catalysis course; and Dr. Madita Einemann, Dr. Karen Resende, Jakub Pazdera, Teresa Schachtl, Aimen Shahpal, Ferdinand Vogelgsang, Mirjam Wenig, Lennart Wahl and all the other members who are not mentioned here, for their help and the great time we have shared in the group.

Special thanks to my best friend, Jingwen Jiang. The unexpected encounter made us the closest friends in Munich. You always gave me unconditional support, encouragement and companionship in my research and my life, which made my days in Munich. Here, I would like to give you my best wishes to finish your Ph.D. in the near future.

Last but not least, I am deeply indebted to my parents and brother for their support in my every decision. Without their understanding, I would not be able to concentrate on my studies. And also, sincerely thanks to my relatives, teachers and friends from whom I've been receiving endless support.

I shall never forget the good days here.

Fuli Deng

Garching, November 2022

Abstract

The mechanism of hydrodeoxygenation of biomass-derived carboxylic acids on Pd-based catalysts has been studied. Palladium hydride (PdH_x) formed by H_2 pretreatment was identified as the active phase for decarboxylation, with one order of magnitude higher activity than metallic Pd. Weak basicity realized by 1 wt. % KHCO_3 increased the activity of PdH_x by nearly 20 times. The high concentration of H in PdH_x facilitates the recombination of the surface intermediate (e.g. Ar-CH^*) with H^* to desorb as product (e.g. Ar-CH_3). The weak basic site induced by KHCO_3 abstracts the proton from the carboxylic acid group to form a carboxylate, which is a reactive precursor to decarboxylate.

Zusammenfassung

Der Mechanismus der Hydrodeoxygenierung von aus Biomasse gewonnenen Carbonsäuren an Katalysatoren auf Pd-Basis wurde untersucht. Das durch die Anwesenheit H_2 gebildete Palladiumhydrid wurde als aktive Phase für die Decarboxylierung identifiziert. Es zeigt eine um eine Größenordnung höheren Aktivität als metallisches Pd. Die schwache Basizität, die durch 1 gew.-% $KHCO_3$ induziert wird erhöhte die Aktivität von PdH_x um fast das 20-fache. Die hohe H-Konzentration in PdH_x begünstigt die Rekombination des Oberflächen-Zwischenprodukts (z. B. $Ar-CH^*$) mit H^* , das als Produkt (z. B. $Ar-CH_3$) desorbiert wird. Die schwache basische Stelle, die durch $KHCO_3$ induziert wird, abstrahiert das Proton von der Carbonsäuregruppe und bildet ein Carboxylat, das ein reaktiver Vorläufer zur Decarboxylierung ist.

Table of Contents

<i>Acknowledgement</i>	I
<i>Abstract</i>	III
<i>Zusammenfassung</i>	IV
<i>Table of Contents</i>	V
<i>Abbreviations</i>	VIII
<i>List of Figures, Schemes and Tables</i>	X
Chapter 1. Introduction	- 1 -
1.1 General background	- 2 -
1.2 Biomass, bio-oils and their upgrading.....	- 4 -
1.3 Carboxylic acids and derivatives.....	- 7 -
1.4 Deoxygenation of carboxylic acids	- 10 -
1.4.1 Hydrodeoxygenation (HDO).....	- 10 -
1.4.2 Decarbonylation	- 12 -
1.4.3 Decarboxylation	- 12 -
1.4.4 Kolbe Electro Catalysis	- 13 -
1.5 Effect of catalysts and H ₂ atmosphere: Palladium-catalyzed deoxygenation of carboxylic acids.....	- 14 -
1.5.1 Active Phases	- 15 -
1.5.2 Catalyst supports	- 16 -
1.5.3 Gaseous atmospheres	- 17 -
1.6 Chemical kinetics	- 19 -
1.7 Scope of this thesis.....	- 25 -
1.8 References	- 27 -
Chapter 2. On the Mechanism of Catalytic Decarboxylation of Carboxylic Acids on Carbon-Supported Palladium Hydride	- 33 -
2.1 Introduction	- 34 -
2.2 Experimental method	- 35 -
2.2.1 Chemicals and Materials	- 35 -

2.2.2 Catalyst Characterizations	- 35 -
2.2.3 Catalytic Reactions.....	- 36 -
2.3 Results and Discussion	- 38 -
2.3.1 On the Role of the Reaction Atmosphere for the Conversion of Hydrocinnamic Acid.....	- 38 -
2.3.2 Identification of the Catalytic Active Species on Pd/C for the Decarboxylation Reaction.....	- 42 -
2.3.3 Role of PdH _x in the Mechanism of Decarboxylation	- 46 -
2.4 Conclusion.....	- 51 -
2.5 Appendix	- 53 -
2.6 Reference.....	- 59 -
Chapter 3. Promotion Effect of KHCO₃ on Palladium Hydride Catalyzed Decarboxylation of Aryl aliphatic Acid.....	- 62 -
3.1 Introduction	- 63 -
3.2 Experimental section	- 64 -
3.2.1 Catalyst preparation.....	- 64 -
3.2.2 Catalytic evaluation and kinetic measurements	- 64 -
3.2.3 Catalyst characterization	- 66 -
3.3 Results and Discussion.....	- 67 -
3.3.1 Decarboxylation reaction of hydrocinnamic acid on α -PdH _x /C.....	- 67 -
3.3.2 Influence of K Content on Catalytic Performance	- 68 -
3.3.3 Physical and Chemical Properties of Catalysts	- 69 -
3.3.4 Temperature-Programmed Surface Reaction (TPSR) in Combination with Operando XANES.....	- 71 -
3.3.5 Temperature programmed desorption of CO ₂ (CO ₂ -TPD) of the Catalysts.....	- 73 -
3.3.6 Effect of KHCO ₃ on on Reaction Kinetics for Hydrocinnamic Acid Decarboxylation	- 74 -
3.3.7 Adsorption States of Hydrocinnamic Acid on PdH _x /C and KHCO ₃ -PdH _x /C catalysts	- 75 -

3.3.8 Mechanism of Hydrocinnamic Acid Decarboxylation on Pd-Elementary Steps and their Reversibility	- 77 -
3.4 Conclusion.....	- 81 -
3.5 Appendix	- 83 -
3.5.1 Supplementary Note 1: Adsorption isotherms of hydrocinnamic acid.....	- 86 -
3.5.2 Supplementary Note 2: Derivation of the substituted deuterium distribution results....	- 89 -
3.5.3 Supplementary Note 3: Derivation of rate equation and reaction order:....	- 90 -
3.5.4 Supplementary Note 4: Derivation of the measured activation energy.....	- 91 -
3.6 Reference.....	- 93 -
Chapter 4. Summary	- 96 -
Curriculum Vitae	- 98 -

Abbreviations

Full name	Abbreviation/Symbol	Unit
Gigatons - or billions of tons - of Carbon	GtC	
Carbon dioxide	CO ₂	
Carbon monoxide	CO	
Dydrodeoxygenation	HDO	
Decarbonylation	DCO	
Hydrocinnamic acid	HDCA	
Ethylbenzene	EB	
Decarboxylation	DCO ₂	
fatty acid methyl esters	FAMEs	
fatty acid ethyl esters	FAEEs	
Uptake of adsorbate	Q	
Uptake at saturation	Q _{sat}	
Coverage of sites x	θ_x	
Adsorption equilibrium constant	$K^{\circ}_{eq.}$	
Adsorption enthalpy	$\Delta H^{\circ}_{ads.}$	kJ mol ⁻¹
Adsorption entropy	$\Delta S^{\circ}_{ads.}$	J mol ⁻¹ K ⁻¹
Universal gas constant	R	J mol ⁻¹ K ⁻¹
Activation energy	E_a	kJ mol ⁻¹
Pre-exponential factor	A	
Reaction rate	r	mol g ⁻¹ _{Pd} s ⁻¹
Rate constant	k	
Reaction order	n	
Atomic absorption spectroscopy	AAS	
Turnover frequency	TOF	h ⁻¹
Palladium hydride	PdH _x	
X-ray absorption near-edge structure	XANES	
Temperature-programmed surface reaction	TPSR	

Abbreviation

Gas chromatography	GC
Mass spectrometer	MS
Nuclear magnetic resonance	NMR
Brunauer, Emmett and Teller	BET
Barrett–Joyner–Halenda	BJH
Weight percentage	wt. %
X-ray diffraction	XRD
Temperature-programmed desorption	TPD

List of Figures, Schemes and Tables

Figures

- Figure 1-1.** (a) Global primary energy consumption by source (1800-2019), (b) total world energy consumption by source (2019). Primary energy denotes the energy which is from nature and has not been subjected to any human engineered conversion process[1]. - 3 -
- Figure 1-2.** Carbon neutral circular framework for biomass..... - 4 -
- Figure 1-3.** Schematic of cellulose, hemicellulose, and lignin components of lignocellulosic biomass and associated molecular building blocks. (Adapted from the website of microbeWiki) - 5 -
- Figure 1-4.** The structure of the carboxylic acids (a), the electronic states of the carboxylic group (b, c), and resonance effect of the C=O (c, d)..... - 8 -
- Figure 1-5.** Structures of typical carboxylic acids..... - 9 -
- Figure 1-6.** Transesterification of oil to a fatty acid methyl/ethyl ester and glycerol. - 9 -
- Figure 1-7.** Energy diagram for the transformation of reactant to products in the non-catalytic and catalytic processes. - 19 -
- Figure 2-1.** Concentrations of products and reactant as a function of time in the reaction of hydrocinnamic acid on Pd/C under different conditions: (a) 20 bar H₂, (b) 1 bar H₂ and 9 bar N₂, (c) 10 bar N₂, and (d) Pd/C pretreated under 1 bar H₂ at 25 °C for 30 min and then reacted in 10 bar N₂ (100 mg of Pd/C, 80 mL of n-dodecane as the solvent, reacted at 300 °C).... - 39 -
- Figure 2-2.** Concentrations of products and reactant as a function of time in the reaction of 3-cyclohexylpropionic acid on Pd/C. (a) Reaction conditions: 100 mg of Pd/C, 80 mL of n-dodecane as the solvent, 5.3 mmol of 3-cyclohexylpropionic acid, reacted at 300 °C, 10 bar N₂. (b) Reaction conditions: 100 mg of Pd/C, 80 mL of n-dodecane as the solvent, 5.3 mmol of 3-cyclohexylpropionic acid, reacted at 300 °C, 1 bar H₂ and 9 bar N₂. - 40 -
- Figure 2-3.** Concentrations of hydrocinnamic acid and products as a function of time on Pd/C in different gas atmospheres. Reaction conditions: 100 mg of Pd/C catalyst, 80 mL of n-dodecane as the solvent, 5.3 mmol of hydrocinnamic acid, reacted at 150 °C..... - 41 -
- Figure 2-4.** (a) Normalized Pd K-edge XANES spectra of the Pd/C catalyst after different treatments. The spectra were collected at room temperature, and the maximum value of spectra was normalized to 1 (the inset shows the enlarged spectra from 24,350 to 24,395 eV). (b)

Normalized Pd K-edge in situ XANES spectra of the Pd species at 25, 40, 50, and 70 °C in a TPSR process; the detailed continuously collected spectra are presented in **Figure A 2-6**. The inset shows the comparison of four XANES spectra without shifting the spectra vertically. **(c)** Rate of toluene formation in the decarboxylation of preadsorbed 2-phenylacetic acid on Pd/C with different pretreatments with programmed increasing temperature, i.e., temperature-programmed surface reaction (TPSR). Orange curve: Pd/C pretreated at 150 °C for 30 min in a H₂ flow (30 mL/ min) and cooled down to the room temperature in a H₂ flow; green curve: Pd/C first pretreated in a H₂ flow (30 mL/min) at 150 °C for 30 min, then switched to N₂ (30 mL/min) flow for 30 min, and cooled down to room temperature in a N₂ flow. After pretreatment, 2-phenylacetic acid preadsorption was conducted in the glove box (temperature ramping rate for the TPSR reaction: 0.5 °C/min from 25 to 40 °C, 0.2 °C/min from 40 to 50 °C, and 2 °C/min from 50 to 150 °C). **(a,b)**: Reproduced with permission from ref 36. Copyright 2021 Royal Society of Chemistry. - 44 -

Figure 2-5. Decarboxylation of arylaliphatic carboxylic acids with different side chain lengths and 3-cyclohexylpropionic acid on a H₂- pretreated Pd/C catalyst..... - 46 -

Figure 2-6. Decarboxylation rate of carboxylic acids as a function of the substituted D atom numbers at the α -C position. - 49 -

Figure 3-1. Concentrations of reactant and product as a function of time in the reaction of hydrocinnamic acid decarboxylation on **(a)** PdH_x/C and **(b)** 1wt. % KHCO₃-PdH_x/C; **(c)** Decarboxylation rate of hydrocinnamic acid on PdH_x/C with and without alkali metal salt with 1wt. % loadings (*:0.5wt.% loading for KOH)..... - 67 -

Figure 3-2. TOF of hydrocinnamic acid decarboxylation as a function of KHCO₃ promoter loading on PdH_x/C..... - 69 -

Figure 3-3. XRD patterns of **(a)** activated carbon, Pd/C and KHCO₃-Pd/C catalysts with different KHCO₃ loadings, **(b)** Comparison among fresh and used 8wt. % KHCO₃-Pd/C, hydrocinnamic acid (Ar-CH₂-CH₂-COOH) and potassium hydrocinnamate (Ar-CH₂-CH₂-COO⁻). - 70 -

Figure 3-4. **(a)** **(a)** Rate of toluene formation in the decarboxylation of pre-adsorbed 2-phenylacetic acid on PdH_x/C and KHCO₃- PdH_x/C in the temperature programmed surface reaction (TPSR). Catalysts wafer were pretreated at 150 °C for 30 min in the H₂ flow (30 mL/min) and cooled down to the room temperature. After pretreatment, 2-phenylacetic acid pre-adsorption was conducted in the glove box. And TPSR was measured in the N₂ flow (30

mL/min). (Temperature ramping rate for TPSR reaction: 5 °C /min from 25 to 150 °C and holding at 150 °C for 1 h); **(b)** Normalized Pd K-edge XANES spectra of Pd foil, Pd/C and KHCO₃-Pd/C catalysts. Pd/C and KHCO₃-Pd/C samples were first pretreated in H₂ flow at 150 °C for 1h and switched to N₂ flow for another 1h pretreatment, then cool down to room temperature in N₂ atmosphere. Spectra were collected at room temperature, and the maximum value of spectra was normalized to 1. (The inset shows the enlarged spectra from 24350 eV to 24400 eV)..... - 72 -

Figure 3-5. CO₂-TPD profiles of the **(a)** Pd/C and KHCO₃-Pd/C catalysts with KHCO₃ loading varies from 0.5 to 8wt. %, and **(b)** decomposition profiles of 1wt. %KHCO₃-Pd/C and pure KHCO₃. - 73 -

Schemes

Scheme 1-1. Photosynthesis process of plants fixing atmospheric CO₂ and transform to organic chemical compounds[20]. - 4 -

Scheme 1-2. Deoxygenation pathways for carboxylic acids and carboxylic acid esters, and side reactions in the gas phase. - 10 -

Scheme 1-3. Proposed reaction mechanism for the Kolbe electrolysis and the generation of the Kolbe, Non-Kolbe and Hofer-Moest products.(Picture adapted from [52]) - 13 -

Scheme 2-1. Reaction Pathways of Hydrocinnamic Acid on the Pd/C Catalyst. - 41 -

Scheme 2-2. Deuterium Substitution of C–H Groups on Hydrocinnamic Acid - 50 -

Scheme 2-3. Proposed mechanisms of **(a)** Decarboxylation of arylaliphatic carboxylic acids on a H₂-pretreated Pd/C catalyst and **(b)** substitution of deuterium toward C–H and –COOH groups on 2-phenylacetic acid..... - 51 -

Scheme 3-1. Schematic illustration of hydrocinnamic acid decarboxylation pathways on KHCO₃-modified Pd catalyst. - 78 -

Tables

Table 2-1. Influence of Pretreatment Conditions on the Decarboxylation Activity of Hydrocinnamic Acid on Pd/C ^a	- 42 -
Table 2-2. Distribution of substituted D atoms in unconverted carboxylic acids after reaction on D ₂ pretreated Pd/C ^a	- 47 -
Table 3-1. Basic physicochemical properties of the Pd/C and KHCO ₃ promoted-Pd/C catalysts.	- 69 -
Table 3-2. Summary of reaction rates, reaction orders, Arrhenius equation derived apparent activation energy for the decarboxylation of hydrocinnamic acid.	- 74 -
Table 3-3. Distribution of Substituted D Atoms in Hydrocinnamic Acid after Reaction on D ₂ -Pretreated Pd catalysts ^a	- 76 -

Chapter 1. Introduction

1.1 General background

The rapidly growing environmental concerns associated with the global warming along with the exponential rise in energy demanding makes developing clean energy strategies an imminent issue. As shown in **Figure 1-1a** [1,2] the global energy consumption exhibited an exponential growth from 1800 to 2019, and the increment was almost covered by fossil fuels, i.e., natural gas, coal and crude oil, which occupied approximately 80% of the overall resources (**Figure 1-1b**). The globe energy demand is expected to rise 2% per annum and the energy consumption is predicted to be twice that of 2001 in 2050. As shown in **Figure 1-1b**[3], renewable resources including biomass, carbon dioxide (CO₂), wind energy, solar energy, etc., are the main renewable and sustainable energies that have been developed accounting for only 17% of the global energy consumption [4]. The most conventional approach nowadays for energy demanding is the conversion of traditional biomass, such as wood fuels, agricultural by-products, which share around 10% of the global final energy consumption over the last half century with minimal improvement [5–8]. It is expected that 30% of the direct fuel production meets the utilization of the renewable biomass resources by 2025 [9]. However, a large amount of biomass is currently utilized by direct combustion, which is extremely inefficient and associated with the CO₂ emission increasing from 6.6 to 11.0 GtC per year, further leading to environmental issues such as global warming and air pollution [10,11]. To halt the trend of climate change causing by CO₂ emission, Paris agreement laid down a target of achieving carbon neutrality by middle-21st century among 195 countries [12].

In response to the growing energy demanding, increasing depletion of the fossil-based feedstocks, and growing environmental concerns over the past centuries, a sensible stratagem is required to reduce the energy reliance on fossil fuels while maintaining the economic development [13–15]. Therefore, the fundamental goal of the whole world is to achieve a sustainable growth of the sustainable economic growth. In fact, biomass is also the only sustainable carbon source in nature, and has been receiving abundant attention as it has the potential to replace fossil feedstocks for the production of essential chemicals such as bio-based transportation fuels, biomaterials and high-value chemicals [16], while other forms of renewable energy thus should be used for stationary power generations. The worldwide raw biomass energy potential has been predicted to be between 150 to 450 EJ/year in 2050 [17].

Pioneering efficient methodology for biomass conversion is an imperative to achieve sustainable energy utilization. As a results, the composition of the future energy supply will

progressively move from high-cost and non-renewable fossil fuels to sustainable and biomass energy.

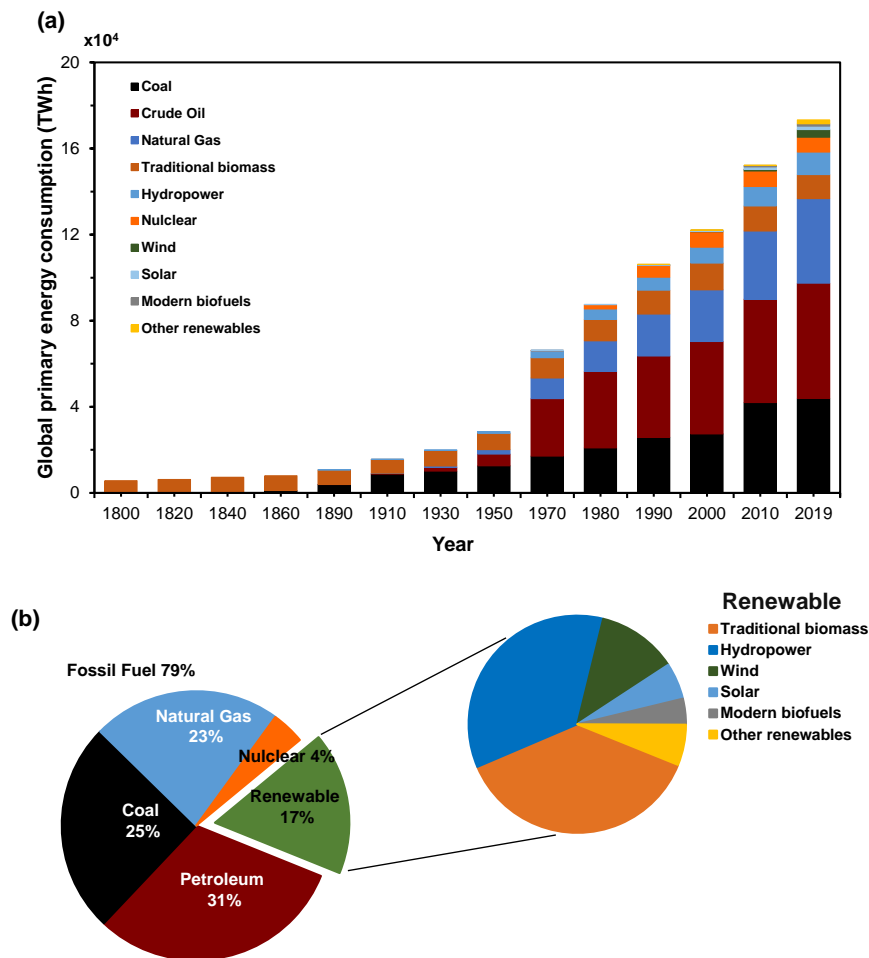


Figure 1-1. (a) Global primary energy consumption by source (1800-2019), (b) total world energy consumption by source (2019). Primary energy denotes the energy which is from nature and has not been subjected to any human engineered conversion process[1].

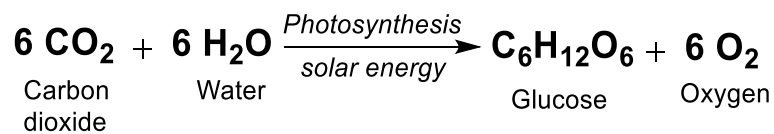
Nevertheless, large amounts of different types of edible biomass (such as corns and wheats) from agricultural production have been converted into bioethanol and first-generation biodiesel manufacturing in recent decades, significantly impacting the food supply and prices and leading to a “food versus fuel” debate, which highlights the importance of utilization of the inedible and waste biomass feedstocks. The expansion of agricultural production for bioenergy will very likely increase the pressure on land and the result in increased deforestation and associated carbon emission [18].

Consequently, in order to guide the use of sustainable biomass energy without competing with the food supply and land, worldwide researchers have been dedicated to developing

effective technologies to transform more inedible biomass to useful chemicals with more efficiency in terms of energy conversion and greenhouse gas emission.

1.2 Biomass, bio-oils and their upgrading

Biomass is a promising alternative sustainable, renewable and carbon-neutral feedstock for energy source with advantages such as renewability, low pollution, wide distribution and abundance of organic carbon resource in nature. The usage of biomass resources helps to avoid the exploitation of fossil resources like oil or gas in the production of chemicals[19]. Biomass contains the chemical energy stored in the forms of glucose or sugar by plants from the radiant energy through the photosynthesis (**Scheme 1-1**) [20].



Scheme 1-1. Photosynthesis process of plants fixing atmospheric CO₂ and transform to organic chemical compounds[20].

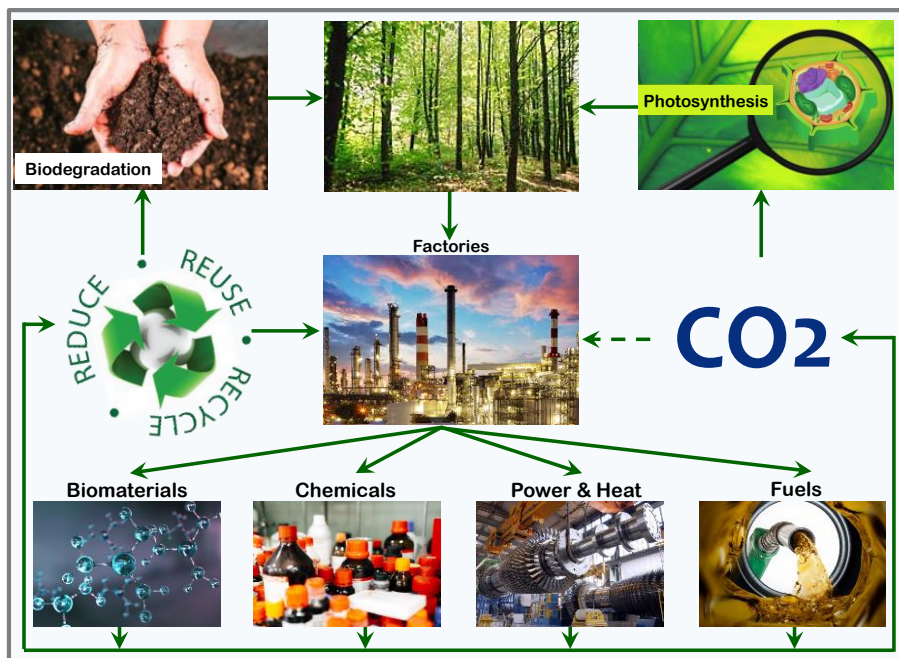


Figure 1-2. Carbon neutral circular framework for biomass.

Thus, Biomass fuels play an increasingly important role in transportation and electricity generation in many developed countries, in order to avoid the CO₂ emission from fossil fuels

combustion. The generation, conversion, and recycling of biomass can achieve a carbon-neutral circular framework as shown in **Figure 1-2**. Biomass initially originates from the plants' photosynthesis with CO₂, which is the main residual gas from the factories. Moreover, the utilization of biomass can be divided into 3 approaches: i) directly combust and produce heat and power for residential and industrial use; ii) thermochemical conversion through pyrolysis and gasification process to produce fuels such as bio-oil, renewable diesel, gasoline, and jet fuels; iii) chemical conversion to produce valuable chemicals and biomaterials. The residual chemicals and materials can be further recycled and reproduced for industrial production or provide essential nutrients for plant growth via biodegradation (**Figure 1-2**).

However, the direct combustion approach usually has the drawback of low efficiency and causing environmental issues. As a result, researchers are focusing on improving the biomass utilization efficiency by chemically separating and purifying raw biomass materials and transforming into high value-added chemicals and energy fuels.

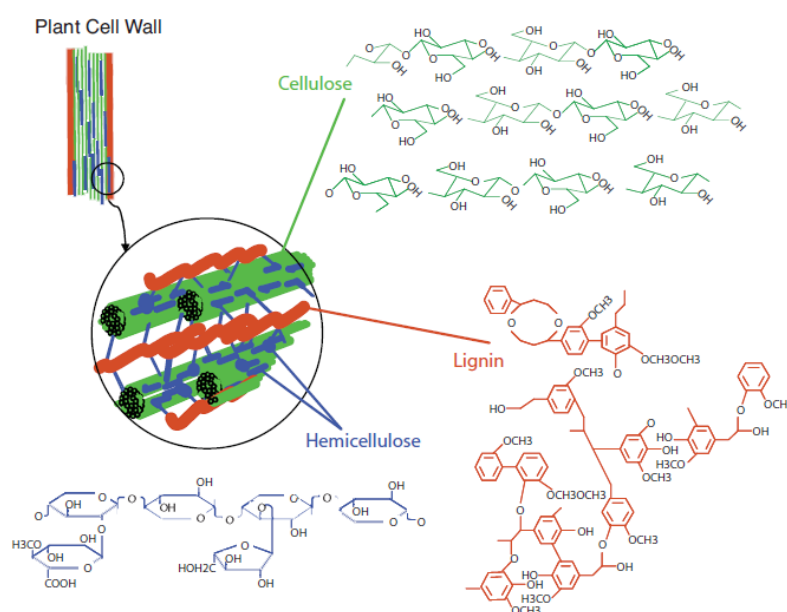


Figure 1-3. Schematic of cellulose, hemicellulose, and lignin components of lignocellulosic biomass and associated molecular building blocks. (Adapted from the website of microbeWiki)

Lignocellulose, as illustrated in **Figure 1-3**, prevalent in plant walls such as wood, grass and agricultural residues, represents the most abundant terrestrial biomass source [21,22]. In general, lignocellulose comprises a mixture of cellulose (38-50%) and hemicellulose (23-32%) carbohydrate polymers embedded in the lignin (15-25%) matrix. Among them, lignin is rich in aromatic functionality and consists mainly of three main primary monomers, namely p-coumaryl, coniferyl, and sinapyl alcohols, which are capable of being converted into high value-

added chemicals and fuels due to their extremely high carbon content[23][24]. Additionally, the structure of lignin varies depending on the biomass resources. Besides, cellulose exhibits a homopolymer structure consisting of β -D-glucopyranose units linked via β -glycosidic bond, which can be decomposed to glucose monomers. Hemicellulose, unlike cellulose, has lower degree of polymerization with branches and exhibits an amorphous structure, which exhibits different structures in according to the lignocellulose sources and may consists of pentoses, hexoses and uronic acids [25]. Therefore, due to the structure complexity and component diversity of compositions, lignocellulose is considered to have great potential to be the alternative feedstocks, which are more practicable, environmental and sustainable for the replacement of fossil fuels.

To transform lignocellulose biomass to fuels and chemicals, comprehensive studies have been focusing on the non-catalytic thermochemical and catalytic biochemical conversion including gasification [26], pyrolysis [6,27,28] and hydrolysis [21], and enzymatic process [29,30]. Enzymatic conversion can be achieved under relatively mild conditions, but, since most of enzymes can only be produced under specific environments and have the shortage of low thermally stability and low productivity, they are industrially expensive and are not widely applied for biomass conversion [31,32]. However, gasification and pyrolysis are thermos routes aiming to convert lignocellulose into syngas and liquid bio-oils which are valuable intermediates for fuels and chemicals [33,34]. However, even though these routes have been gradually matured, harsh conditions such as high temperature and pressure are required in these approaches leading it difficult to control the reaction properly, which further causes the produced chemicals with high fractions of impurities that need further treatment [35]. Compared to gasification and pyrolysis, hydrolysis contains the separation and fraction of product components such as lignin and carbohydrates, which can achieve more precise control of chemical reactions during the conversion process. Obtained lignin is used as fuel for providing heat and electricity, and carbohydrates (namely hemicellulose and cellulose) can convert to target platform chemicals with the help of various catalysts.

The non-catalytic reactions such as above-mentioned gasification and pyrolysis are generally thermochemical process, which is rather unselective and requires harsh conditions, high investment in equipment, and energy-intensive operation, thus greatly limiting their application in the industry. Naturally, catalysts become increasingly important for most chemical reactions, because the catalytic transformation is considered an efficient, highly selective, and economic strategy.

Among all, all the above transformation approaches for lignocellulose biomass result in a mixture of bio-oil, which is a mixture of more than 300 organic compounds. The main compounds of bio-oil include heavy aromatic compounds leading to a low H/C ratio (1.2-1.4), and the O/C ratio of bio-oil is high (0.5) that is caused by significant quantities of water and oxygen containing groups such as phenols, ketones, carboxylic acids, etc., The low H/C ratio but high O/C ratio and strong acidity lead to that bio-oil is not sufficiently stable and is also corrosive, making it difficult for transposition storage and application [26,28].

In view of this, it is necessary to further convert bio-oil to useful liquid hydrocarbon fuels, which can be used as fuels or chemicals, by oxygen removal reactions. Existing methods for eliminating oxygen-containing functional groups in chemicals include dehydration, hydrogenolysis, hydrogenation, decarbonylation, and decarboxylation [36–39]. C-C coupling reactions, including ketonization, oligomerization and hydroxyalkylation etc. [40] were applied to obtain diesel range hydrocarbon products. The major challenge of converting biomass into hydrocarbon fuels is the efficient removal of ubiquitous oxygen-containing groups in the feedstock molecules.

Generally, hydrodeoxygenation (HDO) is widely used method for eliminating oxygen from bio-oil in the form of H₂O; however, CO₂ can be also formed at the same time. General hydrodeoxygenation consists several reactions, such as hydrogenation, cracking, decarbonylation and decarboxylation, which always require hydrogen and catalysts [41]. Among all, hydrodeoxygenation of ketones, phenols are relatively easier as these reactions occur at around 150 to 300 °C or even at room temperature, but the hydrodeoxygenation conversion of carboxylic and phenolic ester requires a high temperature above 300 °C and relatively high H₂ pressure (≥ 2 MPa), accompanied with side reactions and low product selectivity and other shortages. Developing more efficient approaches to convert carboxylic acids, therefore, is a research topic of great potential that can provide more possibilities for the transformation of bio-mass feedstocks.

1.3 Carboxylic acids and derivatives

Carboxylic acids, which can be derived both from natural resources and artificial production, are abundant, structure diverse (e.g., amino acids, fatty acids, vegetable oils, and sugar acids) and generally stable feedstock components, predestining them as versatile starting materials for chemicals synthesis and alternative energy resources [42].

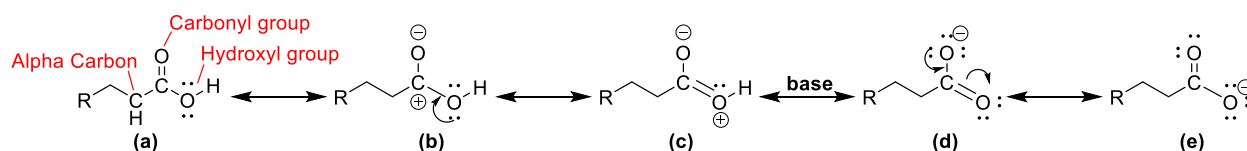


Figure 1-4. The structure of the carboxylic acids (a), the electronic states of the carboxylic group (b, c), and resonance effect of the C=O (c, d).

Figure 1-4 presents the typical structure of carboxylic acid. The carbon and oxygen in the C=O of the carboxylic group are both sp^2 hybridized and are polar as in aldehyde and ketones. The unshared electron pairs in the hydroxyl group (-OH) provide an additional resonance structure to be drawn where one of these pairs is delocalized into the C=O group (b, c). Moreover, the -OH group in the carboxylic acid can deprotonate to the carboxylate ion (d), making the carboxylic acid exhibit acidic properties. However, carboxylic acid exhibits greater acidity than corresponding alcohol due to C=O resonance stabilizing the negative charge on the carboxylate ion that arises by the loss of the OH proton of a carboxylic acid (e). Above all, compared to aldehydes, ketones, and alcohols, carboxylic acids exhibit more stable chemical properties, resulting in the requirement for more severe conditions or catalysts to achieve the removal of the oxygen-containing group in carboxylic acids.

Carboxylic acids can be divided into different types according to their structure and properties. The main types of carboxylic acids include (un)saturated aliphatic acids, aromatic acids, amino acids and etc. The saturated carboxylic acids such as acetic acids, stearic acid, palmitic acid, generally are straight carbon chain with carboxylic group connected to the carbon chain. In the counterpart, unsaturated aliphatic acids which are important in organic chemistry contain C=C bonds in the carbon chain. The most typical sample is α, β -unsaturated acid such as acrylic acid in **Figure 1-5**, in which the double bond is between the second and third carbons of the chain, as well as unsaturated acids, in which the double bond occurs in other positions. Aromatic acids such as benzoic acid are carboxylic acids contain a COOH group bonded to the aromatic ring. Due to the existence of the arene ring, the aromatic acids are similar to other aromatic compounds undergoing electrophilic substitution reactions and the activity of the COOH is suppressed. All these carboxylic acids mostly derive from the biomass, and some of them like aromatic acids were from the waste cooking oils.

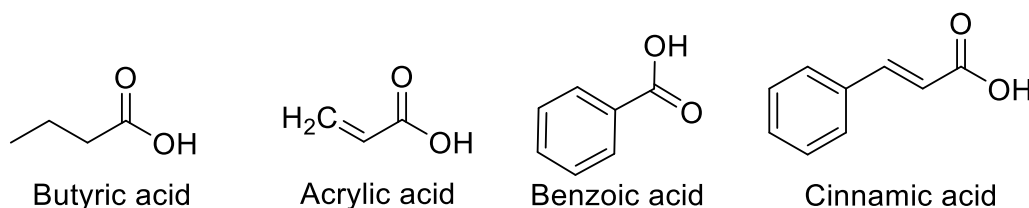
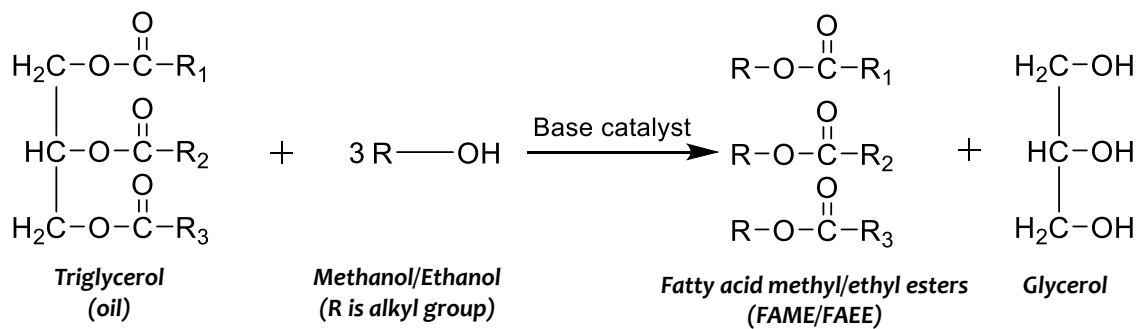


Figure 1-5. Structures of typical carboxylic acids

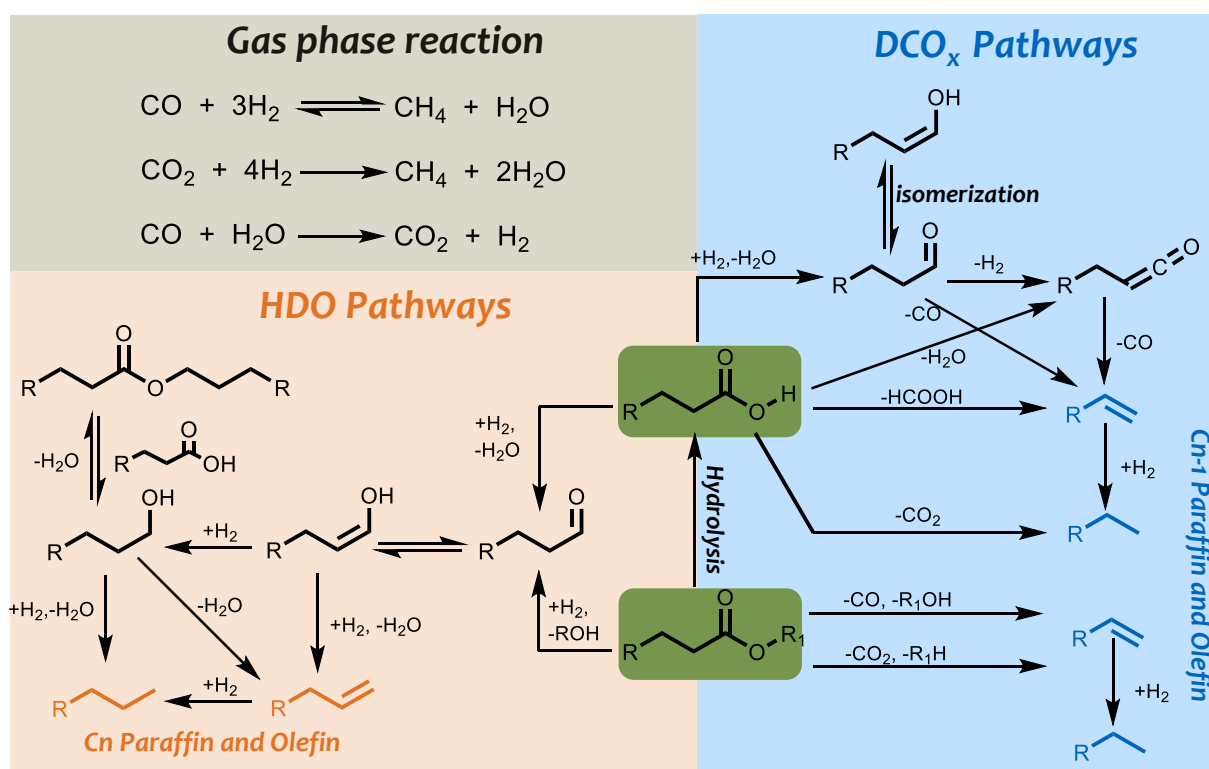
Transesterification reactions convert carboxylic acids into fatty acid methyl esters (FAMES) or fatty acid ethyl esters (FAEEs) (as shown in **Figure 1-6**) which are commonly used as biodiesels. Besides, compounds in which the -OH of the carboxyl group is replaced by certain other groups are carboxylic acid derivatives, the most important of which are acyl halides, acid anhydrides, esters, and amides. Carboxylic acids and derivatives have varied applications in the fields of chemical industry, cosmetics, pharmaceuticals, synthetic polymers, and textiles manufacture.

**Figure 1-6.** Transesterification of oil to a fatty acid methyl/ethyl ester and glycerol.

Therefore, the utilization of carboxylic acids and its derivatives are of significant importance. Nevertheless, these carboxylic acids, carboxylic esters (e.g. FAMES, FAEEs) and derivatives are not fully compatible with conventional fuels due to the high oxygen content of ester groups; Moreover, most of carboxylic acids related chemicals have disadvantages of high acidity, high viscosity, high boiling point, etc. As a result, further upgrading procedures essential for the carboxylic acids and derivatives utilization.

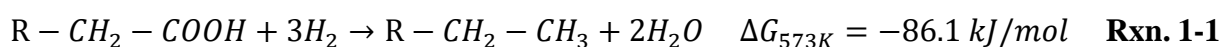
1.4 Deoxygenation of carboxylic acids

Compared to other platform chemicals such as phenols, aldehydes, ketones, researches on the carboxylic acid conversion are rather rare. Nowadays, based on unique chemical structure of carboxylic acids, i.e., have carbonyl group and hydroxyl group, many catalytic decarboxylative strategies for carboxylic acids upgrading to fuels and chemicals have been developed. These catalytic methods convert carboxylic acids to corresponding aldehydes, alcohols, alkanes or alkenes for carboxylic acids utilization, including C-C bond forming reaction for chemical synthesis (Kolbe-electrolysis), C-C bond scission reaction forming CO₂ and alkanes namely decarboxylation (DCO₂), decarbonylation (DCO), hydrodeoxygenation (HDO) reactions. The reaction pathways are presented in **Scheme 1-2**.



Scheme 1-2. Deoxygenation pathways for carboxylic acids and carboxylic acid esters, and side reactions in the gas phase.

1.4.1 Hydrodeoxygenation (HDO)



The hydrodeoxygenation reaction pathway as shown in the **Rxn. 1-1**, which generally is an exothermic reaction, requires high pressure of H₂ that eliminates the oxygen on the

carboxylic acid group as water by a series of hydrogenation and hydrogenolysis reactions. These HDO pathways typically are reduction reactions, which involve molecular H₂ as the reducing agent allowing for a 100% atom efficiency.

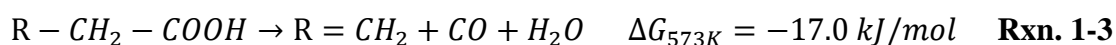
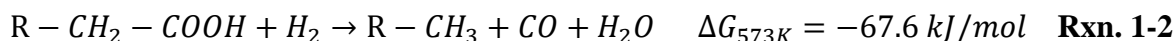
Hydrodeoxygenation starts with removing hydroxyl group of carboxylic acid through hydrogenolysis and generates aldehyde. The intermediates aldehydes can further be converted mainly in 3 different reaction pathways depending on the applied catalysts and reaction conditions. One of them is isomerizing to enol and further hydrogenating to alcohol which could either hydrogenolysis to C_n paraffin or dehydrogenation to C_n olefin; the other 2 pathways involve the indirect decarbonylation reaction steps, which will be described in the next section.

However, catalytic hydrodeoxygenation of carboxylic acids to alcohols and alkanes is a challenging process, due to the low electrophilicity of the carbonyl carbon and the difficulties associated with polarizing the carbonyl group of the reactant carboxylic acids. As a result of the resistance of carboxylic acids to reduction, effective catalysts development is necessary. Current heterogeneous catalytic processes requires harsh conditions including high temperature (200-300 °C) and high H₂ pressure (40-300 bar) [43]. Therefore, side reactions, degradation and deactivation may occur. Alcohols selectivity in this reaction is greatly dependent on the type of catalysts used since alkanes, CO and CO₂, can be produced via decarboxylation and decarbonylation reactions.

Previous research results showed that mono catalysts had nearly negligible results for the carboxylic acids hydrogenation. But bimetallic catalysts comprising early transition carbonyl complexes in combination with a late metal complex achieved extremely high alcohol yield at substantially mild conditions.

The hydrogenation of carboxylic acids and its derivatives is a powerful approach in synthetic organic chemistry. The hydrogenation products aldehydes and alcohols typically formed in such reduction reaction offers great potential for further synthetic functionalization. Therefore, the catalytic reduction of carboxylic acids and their derivatives can yield a vast number of useful products such as bulk platform chemicals or fine-synthesis intermediates.

1.4.2 Decarbonylation



Decarbonylation (DCO) removes oxygen component in the form of CO and H₂O and produces alkanes or alkenes with one carbon atom less than the initial carboxylic acid reactant (**Scheme 1-2**). Above we mentioned the indirect DCO pathways involves hydrogenation reaction steps (**Rxn. 1-2**): after the carboxylic acid first hydrolysis to aldehyde, followed by either aldehyde release CO via decarbonylation to one carbon atom less C_{n-1} paraffin, or aldehyde first dehydrogenates to ketene intermediate and further decarbonylates to C_{n-1} olefin and CO. Direct decarbonylation reaction pathway (**Rxn. 1-3**), however, generates C_{n-1} olefin through the ketene intermediate without any H₂ consumption. All generated olefins in above reaction pathways can further hydrogenate to the saturated paraffin.

An alternative DCO reaction pathway for carboxylic acids has been proposed by Boda et al. [44] according to caprylic acid deoxygenation. This pathway starts with carboxylic acids directly release formic acid (HCOOH) rather than CO₂ as the primary products. Berenblyum et al. [45,46] further proofed this mechanism by the DCO of stearic acid on Pd/WO/ZrO₂ as the methyl formate generated from the methylation step of formic acid.

1.4.3 Decarboxylation



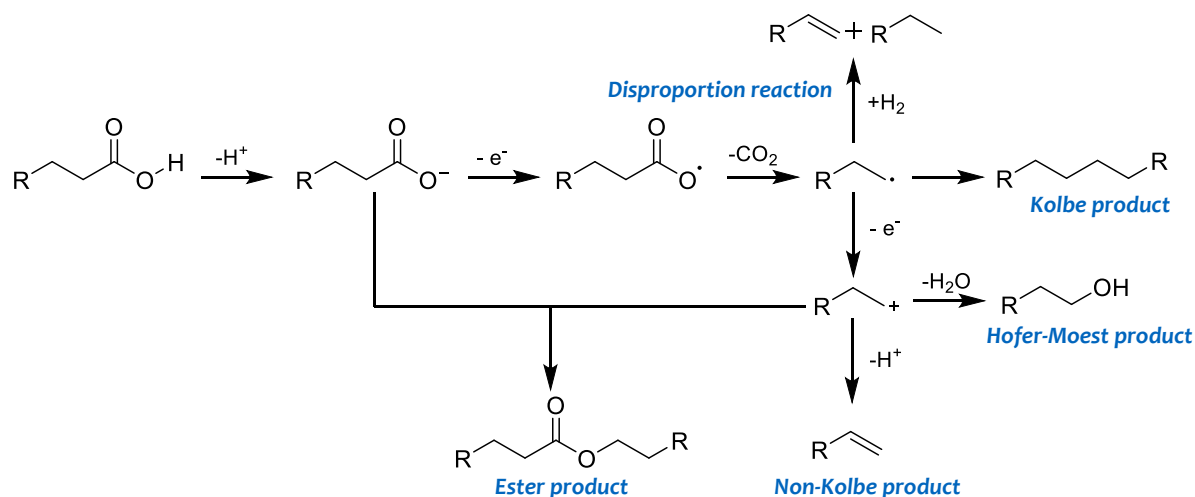
As illustrated in **Rxn. 1-4**, compared to the HDO and DCO, the decarboxylation (DCO₂) pathway directly releases oxygen contain part in the form of CO₂ and produces one carbon atom less alkanes without any H₂ consumption in the stoichiometry. Unlike HDO reaction, DCO₂ is an endothermic reaction which favors high temperature and with almost 100% product selectivity, whereas the HDO reactions may suffer a decrease in products selectivity. Moreover, While HDO is more efficient in regards to atom economy due to the preservation of the number of carbons atoms of the molecular skeleton, DCO_x is more economically attractive because it needs only very low amounts of hydrogen compared with the HDO reaction [47].

In parallel with HDO and DCO_x, other undesirable reactions such as cracking, esterification, ketonization also occur depending on the applied reaction conditions[48]. Meanwhile, other consecutive reactions such as methanation and water gas shift reactions

(shown in **Scheme 1-2** left top) can also take place in the gas phase. Therefore, in order to enhance the selectivity and further enable optimization of the yields for the desired products, it is necessary to have an insightful understanding of the reaction parameters governing the reaction routes and side reactions.

1.4.4 Kolbe Electro Catalysis

In order to achieve high catalytic efficiency in upgrading of carboxylic acids to fuels and chemicals, HDO and DCO_x have been applied in thermos-, photo- and electric-catalysts processes. Compared to traditional deoxygenation process, Kolbe Electrolysis route, however, is usually performed at ambient pressure or without additional pressure and room temperature in aqueous or mildly hazardous solutions. It comprises the anodic decarboxylation of organic acids leading to the formation of prolonged hydro- carbons and CO₂ as the co-product. Tremendous scientific investigations are already available on the topic of Kolbe electrolysis, which in the 21 century, is aiming to build a bridge between the use of renewable electrical energy and the conversion of bio-mass derived carboxylic acids for the production of fuels and chemicals[49,50].



Scheme 1-3. Proposed reaction mechanism for the Kolbe electrolysis and the generation of the Kolbe, Non-Kolbe and Hofer-Moest products.(Picture adapted from [51])

Different theories for the Kolbe electrolysis have been proposed and discussed over one century. A classic example is shown in **Scheme 1-3**, in which radicals are generated electrochemically from carboxylic acids and followed by dimerization [49,51–53]. The Kolbe electrolysis starts with the deprotonation of the carboxylic acid in the base electrolyte. In the

following, the carboxylate adsorbed on the anode surface and an irreversible single electron transfer from the carboxylate to the anode occurs, further is the simultaneous C-C scission to CO_2 and C_{n-1} alkyl radicals followed by the dimerization of two C_{n-1} alkyl radicals and generates which is the main product of the Kolbe reaction. The reaction on the anode surface namely generation of the alkyl radicals requires critical potential lies between 2.1-2.4 V vs. normal hydrogen electrode (NHE). Below this potential, the hydrolysis of water to H_2 and O_2 will mainly occur. However, the generated alkyl radicals can further react to by-products: oxidation reaction on the anode through electron transfer reaction and obtained carbonium ion, which can either convert to alkene via β -H-elimination or with H_2O to alcohol type Hofer-Moest-product. Moreover, the carbenium ion may also react with the deprotonated carboxylic acid leading to the ester side product formation via an esterification reaction. Additionally, on the cathode, occurs the hydrogen evolution reaction, which was also used for the H_2 production.

Pt, Ru, Ir, and graphite are usually used as the working electrode due to their efficient mass and charge transfer contributed by their high conductivity and electrode-electrolyte interface which leads to the higher activity of Kolbe electrolysis. Therefore, tailored electrode materials – especially noble metal free systems, and specifically designed electrolytes are of utmost importance for the development of carboxylic acids conversion via Kolbe electrolysis.

Other decarboxylation methods, such as photocatalytic [54,55] and photo-enzymatic [56,57] decarboxylation are also applied for the carboxylic acid deoxygenation. However, they suffer from the uncontrollable reactivity of the radical intermediates in the photocatalytic reactions. Huang et al. [54] reported that a small amount of hydrogen (≤ 0.2 MPa) can rapidly terminate the photogenerated radicals to C_{n-1} alkanes on the hydrogen-rich surface on the Pt/TiO₂ at ambient temperature. Zhang et al. [57] used *Chlorella variabilis NC64A* (CvFAP) enzyme and achieved the photobiocatalytic decarboxylation of large scope of carboxylic acids with considerable reaction rate. All these research efforts towards carboxylic acids and derivatives open up new methodologies for the conversion of carboxylic acids.

1.5 Effect of catalysts and H_2 atmosphere: Palladium-catalyzed deoxygenation of carboxylic acids

Catalytic activity and selectivity of heterogeneous catalytic reactions are greatly dependent on the reaction and catalyst parameters. More specifically, the active phase, catalyst supports, and gaseous composition have significant effects on the deoxygenation of carboxylic acids.

1.5.1 Active Phases

Transition-metal catalysts are becoming very common for the deoxygenation of carboxylic acids chemicals. The most widely explored catalysts are noble metal Pt, Pd and non-noble metal Ni, which are generally selectively prone to DCO_x pathways. Berenblyum et al. [58] performed a screening of γ -Al₂O₃ supported metal (Ni, Cu, Pt, or Pd) catalysts under 14 bar H₂ atmosphere and 350 °C for stearic acid conversion. Results showed that Ni, Cu, Pt, or Pd/ γ -Al₂O₃ catalysts have high selectivity towards n-heptadecane through a DCO pathway, except Cu/ γ -Al₂O₃, which showed a high selectivity to n-heptadecene. As decarbonylation generated unsaturated olefins, the high selectivity towards paraffin is resulted in the hydrogenation of olefins on the Pd, Pt and Ni catalysts. High n-heptadecene selectivity on Cu/ γ -Al₂O₃, however, is due to the poor hydrogenation abilities of Cu compared to other active metals. Moreover, Snåre et al. [59] also have synthesized and screened various catalysts for their catalytic performances towards the stearic acid DCO_x reactions under an inert condition at 300 °C. The results also exhibited that activities of these catalysts follow a descending order of Pd, Pt, Ni, Rh, Ir, Ru, and Os. Gas-phase analysis demonstrated that the DCO₂ reaction was more profound over the Pd/C catalyst, while the DCO reaction was more evident over the Pt/C catalyst. By combining Berenblyum and Snåre results, we can conclude that in both a H₂-rich and a H₂-free environment that Pd and Pt are selective towards DCO_x reactions [60,61].

In order to further improve the catalytic performance of monometallic catalysts, researchers also developed bimetallic and trimetallic catalysts. Loe et al. modified Ni/ γ -Al₂O₃ catalyst with Cu and Sn metals. Results shows that Cu is an effective promoter of Ni for the DCO_x reactions of stearic acids under H₂ rich atmosphere. The addition of Cu increased both stearic acid conversion and product n-heptadecane selectivity, which was attributed to that Cu enhances the reducibility of Ni and further suppresses cracking reactions and coked caused deactivation. However, the Sn modified Ni/ γ -Al₂O₃ catalyst showed an inhibition effect towards the stearic acid conversion [47,62]. Moreover, NiSnK/SiO₂ catalyst, developing by Chiam et al. [63] for the deoxygenation of palmitic acid, was found to decarboxylate palmitic acid to n-pentadecane accompanied by some DCO and isomerization products.

Except above mentioned transition metal-based catalysts, sulfide catalysts are also used for the carboxylic acids deoxygenation. Sulfide NiMo and CoMo catalysts are only active in the H₂ rich condition, they are reported as being more active towards HDO reaction route.

However, lowering the H₂ pressure over the sulfide catalyst increases the selectivity towards DCO_x reaction routes but decreases the conversion of carboxylic acids, indicating a complete relationship between the HDO and DCO_x reactions. Sulfide catalysts generally have poor chemical and thermal stability because the sulfur is released from the catalytic surface during the high-temperature reaction, leading to oxidation and coking. Therefore, an H₂-rich condition is necessary for sulfide catalysts to maintain activity.

Above all, since the deoxygenation reactions are generally in harsh conditions, catalysts are easily deactivated due to the aggregation and coke deposition, leading to low stability and recyclability. Therefore, development of highly efficient catalysts for the deoxygenation of carboxylic acids is still a challenge, and it would be important to create effective methods for catalyst synthesis and regeneration.

1.5.2 Catalyst supports

Catalyst supports, which play important roles in the heterogeneous catalyst, have been widely researched. One suitable support should be the one that can work in tandem or synergy with the active materials. The most widely used catalyst supports for carboxylic acid deoxygenation reaction include carbon material (activated carbon, carbon nanotubes, etc.), SiO₂, Al₂O₃ and zeolites. The acidity and basicity of the support can significantly impact the activity and selectivity of one catalytic reaction by providing additional reaction sites on the catalytic surface that may be helpful for H₂ dissociation, adsorption of the –COOH group of carboxylic acids, and stabilization of the intermediates.

Al₂O₃, SiO₂ and zeolites are regarded as acidic supports as they containing an abundance of Brønsted acid sites or Lewis acid sites. Brønsted acid sites, which are abundant in zeolites, could promote continuous hydrogenation-dehydrogenation-hydrogenation reaction routes, which is favorable for the HDO reaction pathways mentioned in **Section 1.4.1**. However, since HDO reaction generally occurs at high temperature conditions, supports with too strong acidic sites, such as certain zeolites have been verified to deactivate more easily because of the coke deposition. Supports containing Brønsted acid sites also favor isomerization reactions.

Lewis acid sites, which is plentiful on Al₂O₃ surface, prefer the DCO reactions even under the H₂ rich atmospheres. The influence of support had been studied by Immer et al. [60]. They found that Pd supported on SiO₂ preferred the DCO reaction pathway, whereas Al₂O₃ and activated carbon supported Pd exhibited high DCO₂ activity. Pd/Al₂O₃ was found to deactivate

more rapidly than the Pd/C catalyst. This is because the Pd/Al₂O₃ contains high surface concentration of Lewis acid sites which will further lead to cracking and ketonization reaction. Therefore, the byproducts issued from the side reactions were the main reason causing the catalyst poisoning which leads to rather rapid deactivation and low selectivity of desired hydrocarbons.

Reducible oxide supports which also contains Lewis acid sites such as ZrO₂, TiO₂, and CeO₂ are also ideal supports to reduce carboxylic acids to corresponding aldehydes [64]. These metal oxides support contains oxygen vacancies which could adsorb the oxygenated compounds: Peng et al. proposed that this adsorption process occurs through the abstraction of H atom from the –OH group of carboxylic acid group, and a H atom from α -C position reacted with –OH to produce H₂O and ketene intermediate, which further hydrogenated to aldehyde or decarbonylated to alkanes. As such, the active metal (Ni) and supporting material have synergetic effect for the carboxylic acid deoxygenation [64]. Therefore, the presence of a reducing agent such as H₂ is essential for these reducible supports. Without it, these catalysts with reducible supports cannot maintain the catalytic performances. If a H₂-free system is applied to deoxygenate fatty acid, supports with inert nature such as carbon or SiO₂ are more suitable. However, catalysts with reducible oxide supports are unsuitable for a H₂-free environment as H₂ is required for the catalyst's activation. Under certain reactions, a low-H₂ -containing environment is desired for the selection of a catalyst with reducible oxide material as a support, as they have synergistic effects with relevant catalysts such as Ni that improve the overall activity and selectivity [64].

To sum up, the support of catalysts can affect the catalytic performance and stability of the active metals through the synergetic effect between active metals and the supports; alter the adsorption state of the reactants and further influence reaction pathways, and consequently the products selectivity.

1.5.3 Gaseous atmospheres

The nature of the gaseous atmospheres namely of inert, poor- or rich-hydrogen atmosphere during the reaction also has a significant effect on the carboxylic acids conversion pathways and activities, but resulting effect has strong dependence on the properties of active metals or supports used, on the type of carboxylic acid (saturated or unsaturated acids).

As describe in **Section 1.4**, the HDO and indirect DCO reaction pathways requires a H₂ atmosphere. In **Section 1.5.1**, metal-sulfide and metal-oxide catalysts also prefer a H₂ rich conditions. Peng et al. [64] reveals that higher H₂ pressure (60 bar) benefits the stearic acid HDO pathway on the Ni/H- β catalyst contributing to a higher selectivity of n-octadecane, but lower H₂ pressure (15 bar) favored not only the DCO (n-heptadecane) and iso-octadecane formation.

Compared to HDO and in direct DCO pathway, the DCO and DCO₂ reaction pathways are stoichiometrically H₂-free reactions. However, Several researchers have determined the effect of H₂ concentration on the conversion of carboxylic acids over Pd/C by working on the reaction on dilute H₂ and pure H₂ atmosphere [65–67]. Results showed that though the DCO₂ rate of saturated fatty acid in pure He is faster than in 10% H₂ atmosphere, the presence of H₂ can maintain the stability of catalysts by avoiding generation of the unsaturated products to reach a faster completion. Moreover, unsaturated C₁₈ fatty acids must be hydrogenated first before decarboxylation, and the unsaturated acids can only be deoxygenated in the form of decarbonylation in the inert atmosphere at a slow rate but can be decarboxylated facilely via hydrogenation to saturated carboxylic acids first [66][68]. Maier et al. also reported elimination of the carboxylic group of octanoic acid to n-heptane on Pd/C in a H₂ flow, while it hardly reacted in N₂ [69]. Peng et al. [64] reported that a Ni/ZrO₂ catalyst favors DCO_x reactions for the deoxygenation of palmitic acid under H₂ atmosphere rather an inert atmosphere. A higher selectivity towards conversion were achieved in the H₂ atmosphere. Thus, they conclude that even though Ni/ZrO₂ catalysts favor DCO_x reactions, a source for dissociated hydrogen on the catalyst surface is still required to provide adequate results. Therefore, although the DCO_x of acids without H₂ is possible, deactivation is an issue. An excess of H₂, also inhibit the decarboxylation activity, which could be attributed to the competitive adsorption between the carboxylic acids and H₂ [46,70,71]. Even in the photocatalytic decarboxylation reaction, Huang et al. [54] demonstrated that a hydrogen-rich surface can rapidly terminate the radical intermediates and avoid the dimerization. In addition, indirect DCO reactions appear to be faster than direct DCO reactions. Having certain amount of H₂ in the reaction system would promote indirect DCO to higher activity.

Therefore, a limited amount of H₂ is necessary to achieve desirable products by catalytic decarboxylation of carboxylic acids. A H₂-modest atmosphere should be applied instead of an H₂-free system to achieve higher carboxylic acids deoxygenation activity. However, the role of this trace amount of H₂ is still unclear, especially in a Pd-based catalyst system.

1.6 Chemical kinetics

One heterogeneous reaction generally begins with reactant molecules in the bulk of gaseous/liquid phase diffusing to the catalytic surface, and then adsorbing on the surface-active sites as the initial state with a relatively low free energy level, followed by the surface reaction relating to forming or breaking chemical bonds accompanied by the activated state - transition state generation. Finally, the formed adsorbed products are released from the surface by desorption and further diffuse to the bulk of gaseous/liquid phase.

Figure 1-7 illustrates the energy profiles comparison of non-catalytic reaction and catalytic reaction. Non-catalytic reactions (such as thermochemical reactions) generally have high energy barriers and the chemical process is hardly controllable. When introducing a typical catalyst into one chemical reaction system, the reaction rate can be controlled more precisely either by the catalyst itself or the external reaction conditions. Therefore, catalytic processes are more attractive from environmental as well as economic viewpoints as they exhibit higher atoms and energy efficiencies.

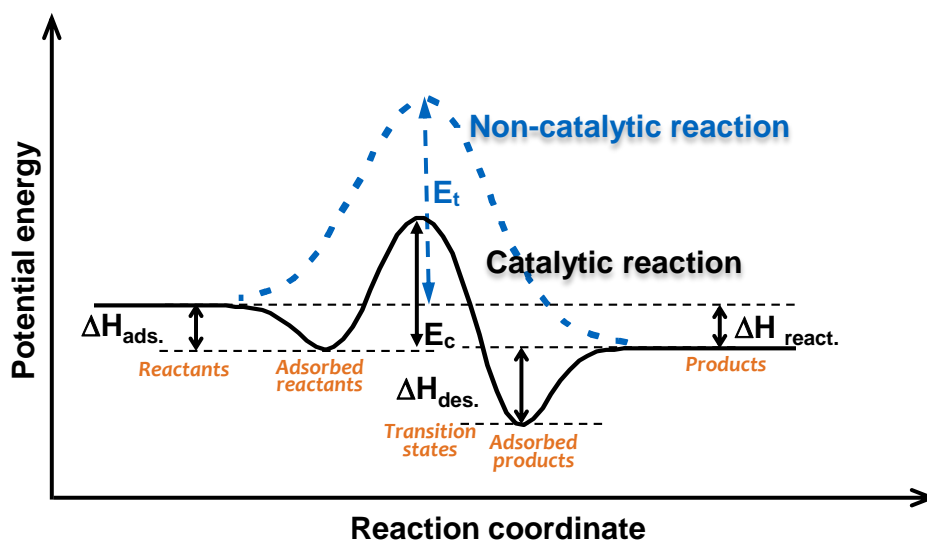


Figure 1-7. Energy diagram for the transformation of reactant to products in the non-catalytic and catalytic processes.

In the catalytic reaction, the overall energy barrier is defined as the difference between the initial state and the transition state, which also reflects the overall reaction rates. Therefore, the

reaction rate or in other words energy barrier of one catalytic reaction can be altered by either changing the composition and morphology of catalysts or the reaction condition.

The initial and final molecules transfer steps between the catalytic surface and bulk of fluid are external diffusions and the mass transfer of these diffusion steps depends on temperature and velocity of fluids [72]. To eliminate the influence of external mass transfer, higher mechanical stirring rate would be helpful [73,74] .

The surface adsorption includes physisorption and chemisorption[75]. Physisorption is achieved by the Van der Waals force driven interaction between the molecule and catalytic surface. In contrast, chemical adsorption forms new chemical bonds between molecules and catalytic active sites. The Van der Waals force induced physisorption is rather weaker than chemisorption which is necessary for the afterwards surface reaction [76,77]. Different chemisorption models have been established and described by adsorption isotherms. The most widely used in heterogeneous catalysis reactions is Langmuir isotherm, which describes the adsorption of a single adsorbate onto a series of equivalent sites onto the surface of the solid basing on the following basic assumptions [78,79]:

- 1) The surface containing the adsorbing sites is perfectly homogeneous without any corrugations. (Chemically heterogeneous surface can also be considered as homogeneous when the adsorbate is bound to specific chemical sites or functional groups on the surface)
- 2) Each site can only hold at most one molecular adsorbent (mono-layer coverage);
- 3) Adsorbate molecules are independent on adjacent sites (no interaction between adsorbed molecules).

Thus, we can derive the mono-site Langmuir adsorption isotherm under equilibrium as **Eq. 1-1** and **Eq. 1-2**:

$$Q = Q_{sat} \frac{K_{eq}^o C_{eq}}{1 + K_{eq}^o C_{eq}} \quad \text{Eq. 1-1}$$

$$\theta = \frac{Q}{Q_{sat}} \quad \text{Eq. 1-2}$$

where Q is the uptake of adsorbate, Q_{sat} is its uptake at saturation, and their quotient ($\theta = Q/Q_{sat}$) is the coverage, namely the fraction of the surface covered with adsorbates, C_{eq} is the concentration of adsorbate in the bulk of liquid/gaseous and K_{eq}^o is the experimentally determined equilibrium constant.

The adsorption entropy and enthalpy can be determined by using of Van't Hoff equation as **Eq. 1-3** [80].

$$\ln K_{eq}^o = -\frac{\Delta H_{ads}^o}{RT} + \frac{\Delta S_{ads}^o}{R} \quad \text{Eq. 1-3}$$

Where ΔH_{ads}^o is standard adsorption enthalpy (kJ/mol), ΔS_{ads}^o is standard adsorption entropy (J/mol/K), T is the absolute temperature (K) and R is the universal gas constant (8.314 J/mol/K). By measuring the equilibrium constant, K_{eq}^o , at different temperatures, the enthalpy and entropy of this adsorbate adsorption process can be easily obtained via the slope and intercept from the Van't Hoff plot.

Surface reactions on catalytic active sites include at least one step of the adsorbed reactants. The mechanisms for these reactions and the rate equation are of extreme importance for heterogeneous catalytic reactions. There are three typical mechanisms commonly applied with respect to the surface reaction steps.

1) Monomolecular reaction

A decomposition reaction namely one reactant breaks down to two or more products [81], it can be represented by the general equation as **Rxn. 1-5**.



The rate equation can be expressed as **Eq. 1-4**.

$$r = kC_{AB}^n \quad \text{Eq. 1-4}$$

where r is the overall reaction rate, which can be affected by reaction conditions, C_{AB} is the initial concentration of reactant A, the exponent n is the reaction order of reactant AB, stating how the reactant concentration affects the reaction rate. The reaction order can be negative, positive and zero order. A chemical reaction, as we described, is composed of one or more elementary steps. Thus, we can describe the decomposition reaction as follows:



where $*$ is the empty site, AB^* , A^* and B^* denote as sorbed reactant AB and sorbed products A and B. k_1 and k_{-1} are equilibrium constants of AB adsorption and desorption.

Rate for the surface reaction is **Eq. 1-8**:

$$r = k_2 C_{AB^*} \quad \text{Eq. 1-8}$$

We define the surface coverage of AB as $\theta_{AB} = C_{AB^*}/C_*$, θ_* is the remaining empty sites, The number of active sites is constant, therefore, $\theta_{AB} + \theta_* = 1$

If we apply steady state approximation to the adsorbed AB, and

$$\frac{dC_{AB^*}}{dt} = k_1 C_{AB} C_* - k_{-1} C_{AB^*} - k_2 C_{AB^*} = 0 \quad \text{Eq. 1-9}$$

We define the surface coverage of AB as $\theta_{AB} = C_{AB^*}/C_*$, so,

$$\frac{dC_{AB^*}}{dt} = k_1 C_{AB} C_* - k_{-1} C_{AB^*} - k_2 C_{AB^*} = k_1 C_{AB} C_* (1 - \theta_{AB}) - k_{-1} C_* \theta_{AB} - k_2 C_* \theta_{AB} = 0 \quad \text{Eq. 1-10}$$

Thus,

$$\theta_{AB} = \frac{k_1 C_{AB}}{k_1 C_{AB} + k_{-1} + k_2} \quad \text{Eq. 1-11}$$

and

$$r = k_2 C_{AB^*} = \frac{k_2 k_1 C_{AB} C_*}{k_1 C_{AB} + k_{-1} + k_2} \quad \text{Eq. 1-12}$$

When the limiting step is adsorption/desorption, namely

$k_2 \gg k_1 C_{AB}, k_{-1}$, so, $r \approx k_1 C_{AB} C_*$, the reaction order of reactant AB is first order.

When the surface reaction is the limiting step,

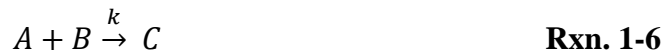
$$k_2 \ll k_1 C_{AB}, k_{-1}, \text{ so, } \theta_{AB} \approx \frac{k_1 C_{AB}}{k_1 C_{AB} + k_{-1}} = \frac{K_1 C_{AB}}{K_1 C_{AB} + 1}$$

where $K_1 = k_1/k_{-1}$ is the adsorption equilibrium constant derived from Langmuir isotherm for the surface coverage, the overall reaction rate becomes:

$$r = k_2 C_{AB^*} = \frac{k_2 K_1 C_{AB} C_*}{k_1 C_{AB} + 1} \quad \text{Eq. 1-13}$$

2) Langmuir-Hinshelwood mechanism (L-H mechanism)

L-H mechanism states two molecules adsorb on neighboring sites and then the surface reaction occurs between the adsorbed molecules [82,83], which can be represented by the general equation as **Rxn. 1-6**:



The overall rate equation can be expressed as:

$$r = -\frac{dC_C}{dt} = k C_A^n C_B^m \quad \text{Eq. 1-14}$$

where C_A and C_B express the concentration of the species A and B. k is the reaction rate constant which is related to the reactant nature and reaction conditions. Exponents n and m are the partial orders with respect to species A and B

The elementary step for a L-H mechanisms type reaction can be presented as:



where $*$ is the empty site, A^* , B^* and C^* denote as sorbed A, B and C. K_A , K_B and K_C are equilibrium constant of A and B adsorption, and C desorption. k_2 is the rate constant for the product formation.

Generally, adsorption and desorption steps are considered as quasi-equilibrium that not limit the reaction. The surface reaction as the slower step which limits the overall reaction. Thus, the reaction rate of every elementary step can be described as:

$$K_A = \frac{\theta_A}{C_A \theta_*} \rightarrow \theta_A = K_A C_A \theta_* \quad \text{Eq. 1-19}$$

$$K_B = \frac{\theta_B}{C_B \theta_*} \rightarrow \theta_B = K_B C_B \theta_* \quad \text{Eq. 1-20}$$

$$r = k_2 \theta_A \theta_B \quad \text{Eq. 1-21}$$

where θ^* , θ_A and θ_B are coverage of empty sites, reactant A and B. K_A , K_B are the equilibrium constant for A and B of the adsorption. k_2 is the reaction rate of the rate-determining step.

The number of active sites is constant, therefore, the sum of θ^* , θ_A , θ_B is one.

$$\theta_A + \theta_B + \theta_* = 1 \quad \text{Eq. 1-22}$$

$$K_A \theta_* + K_B \theta_* + \theta_* = 1 \quad \text{Eq. 1-23}$$

$$\theta_* = \frac{1}{1+K_A+K_B} \quad \text{Eq. 1-24}$$

So, the rate equation can be written as:

$$r = k_2 \theta_A \theta_B = \frac{k_2 K_A K_B C_A C_B}{(1+K_A+K_B)^2} \quad \text{Eq. 1-25}$$

3) Eley–Rideal mechanism

The Eley–Rideal mechanism describes the reaction between an adsorbed molecule A^* and the gas phase molecule B (g) [84–86], which can be expressed as follows **Rxn. 1-7**:



The elementary steps can be expressed as:



The expected rate equation should be:

$$r = k_2 \theta_A P_B \quad \text{Eq. 1-29}$$

$$\theta_A + \theta_* = 1 \quad \text{Eq. 1-30}$$

Thus,

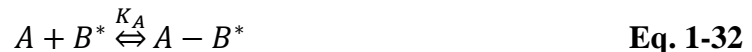
$$r = k_2 \theta_A P_B = \frac{k_2 K_A C_A P_B}{1 + K_A C_A} \quad \text{Eq. 1-31}$$

4) Mars van Krevelen mechanism

The Mars van Krevelen mechanism is different from the E-R mechanism, as it describes one reactant molecular adsorbs and reacts with other components such as O, H, S which had previously been adsorbed in the lattice. The vacancy created by desorption of products will be refilled by the corresponding components [87–89]. Therefore, the overall reaction equation can be expressed as **Rxn. 1-8**:



The elementary steps can be written as follows:



The adsorption of B is present at last step since the empty sites is created by the reaction rather than being present on the fresh catalyst.

When analyzing this mechanism from kinetic perspective, the first 2 steps are combined, assuming that the products are formed as soon as A interacts with adsorbed B. The desorption step is also considered as quasi-equilibrated.

Thus, the rate equation can be expressed as

$$r_2 = k_2 C_A \theta_B \quad \text{Eq. 1-36}$$

In addition, the adsorption of B can be expressed as

$$r_B = k_B C_B \theta_* \quad \text{Eq. 1-37}$$

Note that

$$\theta_B + \theta_* = 1 \quad \text{Eq. 1-38}$$

Under the steady state, when $r_2 = r_B$, we get

$$r_B = k_B C_B \theta_* = k_B C_B (1 - \theta_B) \quad \text{Eq. 1-39}$$

$$\theta_B = \frac{k_B C_B}{k_2 C_A + k_B C_B} \quad \text{Eq. 1-40}$$

$$r_2 = k_2 C_A \theta_B = \frac{k_2 C_A k_B C_B}{k_2 C_A + k_B C_B} \quad \text{Eq. 1-41}$$

1.7 Scope of this thesis

The successful conversion of biomass derived carboxylic acids and derivatives to the useful hydrocarbon fuels and chemicals via a heterogeneous catalytic system depends on the active species and the reaction parameters such as temperature and gaseous compositions. Decarboxylation pathways have been showing great potential in chemical synthesis and bio-oil upgrading. Thus, identifying the active species of Pd-based catalysts and understanding the fundamental reaction mechanism for the decarboxylation processes are of significant importance.

In this context, we focus on the simple Pd-based catalysts in the aryl-substituted aliphatic carboxylic acid ($\text{Ar-C}_n\text{H}_{2n}\text{-COOH}$, $n \geq 1$) deoxygenation reactions in a heterogeneous liquid-solid system. We aim to explore ideal reaction parameters for the better deoxygenation of carboxylic acids in terms of high the reactivity and selectivity. Moreover, due to the special chemical property of applied Pd catalyst which forms palladium hydride (PdH_x) under H_2 atmosphere, the identification of the active species during the reaction, which have not been addressed in previous studies, are identified in this thesis, in order to have a deep understanding

of the reaction mechanism. The ultimate goal of this research is rational design of novel catalysts by taking advantage of the fundamental insights into the reaction mechanisms.

Exploring the suitable reaction conditions for the successful deoxygenation of carboxylic acids is one of the key tasks in the upgrading of the bio-derived chemicals. Therefore, in the second chapter of this thesis, we first investigated the reaction parameters such as the reaction temperatures, gaseous composition using Pd/C as the catalyst for the deoxygenation of the aryl-substituted aliphatic carboxylic acid which was used as a model carboxylic acid. We reported how the gaseous compositions influence the reaction pathways and find a more efficient deoxygenation approach. Furthermore, the in-situ X-ray absorption near edge spectroscopy (XANES) in combination of the temperature programmed surface reaction (TPSR) identified that the PdH_x has higher decarboxylation activity than metallic Pd. The specific role of hydrogen in the decarboxylation reaction was explored by the isotopic labeling of gaseous H₂ and deuterium substitution reaction. With all these results, the carboxylic acid decarboxylation mechanism was also proposed.

In the third chapter, the study focused on revealing the promotion effect of alkali-metal salts modifiers to the PdH_x/C catalyst. Various alkali metal compounds such as KOH, KCl, K₂CO₃, KHCO₃ etc., and modified PdH_x/C catalysts were synthesis via simple two-step continuous incipient wetness method. PdH_x/C catalysts with different modifiers exhibited quite different activities, and among all the catalysts, 1wt. % KHCO₃-PdH_x/C catalyst most elevate the hydrocinnamic acid decarboxylation rate. Characterizations including XANES, CO₂-TPD, CO/H₂-chemisorption etc. were applied to identify the surface properties of the modified catalysts, which reveals that introduction of alkali-metal compounds create basic sites on the PdH_x/C surface. Moreover, reaction rate and reaction orders were measured on PdH_x/C catalysts with different KHCO₃ loadings (0.5 to 8 wt. %). With kinetic analysis, we confirmed that the C-C bond scission is the rate-determining step, and the KHCO₃ modifier promotes the dissociation of COOH group of carboxylic acid and makes the dissociated carboxylate species dominating the active sites on the surface, which contributes to the higher decarboxylation activity.

The final chapter summarizes the whole thesis and generates insights towards the rational catalysts design and mechanistic understanding for the upgrading of biomass-derived carboxylic acids into desired fuels and chemicals.

1.8 References

- [1] H. Ritchie, M. Rose, Energy Production and Consumption, Our World Data. (2021).
- [2] H. Khan, I. Khan, T.T. Binh, The heterogeneity of renewable energy consumption, carbon emission and financial development in the globe: A panel quantile regression approach, *Energy Reports*. 6 (2020) 859–867.
- [3] M. Azam, A. Gohar, F.V. Bekun, Estimating the energy consumption function: evidence from across the globe, *Environ. Sci. Pollut. Res.* 29 (2022) 59060–59075.
- [4] M.A. Abdelkareem, A.G. Olabi, Renewable energy and climate change, *Renew. Sustain. Energy Rev.* 158 (2022) 12111.
- [5] M. Balat, G. Ayar, Biomass energy in the world, use of biomass and potential trends, *Energy Sources*. 27 (2005) 931–940.
- [6] Y. K N, P.D. T, S. P, K. S, Y.K. R, S. Varjani, S. AdishKumar, G. Kumar, R.B. J, Lignocellulosic biomass-based pyrolysis: A comprehensive review, *Chemosphere*. 286 (2022) 131824.
- [7] S.A. Akhade, N. Singh, O.Y. Gutierrez, J. Lopez-Ruiz, H. Wang, J.D. Holladay, Y. Liu, A. Karkamkar, R.S. Weber, A.B. Padmaperuma, M.S. Lee, G.A. Whyatt, M. Elliott, J.E. Holladay, J.L. Male, J.A. Lercher, R. Rousseau, V.A. Glezakou, Electrocatalytic hydrogenation of biomass-derived organics: A review, *Chem. Rev.* 120 (2020) 11370–11419.
- [8] V.R. Ashokkumar V, et al Jayashree S, Recent advances in lignocellulosic biomass for biofuels and value-added bioproducts-A critical review, *Bioresour. Technol.* 344 (2022) 126195.
- [9] M.P. Koh, W.K. Hoi, Sustainable biomass production for energy in Malaysia, *Biomass and Bioenergy*. 25 (2003) 517–529.
- [10] R. Waheed, S. Sarwar, C. Wei, The survey of economic growth, energy consumption and carbon emission, *Energy Reports*. 5 (2019) 1103–1115.
- [11] K.H. Nguyen, M. Kakinaka, Renewable energy consumption, carbon emissions, and development stages: Some evidence from panel cointegration analysis, *Renew. Energy*. 132 (2019) 1049–1057.
- [12] Key aspects of the Paris Agreement, United Nations Clim. Chang. (2015). <https://unfccc.int/most-requested/key-aspects-of-the-paris-agreement>.
- [13] F. Wang, J.D. Harindintwali, Z. Yuan, M. Wang, F. Wang, S. Li, Z. Yin, L. Huang, Y. Fu, L. Li, S.X. Chang, J. Lehmann, Y.G. Zhu, H. Jin, A. Schäffer, J.M. Tiedje, J.M. Chen, Technologies and perspectives for achieving carbon neutrality, *Innov.* 2 (2021).
- [14] M.J.B. Kabeyi, O.A. Olanrewaju, Sustainable Energy Transition for Renewable and Low Carbon Grid Electricity Generation and Supply, *Front. Energy Res.* 9 (2022) 1–45.
- [15] M. Larsson, Global energy transformation: Four necessary steps to make clean energy the next success story, 2009.
- [16] G.W. Huber, S. Iborra, A. Corma, Synthesis of transportation fuels from biomass: Chemistry, catalysts, and engineering, *Chem. Rev.* 106 (2006) 4044–4098.

- [17] I.E.A. Iea, *Biofuels for Transport: An International Perspective*, Int. Energy Agency. (2004) 216. <http://www.iea.org/textbase/nppdf/free/2004/biofuels2004.pdf>.
- [18] *Liquid Biofuels for Transport Prospects, risks and opportunities*, Green Facts. (2009). <https://www.greenfacts.org/en/biofuels/1-2/1-definition.htm>.
- [19] X. Zhang, K. Wilson, A.F. Lee, Heterogeneously Catalyzed Hydrothermal Processing of C5-C6 Sugars, *Chem. Rev.* 116 (2016) 12328–12368.
- [20] A. Stirbet, D. Lazár, Y. Guo, G. Govindjee, Photosynthesis: Basics, history and modelling, *Ann. Bot.* 126 (2020) 511–537.
- [21] M. Möller, U. Schröder, Hydrothermal production of furfural from xylose and xylan as model compounds for hemicelluloses, *RSC Adv.* 3 (2013) 22253–22260.
- [22] C.H. Zhou, X. Xia, C.X. Lin, D.S. Tong, J. Beltramini, Catalytic conversion of lignocellulosic biomass to fine chemicals and fuels, *Chem. Soc. Rev.* 40 (2011) 5588–5617.
- [23] J. Zakzeski, P.C.A. Bruijninx, A.L. Jongerius, B.M. Weckhuysen, The catalytic valorization of lignin for the production of renewable chemicals, *Chem. Rev.* 110 (2010) 3552–3599.
- [24] A.M. Borrero-López, C. Valencia, J.M. Franco, Lignocellulosic Materials for the Production of Biofuels, Biochemicals and Biomaterials and Applications of Lignocellulose-Based Polyurethanes: A Review, *Polymers (Basel)*. 14 (2022).
- [25] K. Alper, K. Tekin, S. Karagöz, A.J. Ragauskas, Sustainable energy and fuels from biomass: A review focusing on hydrothermal biomass processing, *Sustain. Energy Fuels*. 4 (2020) 4390–4414.
- [26] D.A. Bulushev, J.R.H. Ross, Catalysis for conversion of biomass to fuels via pyrolysis and gasification: A review, *Catal. Today*. 171 (2011) 1–13.
- [27] Z. He, X. Wang, Hydrodeoxygenation of model compounds and catalytic systems for pyrolysis bio-oils upgrading, *Catal. Sustain. Energy*. 1 (2013) 28–52.
- [28] G. Wang, G. Dai, S. Ding, J. Wu, S. Wang, A new insight into pyrolysis mechanism of three typical actual biomass: The influence of structural differences on pyrolysis process, *J. Anal. Appl. Pyrolysis*. 156 (2021) 105184.
- [29] J.S. Gan, H.M.N. Iqbal, P.L. Show, A. Rahdar, M. Bilal, Upgrading recalcitrant lignocellulosic biomass hydrolysis by immobilized cellulolytic enzyme-based nanobiocatalytic systems: a review, *Biomass Convers. Biorefinery*. (2022).
- [30] R. Saini, A.K. Patel, J.K. Saini, C.W. Chen, S. Varjani, R.R. Singhania, C. Di Dong, Recent advancements in prebiotic oligomers synthesis via enzymatic hydrolysis of lignocellulosic biomass, *Bioengineered*. 13 (2022) 2139–2172.
- [31] G. Banerjee, J.S. Scott-Craig, J.D. Walton, Improving enzymes for biomass conversion: A basic research perspective, *Bioenergy Res.* 3 (2010) 82–92.
- [32] Z. Zhang, A.A. Donaldson, X. Ma, Advancements and future directions in enzyme technology for biomass conversion, *Biotechnol. Adv.* 30 (2012) 913–919.
- [33] D. Lee, H. Nam, M.W. Seo, S.H. Lee, D. Tokmurzin, S. Wang, Y.-K. Park, Recent progress in the catalytic thermochemical conversion process of biomass for biofuels, *Chem. Eng. J.* 447 (2022) 137501.

- [34] Y. Wu, W. Haoyu, L. Haoyang, H. Xue, Z. Mingyuan, S. Yan, F. Xudong, T. Ren, Z. Yimin, X.C. Charles, X. Xiwei, Applications of catalysts in thermochemical conversion of biomass (pyrolysis, hydrothermal liquefaction and gasification): A critical review, *Renew. Energy*. 196 (2022) 462–481.
- [35] S. Mariyam, M. Shahbaz, T. Al-Ansari, H.R. Mackey, G. McKay, A critical review on co-gasification and co-pyrolysis for gas production, *Renew. Sustain. Energy Rev.* 161 (2022) 112349.
- [36] M.W. Nolte, B.H. Shanks, A Perspective on Catalytic Strategies for Deoxygenation in Biomass Pyrolysis, *Energy Technol.* 5 (2017) 7–18.
- [37] S. Dutta, Deoxygenation of biomass-derived feedstocks: Hurdles and opportunities, *ChemSusChem*. 5 (2012) 2125–2127.
- [38] M. Shiramizu, F.D. Toste, Deoxygenation of biomass-derived feedstocks: Oxorhenium-catalyzed deoxydehydration of sugars and sugar alcohols, *Angew. Chemie - Int. Ed.* 51 (2012) 8082–8086.
- [39] K.C. Kwon, H. Mayfield, T. Marolla, B. Nichols, M. Mashburn, Catalytic deoxygenation of liquid biomass for hydrocarbon fuels, *Renew. Energy*. 36 (2011) 907–915.
- [40] M.J. Climent, A. Corma, S. Iborra, Conversion of biomass platform molecules into fuel additives and liquid hydrocarbon fuels, *Green Chem.* 16 (2014) 516–547.
- [41] D.C. Elliott, Historical developments in hydroprocessing bio-oils, *Energy and Fuels*. 21 (2007) 1792–1815.
- [42] W.H. Brown, J. March, A. Augustyn, T.K. Bhutia, G. Lotha, M. Metych, R. Pallardy, N. Parwani, K. Rogers, *Carboxylic Acid*, *Britannica*. (2022).
- [43] H. Adkins, R. Connor, The catalytic hydrogenation of organic compounds over copper chromite, *J. Am. Chem. Soc.* 53 (1931) 1091–1095.
- [44] L. Boda, G. Onyestyák, H. Solt, F. Lónyi, J. Valyon, A. Thernesz, Catalytic hydroconversion of tricaprylin and caprylic acid as model reaction for biofuel production from triglycerides, *Appl. Catal. A Gen.* 374 (2010) 158–169.
- [45] A.S. Berenblyum, V.Y. Danyushevsky, E.A. Katsman, T.A. Podoplelova, V.R. Flid, Production of engine fuels from inedible vegetable oils and fats, *Pet. Chem.* 50 (2010) 305–311.
- [46] A.S. Berenblyum, T.A. Podoplelova, R.S. Shamsiev, E.A. Katsman, V.Y. Danyushevsky, On the mechanism of catalytic conversion of fatty acids into hydrocarbons in the presence of palladium catalysts on alumina, *Pet. Chem.* (2011).
- [47] K.A. Rogers, Y. Zheng, Selective Deoxygenation of Biomass-Derived Bio-oils within Hydrogen-Modest Environments: A Review and New Insights, *ChemSusChem*. 9 (2016) 1750–1772.
- [48] R.W. Gosselink, S.A.W. Hollak, S.W. Chang, J. Van Haveren, K.P. De Jong, J.H. Bitter, D.S. Van Es, Reaction pathways for the deoxygenation of vegetable oils and related model compounds, *ChemSusChem*. 6 (2013) 1576–1594.
- [49] H.-J. Schäfer, Recent contributions of Kolbe electrolysis to organic synthesis, *Electrochem. IV.* (2005) 91–151.

- [50] H. Kolbe, a N N a L E N Chemie Pharmacle, Justus Liebigs Ann. Chem. 69 (1849) 257–294.
- [51] F.J. Holzhäuser, J.B. Mensah, R. Palkovits, (Non-)Kolbe electrolysis in biomass valorization—a discussion of potential applications, Green Chem. 22 (2020) 286–301.
- [52] G. Yuan, C. Wu, G. Zeng, X. Niu, G. Shen, L. Wang, X. Zhang, R. Luque, Q. Wang, Kolbe Electrolysis of Biomass-Derived Fatty Acids Over Pt Nanocrystals in an Electrochemical Cell, ChemCatChem. 12 (2020) 642–648.
- [53] D. Klüh, W. Waldmüller, M. Gaderer, Kolbe Electrolysis for the Conversion of Carboxylic Acids to Valuable Products—A Process Design Study, Clean Technol. 3 (2021) 1–18.
- [54] Z. Huang, Z. Zhao, C. Zhang, J. Lu, H. Liu, N. Luo, J. Zhang, F. Wang, Enhanced photocatalytic alkane production from fatty acid decarboxylation via inhibition of radical oligomerization, Nat. Catal. 3 (2020) 170–178.
- [55] H. Zhang, P. Zhou, H. Ji, W. Ma, C. Chen, J. Zhao, Enhancement of photocatalytic decarboxylation on TiO₂ by water-induced change in adsorption-mode, Appl. Catal. B Environ. 224 (2018) 376–382.
- [56] D. Sorigué, B. Légeret, S. Cuiné, S. Blangy, S. Moulin, E. Billon, P. Richaud, S. Brugière, Y. Couté, D. Nurizzo, P. Müller, K. Brettel, D. Pignol, P. Arnoux, Y. Li-beisson, G. Peltier, F. Beisson, An algal photoenzyme converts fattyacids to hydrocarbons, Science (80-.). 357 (2017) 903–907.
- [57] W. Zhang, M. Ma, M.M.E. Huijbers, G.A. Filonenko, E.A. Pidko, M. Van Schie, S. De Boer, B.O. Burek, J.Z. Bloh, W.J.H. Van Berkel, W.A. Smith, F. Hollmann, Hydrocarbon Synthesis via Photoenzymatic Decarboxylation of Carboxylic Acids, J. Am. Chem. Soc. 141 (2019) 3116–3120.
- [58] A.S. Berenblyum, R.S. Shamsiev, T.A. Podoplelova, V.Y. Danyushevsky, The influence of metal and carrier natures on the effectiveness of catalysts of the deoxygenation of fatty acids into hydrocarbons, Russ. J. Phys. Chem. A. 86 (2012) 1199–1203.
- [59] M. Snåre, Kubic̆kova´, P. IvaMäki-Arvela, K. Eränen, D.Y. Murzin, Heterogeneous Catalytic Deoxygenation of Stearic Acid for Production of Biodiesel, Ind. Eng. Chem. Res. 45 (2006) 5708–5715.
- [60] R. Bartosz, M.-A. Päivi, T. Anton, L. Anne Riikka, E. Kari, D.Y. Murzin, Influence of hydrogen in catalytic deoxygenation of fatty acids and their derivatives over Pd/C, Ind. Eng. Chem. Res. 51 (2012) 8922–8927.
- [61] E. Santillan-Jimenez, M. Crocker, Catalytic deoxygenation of fatty acids and their derivatives to hydrocarbon fuels via decarboxylation/decarbonylation, J. Chem. Technol. Biotechnol. 87 (2012) 1041–1050.
- [62] R. Loe, E. Santillan-Jimenez, T. Morgan, L. Sewell, Y. Ji, S. Jones, M.A. Isaacs, A.F. Lee, M. Crocker, Effect of Cu and Sn promotion on the catalytic deoxygenation of model and algal lipids to fuel-like hydrocarbons over supported Ni catalysts, Appl. Catal. B Environ. (2016).
- [63] L.T. Chiam, C.T. Tye, Deoxygenation of plant fatty acid using NiSnK/SiO₂ as catalyst, Malaysian J. Anal. Sci. 17 (2013) 129–138.

- [64] B. Peng, C. Zhao, S. Kasakov, S. Foraita, J.A. Lercher, Manipulating catalytic pathways: Deoxygenation of palmitic acid on multifunctional catalysts, *Chem. - A Eur. J.* 19 (2013) 4732–4741.
- [65] H. Bernas, K. Eränen, I. Simakova, A.R. Leino, K. Kordás, J. Myllyoja, P. Mäki-Arvela, T. Salmi, D.Y. Murzin, Deoxygenation of dodecanoic acid under inert atmosphere, *Fuel*. 89 (2010) 2033–2039.
- [66] M. Snåre, I. Kubičková, P. Mäki-Arvela, D. Chichova, K. Eränen, D.Y. Murzin, Catalytic deoxygenation of unsaturated renewable feedstocks for production of diesel fuel hydrocarbons, *Fuel*. 87 (2008) 933–945.
- [67] I. Kubičková, M. Snåre, K. Eränen, P. Mäki-Arvela, D.Y. Murzin, Hydrocarbons for diesel fuel via decarboxylation of vegetable oils, *Catal. Today*. 106 (2005) 197–200.
- [68] J.G. Immer, M.J. Kelly, H.H. Lamb, Catalytic reaction pathways in liquid-phase deoxygenation of C18 free fatty acids, *Appl. Catal. A Gen.* 375 (2010) 134–139.
- [69] W.F. Maier, W. Roth, I. Thies, P.U. Ragukschleyer, C. Ber, W.F. Maier, W. Roth, I. Thies, P.V.R. Schleyer, *Gas Phase Decarboxylation of Carboxylic Acids*, n.d.
- [70] B. Peng, Y. Yao, C. Zhao, J.A. Lercher, Towards Quantitative Conversion of Microalgae Oil to Diesel-Range Alkanes with Bifunctional Catalysts, *Angew. Chemie*. 124 (2012) 2114–2117.
- [71] J. Lu, S. Behtash, M. Faheem, A. Heyden, Microkinetic modeling of the decarboxylation and decarbonylation of propanoic acid over Pd(1 1 1) model surfaces based on parameters obtained from first principles, *J. Catal.* 305 (2013) 56–66.
- [72] R. Klaewkla, M. Arend, W. F., A Review of Mass Transfer Controlling the Reaction Rate in Heterogeneous Catalytic Systems, *Mass Transf. - Adv. Asp.* (2011).
- [73] A.K. Prajapati, P. Verma, S. Singh, M.K. Mondal, M.R.R. Kooh, Adsorption-Desorption Surface Bindings, Kinetics, and Mass Transfer Behavior of Thermally and Chemically Treated Great Millet Husk towards Cr(VI) Removal from Synthetic Wastewater, *Adsorpt. Sci. Technol.* 2022 (2022).
- [74] M. Malayeri, C.S. Lee, F. Haghghat, L. Klimes, Modeling of gas-phase heterogeneous photocatalytic oxidation reactor in the presence of mass transfer limitation and axial dispersion, *Chem. Eng. J.* 386 (2020) 124013.
- [75] J. P. Gaspard, Physisorption and Chemisorption, *Interfacial Asp. Phase Transform.* 87 (1982) 103–118.
- [76] F. Ding, B.I. Yakobson, Challenges in hydrogen adsorptions: From physisorption to chemisorption, *Front. Phys.* 6 (2011) 142–150.
- [77] F. Huber, J. Berwanger, S. Polesya, S. Mankovsky, H. Ebert, F.J. Giessibl, Chemical bond formation showing a transition from physisorption to chemisorption, *Science* (80-.). 366 (2019) 235–238.
- [78] E. Czepirski, L., Balys, M. R., & Komorowska-Czepirska, Some generalization of Langmuir adsorption isotherm, *J. Chem.* 3 (2000) 1099-8292.
- [79] L. Largette, R. Pasquier, A review of the kinetics adsorption models and their application to the adsorption of lead by an activated carbon, *Chem. Eng. Res. Des.* 109 (2016) 495–504.

- [80] H. Naghibi, A. Tamura, J.M. Sturtevant, Significant discrepancies between van't Hoff and calorimetric enthalpies, *Proc. Natl. Acad. Sci. U. S. A.* 92 (1995) 5597–5599.
- [81] A. Janda, B. Vlasisavljevich, L.C. Lin, B. Smit, A.T. Bell, Effects of Zeolite Structural Confinement on Adsorption Thermodynamics and Reaction Kinetics for Monomolecular Cracking and Dehydrogenation of n-Butane, *J. Am. Chem. Soc.* 138 (2016) 4739–4756.
- [82] M. Žula, M. Grilc, B. Likozar, Hydrocracking, hydrogenation and hydro-deoxygenation of fatty acids, esters and glycerides: Mechanisms, kinetics and transport phenomena, *Chem. Eng. J.* 444 (2022).
- [83] S. Wei, H. He, Y. Cheng, C. Yang, G. Zeng, L. Qiu, Performances, kinetics and mechanisms of catalytic oxidative desulfurization from oils, *RSC Adv.* 6 (2016) 103253–103269.
- [84] S. Zhang, B. Zhang, B. Liu, S. Sun, A review of Mn-containing oxide catalysts for low temperature selective catalytic reduction of NO: X with NH₃: Reaction mechanism and catalyst deactivation, *RSC Adv.* 7 (2017) 26226–26242.
- [85] F. Gao, X. Tang, H. Yi, S. Zhao, C. Li, J. Li, Y. Shi, X. Meng, A review on selective catalytic reduction of NO_x by NH₃ over Mn-based catalysts at low temperatures: Catalysts, mechanisms, kinetics and DFT calculations, 2017.
- [86] T. Aditya, A. Pal, T. Pal, Nitroarene reduction: A trusted model reaction to test nanoparticle catalysts, *Chem. Commun.* 51 (2015) 9410–9431.
- [87] C. Doornkamp, V. Ponec, The universal character of the Mars and Van Krevelen mechanism, *J. Mol. Catal. A Chem.* 162 (2000) 19–32.
- [88] P. Schlexer, A. Ruiz Puigdollers, G. Pacchioni, Role of Metal/Oxide Interfaces in Enhancing the Local Oxide Reducibility, *Top. Catal.* 62 (2019) 1192–1201.
- [89] W. Wang, H. Zhang, S. Zhang, Y. Liu, G. Wang, C. Sun, H. Zhao, Potassium-Ion-Assisted Regeneration of Active Cyano Groups in Carbon Nitride Nanoribbons: Visible-Light-Driven Photocatalytic Nitrogen Reduction, *Angew. Chemie - Int. Ed.* 58 (2019) 16644–16650.
- [90] C.R. Glein, I.R. Gould, E.D. Lorange, H.E. Hartnett, E.L. Shock, Mechanisms of decarboxylation of phenylacetic acids and their sodium salts in water at high temperature and pressure, *Geochim. Cosmochim. Acta.* 269 (2020) 597–621.
- [91] G.C.Q. Da Silva, T.M. Cardozo, G.W. Amarante, C.R.A. Abreu, B.A.C. Horta, Solvent effects on the decarboxylation of trichloroacetic acid: Insights from: Ab initio molecular dynamics simulations, *Phys. Chem. Chem. Phys.* 20 (2018) 21988–21998.
- [92] F.H. Verhoek, The Kinetics of the Decomposition of Trichloroacetates in Ethyl Alcohol, *J. Am. Chem. Soc.* 67 (1945) 1062–1064.
- [93] F.H. Verhoek, The Kinetics of the Decomposition of the Trichloroacetates in Various Solvents, *J. Am. Chem. Soc.* 56 (1934) 571–577.

Chapter 2. On the Mechanism of Catalytic Decarboxylation of Carboxylic Acids on Carbon-Supported Palladium Hydride

The high chemical stability of aliphatic carboxylic acid makes catalytic decarboxylation at low temperatures challenging. We show that arylaliphatic acids (Ar-C_nH_{2n}-COOH, n ≥ 1) decarboxylate on carbon-supported Pd nanoparticles (Pd/C) at 90 °C with 100% selectivity. In situ XANES during decarboxylation of pre-adsorbed substrates indicates that the active phase is α -phase palladium hydride (α -PdH_x). The reaction rate is enhanced by one order of magnitude when hydrogen is pre-adsorbed. Tracing deuterium labeling positions, it is concluded that carboxylic acid (Ar-C_nH_{2n}-COOH) undergoes an α -C–H bond dissociation on the Pd surface to the Ar-(CH₂)_{n-1}-CH*–COO* intermediate in the first step, followed by the C–COO scission, and finally, Ar-(CH₂)_{n-1}-CH* reacts with two sorbed H to produce Ar-(CH₂)_{n-1}-CH₃. The high rates are related to the concentration of hydride present on the catalyst particles to complete the catalytic cycle in a Mars–van Krevelen-type mechanism and the rate of H/D exchange at the α -C–H position.

This chapter is based on the article: On the Mechanism of Catalytic Decarboxylation of Carboxylic Acids on Carbon Supported Palladium Hydride, *ACS Catalysis*, (2021) 14625–14634.

2.1 Introduction

Carboxylic acids are abundant and inexpensive substrates that are available both from natural and synthetic sources. They have emerged as promising starting materials for catalytic transformations to hydrocarbon fuels and high-value pharmaceutical intermediates. [1] Direct decarboxylation of carboxylic acids is an efficient way to achieve the elimination of the COOH functional group by carbon-carbon bond cleavage to release 1 equiv of CO₂ along with the formation of the corresponding product. However, methods available for decarboxylation are mostly dedicated to acid substrates with functional groups adjacent to the reactive carbon,[2-4] while un-functionalized acids, i.e., aliphatic carboxylic acids, usually need severe reaction conditions including elevated temperature (≥ 250 °C) and high H₂ pressure (≥ 1 MPa)[5-11] or prior modification with a stoichiometric reagent.[12-14]

Transition metal-based catalysts such as Pd, [5, 6, 15-17] Ni, [7, 18, 19] Pt, [8-10] and Ru [11, 20] were used as heterogeneous catalysts for the elimination of carboxylic groups of aliphatic acids. Even on these catalysts, the reaction tends to proceed dominantly via decarbonylation after OH elimination ($-\text{H}_2\text{O}-\text{CO}$) rather than direct decarboxylation ($-\text{CO}_2$). The high chemical stability of alkyl carboxylic acid challenges the development of effective heterogeneous catalysts active at low temperatures for the decarboxylation of aliphatic carboxylic acid.

In principle, H₂ is not involved in stoichiometric decarboxylation ($\text{R}-\text{COOH} \rightarrow \text{R}-\text{H}+\text{CO}_2$). Several groups, however, have reported that H₂ is not inert for the reaction. For Pd/C-catalyzed stearic acid decarboxylation, for example, co-feeding of H₂ (25%) and N₂ (75%) was critical to achieve stability, because H₂ was required to accelerate the desorption of products and inhibited aromatization, deactivating the catalyst.[21,22] Also, Maier et al. reported elimination of the carboxylic group of octanoic acid to n-heptane on Pd/C in a H₂ flow, while it hardly reacted in N₂. [23] This leads to the hypothesis that the active phase may not be Pd but rather palladium hydride (PdH_x). However, neither the existence of PdH_x nor its role has been investigated [23]. In this chapter, we report that aryl-substituted aliphatic carboxylic acid ($\text{Ar}-\text{C}_n\text{H}_{2n}-\text{COOH}$, $n \geq 1$) decarboxylates on hydrogen-pretreated Pd supported on carbon (Pd/C) under relatively mild conditions (150 °C, 10 bar N₂, with a TOF (turnover frequency) of 54 h⁻¹). Combining detailed kinetic investigations with isotope labeling and tracing, in situ X-ray absorption near-edge structure (XANES), and temperature-programmed surface reaction (TPSR), the active sites, the role of hydrogen, and the reaction mechanism of arylaliphatic carboxylic acid decarboxylation have been investigated. We show that on metallic Pd, the most

challenging step is not the cleavage of the C–COO bond, as conventionally argued, but the hydrogen addition to the phenyl-alkyl group (Ar-C_nH_{2n}^{*}), forming phenyl-alkane (Ar-C_nH_{2n+1}). On PdH_x, a high concentration of the surface or subsurface hydrogen facilitates this step, thus leading to a higher rate.

2.2 Experimental method

2.2.1 Chemicals and Materials

All chemicals were purchased from Sigma-Aldrich and used without further purification: hydrocinnamic acid (≥99.0%), benzoic acid (≥99.0%), 2-phenylacetic acid (≥99.0%), 4-phenylbutyric acid (≥99.0%), 5-phenylvaleric acid (≥99.0%), 3-cyclohexylpropionic acid (≥99.0%), n-dodecane, n-hexane, and D₂O. Deuterium gas was also purchased from Sigma-Aldrich.

Pd/C catalyst (5 wt. %) was purchased from Sigma-Aldrich. It has a Pd dispersion of 19%, determined by H₂-chemisorption, corresponding to an average-sized of 5.9 nm. The specific surface area is 1236 m²/g, determined by N₂ adsorption–desorption based on the Brunauer–Emmett–Teller (BET) analysis method and Barrett–Joyner–Halenda (BJH) model. The detailed H₂ chemisorption and N₂ adsorption profiles are shown in **Figure A 2-1**. There is hardly loss of Pd during the reaction as the Pd loading values of fresh and spent catalysts are 4.83 ± 0.05 and 4.76 ± 0.05 wt. % (measured by atomic absorption spectroscopy (AAS)), respectively.

2.2.2 Catalyst Characterizations

2.2.2.1 N₂-physisorption

The surface area of the catalysts was determined by N₂ adsorption at 77 K on a PMI automated BET sorptometer. Before measurements, the samples were outgassed at 523 K for 2 h.

2.2.2.2 Atomic absorption spectroscopy

Atomic absorption spectroscopy (AAS) was employed to analyze Pd content in catalysts with a UNICAM 939 AA-Spectrometer.

2.2.2.3 H₂-Chemisorption

The dispersion of Pd was determined by H₂ chemisorption. Pd/C was pretreated under vacuum at 588 K for 1 h and then cooled to 313 K. The first hydrogen adsorption isotherm was measured at 1–40 kPa H₂. Afterward, the sample was outgassed at 313 K for 1 h and a second set of isotherms was measured. The concentrations of chemisorbed H₂ on the metal were determined by extrapolating the difference isotherm of the two to zero hydrogen pressure. The dispersion of Pd was estimated from the concentration of chemisorbed H₂, assuming a stoichiometry of 1:1 metal to hydrogen atoms.

2.2.2.4 X-ray absorption near-edge structure

X-ray absorption near-edge structure (XANES) measurements were performed at the Munich Compact Light Source (MuCLS) of Technical University of Munich (**Figure A 2-2**), which is a miniature synchrotron facility.[41] The experimental setup is shown in **Figure A 2-2b**. The X-ray source energy was tuned to 25 keV configuration with a bandwidth of ~4%. Test samples were mixed with BN and then pressed to a powdered pellet of 13 mm diameter. Sample pellets were placed in a home-designed reaction cell with two Kapton windows on both sides so that X-rays can pass through. The reaction cell was equipped with heating wire as well as gas flow, therefore allowing in situ measurements under specific conditions.

2.2.3 Catalytic Reactions

2.2.3.1 Batch Reaction

Catalytic conversions of arylaliphatic carboxylic acids were performed in a high-pressure stainless-steel autoclave (300 mL) with a mechanical agitator. In a typical experiment, 100 mg of catalyst, 80 mL of alkane solvent (n-dodecane or n-hexane), and 5.3 mmol of substrates were added into the autoclave and purged with N₂ three times to remove any presence of air, and afterward, a specific pressurized reaction gas (H₂ or N₂ varied from 1 bar to 60 bar) was introduced into the autoclave at room temperature. The autoclave was then rapidly heated to the desired temperature (150 to 300 °C) by a heating jacket. Samples of the liquid phase in each experiment were continuously taken through a sampling tube with a filter at certain intervals. The stirring rate was kept at 600 r/min during the reaction. For some of the reactions, the Pd/C catalyst was first pretreated under certain conditions before adding the substrate. The pretreatment processes were described as follows: 100 mg of Pd/C catalyst was first dispersed in 80 mL of solvent in the autoclave, and then the reactor was purged with H₂ of different

pressures at a certain temperature for 30 min. After pretreatment, the reactor was cooled down to room temperature, and substrate acid was added to the reactor, then purged with 10 bar N₂, and reacted at a certain temperature.

The product solution was analyzed by gas chromatography (Shimadzu GC 2010) equipped with an HP-5 Agilent column (30.0 m × 0.25 μm) and gas chromatography–mass spectrometry (Agilent, GC–MS 2010) equipped with an HP-5 Agilent column (30.0 m × 0.25 μm). N-Decane was used as an internal standard. Products in the gas phase were collected by a gasbag and analyzed by a mass spectrometer (OmniStar Gas analysis system).

2.2.3.2 Deuterium Substitution Reaction

The deuterium substitution reaction was also conducted in the high-pressure stainless-steel autoclave (300 mL). One hundred milligrams of catalyst was first dispersed in 80 mL of solvent (n-hexane) in the autoclave and pretreated with 1 bar deuterium (D₂) under 150 °C for 30 min. After the pretreatment, the mixture was cooled to room temperature and 0.53 mmol of substrate was then added, purged, and pressurized with N₂ to 10 bar at room temperature. Then, the autoclave was rapidly heated to 100 or 200 °C for the substitution reaction. Liquid samples were collected at a different time during the reaction and analyzed by GC–MS. After the reaction, the component in the solution was extracted with D₂O and characterized by the ¹H NMR spectra. The deuterium substitution results were obtained based on the GC–MS results and ¹H NMR spectra according to Liu *et al.*'s research. [37]

2.2.3.3 Temperature-Programmed Surface Reaction (TPSR) with In Situ XANES. Temperature-programmed

Temperature-programmed surface reaction (TPSR) was applied in a homemade reaction cell (**Figure A 2-3**) equipped with heating wire, gas flow, and two windows on both sides for the X-ray beam. The gas outlet connects to a mass spectrometer to detect the formed gaseous products. The Pd/C catalyst was well mixed with BN and pressed to a wafer of 13 mm diameter. The prepared wafer was then placed in the sample holder of the reaction cell. In this cell, the wafer was first pretreated under selected conditions and cooled down to room temperature. Then, the sealed reaction cell together with the pretreated sample inside was put into a glove box with N₂ protection. In the glove box, a certain amount of 2- phenylacetic acid/n-hexane solution was preadsorbed to the wafer with N₂ protection for the temperature-programmed surface reaction.

In situ XANES with TPSR was applied in the homemade reaction cell with a sample wafer preadsorbed with 2- phenylacetic acid inside. The continuous in situ XANES spectra were collected while progressively increasing the temperature of the cell, and the online MS results of 2- phenylacetic acid decarboxylation were measured at the same time.

2.3 Results and Discussion

2.3.1 On the Role of the Reaction Atmosphere for the Conversion of Hydrocinnamic Acid

In the first step, hydrocinnamic acid (3-phenylpropionic acid) in n-dodecane was catalytically converted on Pd/C under H₂ and N₂.

Figure 2-1a shows the reaction at a high temperature (300 °C) and high pressure of H₂ (20 bar), in analogy to the widely reported approach to eliminate the carboxylic group developed for fatty acids. [24,25] Already during the temperature increase to 300 °C, the arene ring of hydrocinnamic acid was rapidly saturated such that 98% 3-cyclohexylpropionic acid was present as the final temperature was reached. Subsequently, the concentration of 3-cyclohexylpropionic acid gradually decreased as ethyl- cyclohexane was formed. The gas-phase product was mainly CO₂, indicating that ethylcyclohexane is generated by decarboxylation of 3-cyclohexylpropionic acid. Using 3-cyclohexylpropionic acid directly as a substrate led to nearly identical results (**Figure A 2-4**).

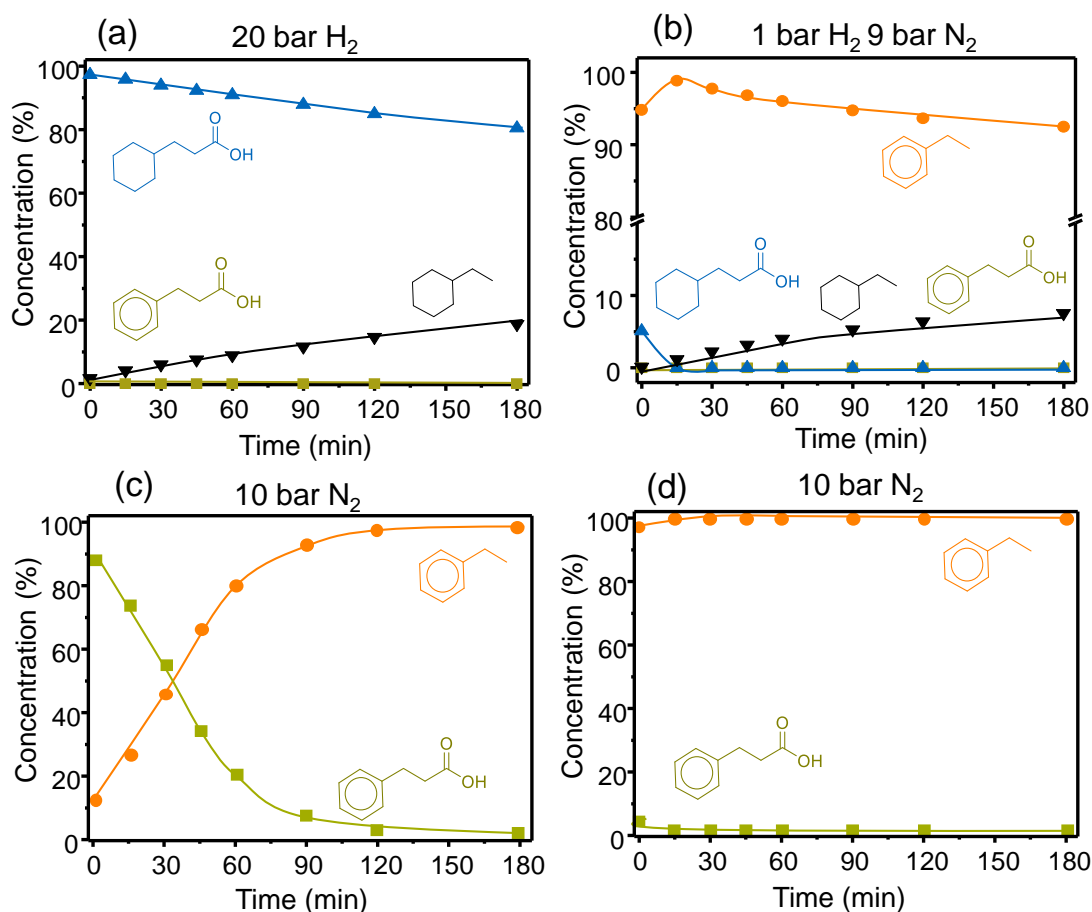


Figure 2-1. Concentrations of products and reactant as a function of time in the reaction of hydrocinnamic acid on Pd/C under different conditions: **(a)** 20 bar H₂, **(b)** 1 bar H₂ and 9 bar N₂, **(c)** 10 bar N₂, and **(d)** Pd/C pretreated under 1 bar H₂ at 25 °C for 30 min and then reacted in 10 bar N₂ (100 mg of Pd/C, 80 mL of n-dodecane as the solvent, reacted at 300 °C).

Under a lower (1 bar) H₂ pressure, ethylbenzene was the main product with a yield of 92.5% after 3 h (**Figure 2-1b**). Ethylcyclohexane increased slowly as a minor product, reaching a yield of 7.3% after 3 h. The sequence of products suggests that ethylbenzene was hydrogenated to ethyl- cyclohexane at a slow rate.

If the reaction was carried out in a N₂ atmosphere above hydrocinnamic acid in n-dodecane, hydrocinnamic acid was selectively converted to ethylbenzene with a TOF of 258 h⁻¹ (**Figure 2-1c**). Also, in this case, CO₂ was the main gas-phase product. The rate of this decarboxylation reaction was, however, significantly higher if Pd/C was pretreated under 1 bar H₂ at 25 °C for 30 min in the autoclave prior to the addition of hydrocinnamic acid. With the H₂-pretreated Pd/C, the decarboxylation to ethylbenzene was already complete when the temperature reached 300 °C (**Figure 2-1d**). Even upon decreasing the reaction temperature to 150 °C, this H₂-

pretreated catalyst still showed a reaction TOF of 54 h⁻¹, contrasted by less than 0.1 h⁻¹ for the catalyst without H₂ pretreatment.

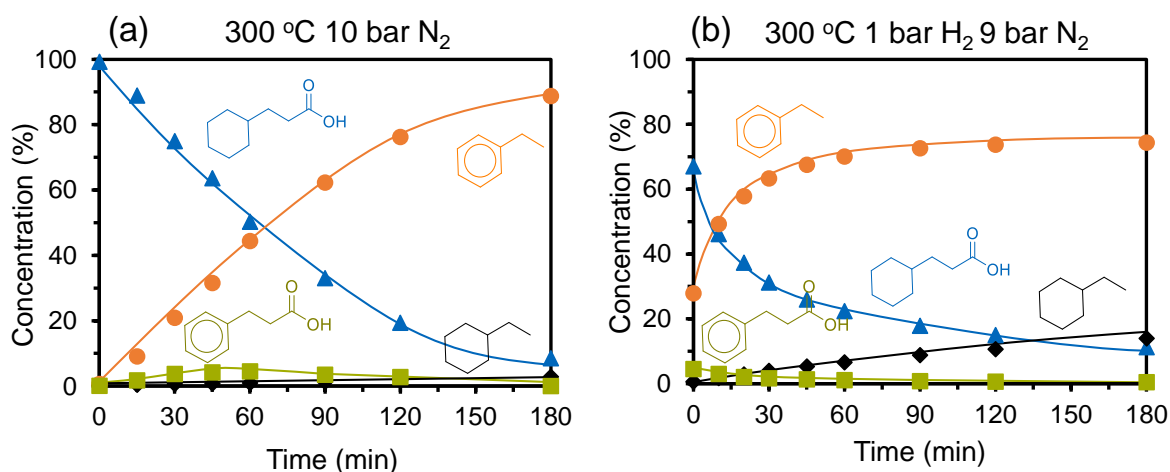
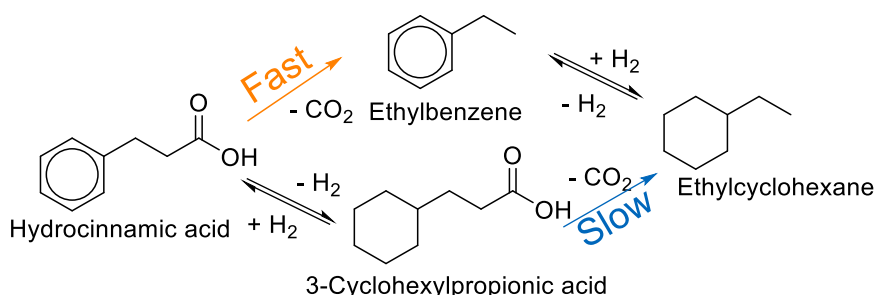


Figure 2-2. Concentrations of products and reactant as a function of time in the reaction of 3-cyclohexylpropionic acid on Pd/C. (a) Reaction conditions: 100 mg of Pd/C, 80 mL of n-dodecane as the solvent, 5.3 mmol of 3-cyclohexylpropionic acid, reacted at 300 °C, 10 bar N₂. (b) Reaction conditions: 100 mg of Pd/C, 80 mL of n-dodecane as the solvent, 5.3 mmol of 3-cyclohexylpropionic acid, reacted at 300 °C, 1 bar H₂ and 9 bar N₂.

To further investigate the pathways of hydrocinnamic acid conversion on Pd/C, one of the intermediates, 3-cyclohexylpropionic acid, was used as a substrate and reacted under H₂ or N₂ at 300 °C. In a N₂ atmosphere (**Figure 2-2a**), the main product was not ethylcyclohexane (only 3% yield after 3 h of reaction) but ethylbenzene, which was generated rapidly and reached 89% yield after 3 h. Very small concentrations of hydrocinnamic acid (<5%) were also detected, although decreasing further slowly with reaction time. Ethylcyclohexane appeared with a very low rate that had only 3% yield after 3 h. This result shows that 3-cyclohexylpropionic acid rapidly dehydrogenates to hydrocinnamic acid, followed by decarboxylation to ethylbenzene, whereas decarboxylation to ethylcyclohexane is very slow. When introducing 1 bar H₂ into the reactor (**Figure 2-2b**), the evolution sequence of products was unchanged, but ethylbenzene increased rapidly at the beginning and reached a constant level of 73% yield after 90 min, while the formation rate of ethylcyclohexane was five times higher than that in the 10 bar N₂ condition shown in **Figure 2-2a**. Since the ratio of hydrocinnamic acid to 3-cyclohexylpropionic acid approached a constant value of 0.04 (**Figure A 2-5**), we conclude that a quasi-equilibrium of hydrogenation and dehydrogenation of the arene ring in these two molecules has been achieved.

Ethylcyclohexane was produced mainly from the hydrogenation of ethylbenzene (TOF = 18 h⁻¹) and partially from direct decarboxylation of 3-cyclohexylpropionic acid (TOF = 3.0 h⁻¹).



Scheme 2-1. Reaction Pathways of Hydrocinnamic Acid on the Pd/C Catalyst.

These results lead to establishing the general reaction pathways for decarboxylation of hydrocinnamic acid depicted in **Scheme 2-1**. Two parallel reaction pathways exist on Pd/C depending on prominence on the reaction conditions. One pathway starts with reversible arene ring saturation of hydrocinnamic acid to 3-cyclohexylpropionic acid, decarboxylating subsequently to ethylcyclohexane. The other faster pathway is the direct decarboxylation of hydrocinnamic acid to ethylbenzene that is hydrogenated further to ethylcyclohexane reversibly.

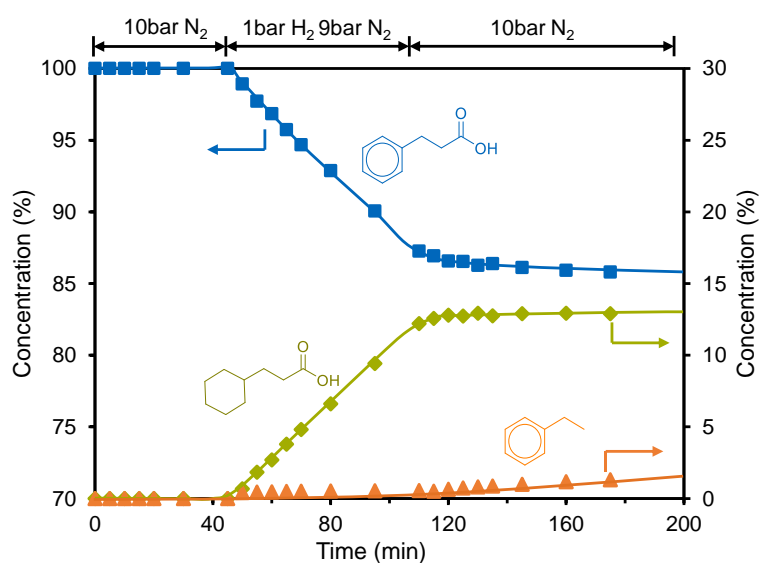


Figure 2-3. Concentrations of hydrocinnamic acid and products as a function of time on Pd/C in different gas atmospheres. Reaction conditions: 100 mg of Pd/C catalyst, 80 mL of n-dodecane as the solvent, 5.3 mmol of hydrocinnamic acid, reacted at 150 °C.

The impact of the presence of H₂ on the two reaction pathways for conversion is shown in **Figure 2-3**. While in the absence of H₂, hydrocinnamic acid almost did not react at 150 °C, introducing 1 bar H₂ led to the hydrogenation of the arene ring (TOF = 62 h⁻¹). In parallel, a

small amount of ethylbenzene was detected (TOF = 1.0 h⁻¹). When changing the atmosphere back to 10 bar N₂, the hydrogenation of the arene ring nearly stopped, but the decarboxylation increased moderately (TOF = 5.0 h⁻¹). This indicates that the catalytic activity for the decarboxylation of hydrocinnamic acid was promoted by short exposure to H₂; however, the presence of excess H₂ inhibited the decarboxylation.

2.3.2 Identification of the Catalytic Active Species on Pd/C for the Decarboxylation Reaction.

Having shown that the catalytic activity of Pd/C for decarboxylation of hydrocinnamic acid is positively influenced by H₂, let us address the active species of Pd that are formed after being exposed to H₂. In general, two types of impact of the exposure to H₂ may exist, i.e., one is that H₂ partially reduces oxidized PdO to metallic Pd, and the other is that Pd reacts with H₂ to form Pd hydride (PdH_x) species.[26,27] To better understand the relation between the nature of the palladium site and the catalytic performance, different pretreatments have been compared.

2.3.2.1 H₂ Pretreatment of Pd/C.

Table 2-1. Influence of Pretreatment Conditions on the Decarboxylation Activity of Hydrocinnamic Acid on Pd/C^a

Entry		H ₂ pressure [bar]	Time [min]	TOF [h ⁻¹]
1		(no pretreatment)		47
2		1	30	844
3		1	60	887
4		10	30	854
5		50	30	867
6 ^b (Two steps)	(1st step)	1	30	207
	(2nd step)	1 (N ₂)	30	
7 ^c	Activated carbon	1	30	288

^a: 100 mg of Pd/C and 80 mL of n-dodecane as the solvent. The pretreatment temperature was 150 °C for all entries. Hydrocinnamic acid (5.3 mmol) was fed into the reactor after pretreatment. Reaction conditions: 200 °C and 10 bar N₂. ^b The Pd/C catalyst was first pretreated with 1 bar H₂ at 150 °C for 30 min (1st step), and then the gas phase was changed to 1 bar N₂ for another 30 min of treatment (2nd step). ^c 100 mg of activated carbon was dispersed in the solvent and pretreated with 1 bar H₂ at 150 °C for 30 min, and then hydrocinnamic acid and 100 mg of unpretreated Pd/C were added into the reactor for reaction at 200 °C and 10 bar N₂.

Table 2-1 compiles the rates normalized to accessible Pd for decarboxylation of hydrocinnamic acid on Pd/C at 200 °C after pretreatment in H₂. After exposure in 1 bar H₂ (entry 2), a much higher rate (TOF = 844 h⁻¹) was observed than without H₂ pretreatment (entry 1, TOF = 47 h⁻¹). Prolonging the pretreatment time (entry 3) or increasing H₂ pressure (entries 4 and 5) did not lead to higher activity. However, eliminating the external H₂ by purging with N₂ at 150 °C for 30 min led to a TOF that was about a fourth of the value after being only exposed to H₂ (entry 6). Moreover, H₂-pretreated activated carbon together with an unpretreated Pd/C catalyst showed a decarboxylation TOF of 288 h⁻¹ (entry 7). These values suggest that after reduction of PdO to metallic Pd, PdH_x may subsequently form in the presence of H₂. The low TOF after sequential H₂ and N₂ exposure (entry 6) is attributed to PdH_x being depleted in H. H₂ adsorbed on a carbon support can also serve to produce PdH_x with Pd; however, this route is less efficient than direct treatment under H₂ gas.

It is hypothesized that the residual amount of H on the catalyst is lowered or PdH_x is decomposed and metallic Pd is formed in the absence of H₂ and at a high temperature.[26,28] PdO can be completely reduced to Pd under 25 °C and 1 bar H₂, and a change in the particle size caused by the treatment can be excluded, as changes in the Pd particle size were reported negligible below 300 °C.[29,30] Therefore, we hypothesize that the H₂ pretreatment reduces (the surface) PdO species to metallic Pd and forms PdH_x.

Intermediates from decarboxylation may oligomerize further and strongly adsorb and accumulate on active sites. Note that the hydrogen on/in Pd and that dissolved in n-dodecane will limit the probability of oligomerization by reducing the lifetime of reactive intermediates. [5, 31]

2.3.2.2 Temperature-Programmed Surface Reaction (TPSR) in Combination with In Situ XANES.

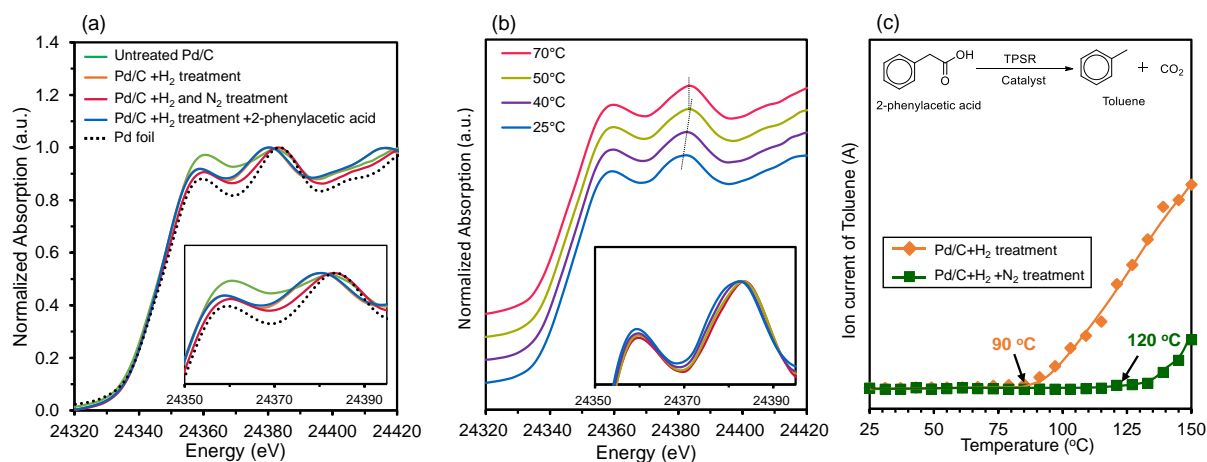


Figure 2-4. (a) Normalized Pd K-edge XANES spectra of the Pd/C catalyst after different treatments. The spectra were collected at room temperature, and the maximum value of spectra was normalized to 1 (the inset shows the enlarged spectra from 24,350 to 24,395 eV). (b) Normalized Pd K-edge in situ XANES spectra of the Pd species at 25, 40, 50, and 70 °C in a TPSR process; the detailed continuously collected spectra are presented in **Figure A 2-6**. The inset shows the comparison of four XANES spectra without shifting the spectra vertically. (c) Rate of toluene formation in the decarboxylation of preadsorbed 2-phenylacetic acid on Pd/C with different pretreatments with programmed increasing temperature, i.e., temperature-programmed surface reaction (TPSR). Orange curve: Pd/C pretreated at 150 °C for 30 min in a H₂ flow (30 mL/min) and cooled down to the room temperature in a H₂ flow; green curve: Pd/C first pretreated in a H₂ flow (30 mL/min) at 150 °C for 30 min, then switched to N₂ (30 mL/min) flow for 30 min, and cooled down to room temperature in a N₂ flow. After pretreatment, 2-phenylacetic acid preadsorption was conducted in the glove box (temperature ramping rate for the TPSR reaction: 0.5 °C/min from 25 to 40 °C, 0.2 °C/min from 40 to 50 °C, and 2 °C/min from 50 to 150 °C). (a,b): Reproduced with permission from ref [36]. Copyright 2021 Royal Society of Chemistry.

To further characterize the active sites, Pd/C was investigated during the temperature-programmed surface reaction (TPSR) of pre-adsorbed 2-phenylacetic acid by XANES. **Figure 2-4a** shows Pd K-edge XANES of Pd/C samples after different pretreatments and the XANES spectrum of a Pd foil as a reference. Compared to the Pd foil, the spectrum of untreated Pd/C has two characteristic peaks at 24,360 and 24,383 eV, the peak positions of which are similar to the reference spectrum of metallic Pd, [32, 33] but the intensity of the first peak is rather different. The spectrum difference between untreated Pd/C and Pd foil reference was due to the partial oxidation of the Pd/C powders in air. After H₂ pretreatment, the absorption edge and the first two peaks shifted to lower energy, and the intensity of the peak at 24,360 eV increased relative to the intensity of the peak at 24,384 eV compared to the Pd foil, i.e., characteristic of

the formation of PdH_x. [34, 35] After pre-adsorbing 2-phenylacetic acid on this PdH_x sample, its spectrum was hardly changed, indicating that the PdH_x species were maintained after adsorbing 2-phenylacetic acid at ambient temperature. The spectrum of Pd/C pretreated sequentially with H₂ and N₂ indicates a strong depletion in H, as the shape and peak positions of its spectrum are in good agreement with those of reference Pd at ambient temperature. The results of XANES in **Figure 2-4a** echo the results from **Table 2-1**, indicating that H₂ pretreatment forms a PdH_x species (entry 2), while subsequent N₂ treatment leads to its decomposition or marked depletion in H (entry 6).

To investigate whether PdH_x are maintained under decarboxylation conditions, the in situ XANES spectra were collected during the temperature increase. In **Figure 2-4b** and **Figure A 2-6**, the spectra of the H₂-pretreated Pd/C (PdH_x) with sorbed 2-phenylacetic acid had no apparent change at room temperature but slowly shifted to higher energy as the temperature increased from room temperature to 50 °C and finally almost overlapped with the spectrum of metallic Pd at 50 °C and without changing when further increasing the temperature, indicating that the PdH_x of Pd/C is stable under mild conditions but begins decomposing when ramping up the temperature and finally transfers to metallic Pd or hydride with very low hydride species (α -PdH_x) at around 50 °C in a N₂ atmosphere. The decarboxylation product of 2-phenylacetic acid, toluene, was detected in the gas phase only when further increasing the reaction temperature above 90 °C (**Figure 2-4c**, orange curve). For comparison, the same TPSR process was applied to the Pd/C catalyst pretreated sequentially with H₂ and N₂ samples, which exhibited a metallic Pd species after the treatment. The TPSR result (**Figure 2-4c**, green curve) shows that the decarboxylation reaction started at above 120 °C, which is 30 °C higher than the H₂-pretreated Pd/C.

These results allow us to conclude that the metallic Pd is capable of catalyzing the decarboxylation; however, the activity is much lower than the counterpart after H₂ treatment. The H₂-pretreated Pd/C is concluded to be an α -PdH_x species as the small amount of hydrogen of α -PdH_x can occupy the free space in the palladium lattice without swelling; [32] thus, the spectral shape of α -PdH_x highly resembles that of metallic Pd. The higher activity of H₂-pretreated Pd/C is attributed to the promotion of decarboxylation by residual-incorporated H.

2.3.2.3 Influence of different metal species.

In addition to palladium catalysts, the decarboxylation of hydrocinnamic acid was also investigated by using several noble and non-noble metal-based catalysts such as Cu, Ni, Pt, and

Rh, which are the active metals for the conversion of carboxylic acids and their derivatives to hydrocarbons. Among the mentioned metal species, Pd, Cu and Ni can form metal-hydride complex under certain conditions, but only H₂ pretreated Pd/C catalyst, as shown in **Table A 2-1**, illustrated an extremely high catalytic performance as TOF is 54 h⁻¹, this result can be ascribed to the applied conditions are not suitable for copper and nickel to form hydride complexes, or this reaction conditions are not suitable for the carboxylic acid conversion on these catalysts. In addition, Pt/C and Rh/C catalysts, which cannot form hydride complex, have lower TOFs compared to Pd/C catalysts, owing to the metallic Pt and Rh themselves have the relatively low decarboxylative ability.

2.3.3 Role of PdH_x in the Mechanism of Decarboxylation

The decarboxylation rates of arylaliphatic carboxylic acids with varying side chain lengths and 3-cyclohexylpropionic acid are compiled in **Figure 2-5**. Pd/C exposed to H₂ was capable of catalyzing the decarboxylation of several arylaliphatic carboxylic acids.

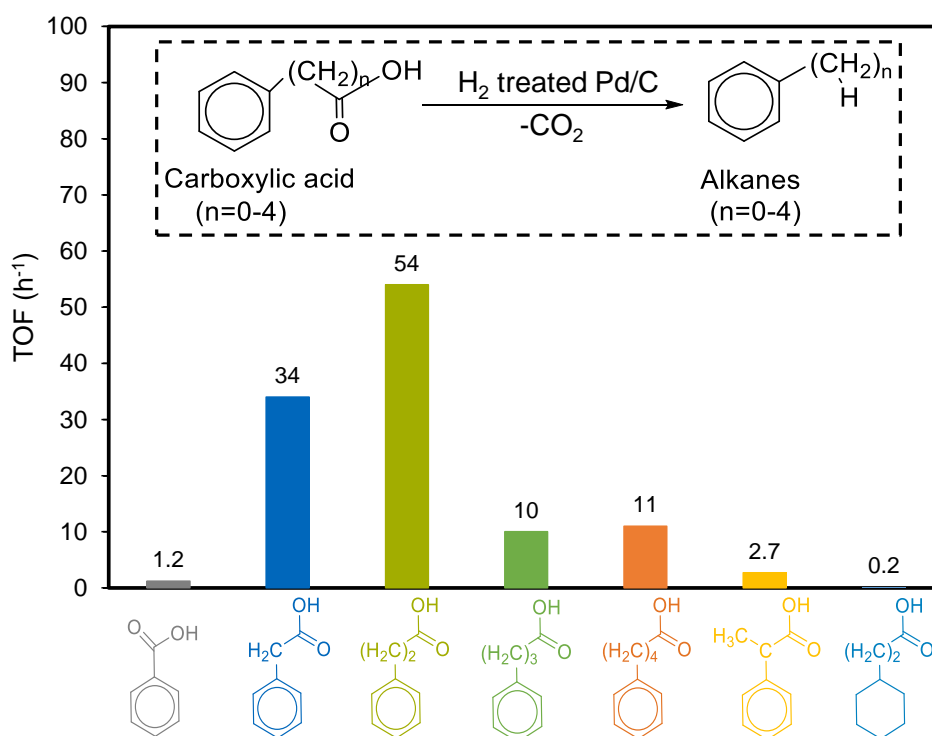


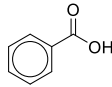
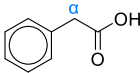
Figure 2-5. Decarboxylation of arylaliphatic carboxylic acids with different side chain lengths and 3-cyclohexylpropionic acid on a H₂- pretreated Pd/C catalyst.

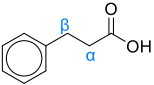
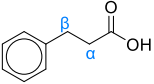
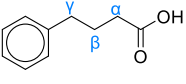
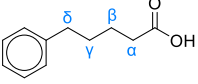
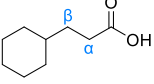
Reaction conditions: 100 mg of Pd/C catalyst pretreated at 150 °C and 1 bar H₂ for 30 min, 80 mL of n-hexane as the solvent, 5.3 mmol of carboxylic acid, reacted at 150 °C, 10 bar N₂.

However, the reaction rates depend on the length of branch carbon chains and the presence of the arene ring. Among the studied carboxylic acids, hydrocinnamic acid with two methylene groups between the arene ring and the carboxylic acid group had the highest decarboxylation activity (TOF = 54 h⁻¹), and 2-phenylacetic acid had a comparable TOF of 34 h⁻¹ with hydrocinnamic acid. Benzoic acid, having the carboxylic acid group directly connected with the arene ring, had the lowest decarboxylation TOF of 1.2 h⁻¹, which was caused by the *p*- π conjugated effect of the arene ring and carboxylic group, strengthening the arene C(sp²)-COO bond. In addition, the TOF of 3-cyclohexylpropionic acid lacking an aromatic group was only 0.2 h⁻¹, indicating that the presence of an arene ring is critical for the decarboxylation on Pd/C.

To investigate the reason for the variations in the reaction rate and, in particular, whether this property relates to the H₂ pretreatment of Pd, we used D₂-pretreated Pd/C to catalyze the reactions. The reaction temperature was chosen at 100 °C because the catalyst showed activity starting from 90 °C in the TPSR test (**Figure 2-4c, orange curve**). However, the decarboxylation rate at 100 °C in the liquid–solid reaction system was very low, showing less than 1% conversion after 6 h. However, a substantial substitution of C–H with C–D was observed, indicating an activation of the C–H bonds under these conditions. For example, the mass spectrometry (MS) spectra (**Figure A 2-7a**) of unconverted hydrocinnamic acid after 0.5 h of reaction showed an increase in molecular weight from 150.1 g/mol to 151.1 g/mol, and its ¹H NMR spectrum showed that the H atom ratio from ortho plus para and meta positions of the arene ring and α -C–H and β -C–H of the hydrocinnamic acid changed from 1:1.5:1:1 to 1:1.5:0.66:0.66. This indicates that 0.61 out of 2 of the α - and β -C–H groups was partly substituted to the C–D group by the D atoms preadsorbed on Pd/C (**Table 2-2, entry 3**).

Table 2-2. Distribution of substituted D atoms in unconverted carboxylic acids after reaction on D₂ pretreated Pd/C^a

Entry	Substrate	Reaction time [min]	Substituted D atom numbers ^b				
			Arene ring	α	β	Γ	δ
1		60	0	-	-	-	-
2		60	0.28	0.42	-	-	-

3		30	0	0.61	0.61	-	-
4		60	0.39	1.02	1.02	-	-
5		60	0.05	0.29	0.43	0.41	-
6		60	0.02	0.28	0.46	0.46	0.45
7		60	0	0	0	-	-

^a Reaction conditions: 100 mg of Pd/C catalyst pretreated at 150 °C and 1 bar D₂ for 30 min, 80 mL of n-hexane as the solvent, 0.53 mmol of carboxylic acid, reacted at 100 °C, 10 bar N₂ for a certain time. ^b Substituted D atom numbers were calculated from GC-MS and ¹H NMR results based on Liu *et al.*'s research [37].

Prolonging the reaction time to 1 h, 1.02 out of 2 of the α - and β -C-H groups was converted to C-D, and 0.39 out of 5 of aromatic C-H was also substituted (**Table 2-2**, entry 4). The reaction results of other acids are summarized in **Table 2-2**. Except for benzoic acid, all the C-H of alkyl side chains in the arylaliphatic carboxylic acids were substituted with C-D to different degrees. The substitution rate on the alkyl chains was higher than that on the arene ring. For hydrocinnamic acid, the α -C-H had the same substitution rate as β -C-H, whereas for 4-phenylbutyric acid and 5-phenylpentanoic acid, the α -C-H had a lower substitution rate than the other C-H, which is attributed to the negative inductive effect of the arene ring, helping in stabilizing the Ar-(CH₂)_n-CH*-COO* intermediate. The inductive effect decreases with the carbon chain. Moreover, when further increasing the D-substitution reaction temperature to 200 °C, the hydrocinnamic acid fully converted to ethylbenzene. Substituted ethylbenzenes with up to 4D atoms were identified, with an average 2D substitution (**Figure A 2-7b**). Excluding the D-substitution of ethylbenzene itself on PdD_x (**Figure A 2-7b**), it is concluded that a hydrocinnamic acid molecule has undergone several C-H/C-D substitutions on PdD_x before a single turnover of C-COO bond cleavage. Interestingly, 3-cyclohexylpropionic acid did not show substitution of C-H and had the lowest decarboxylation activity, indicating that the presence of the arene ring is critical for decarboxylation. The high reactivity of hydrocinnamic acid is concluded to be induced by the negative inductive effect of the arene ring on the adjacent -CH₂- groups, stabilizing the Ar-(CH₂)_n-CH*-COO* intermediate.

According to Sajiki et al. [38] who showed the Pd-catalyzed regioselective deuteration at the benzylic position of different organic compounds, the C–H to C–D substitution occurs first at the benzylic site of 4-phenylbutyric acid, and the nonbenzylic position(s) of the alkyl side chain and arene ring itself further deuterated in sequence at a longer time or higher temperatures. [38]

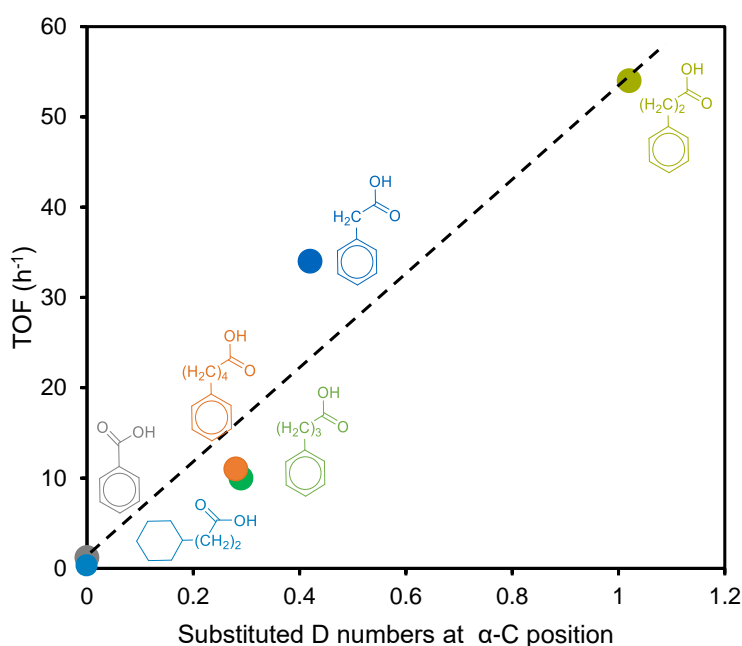


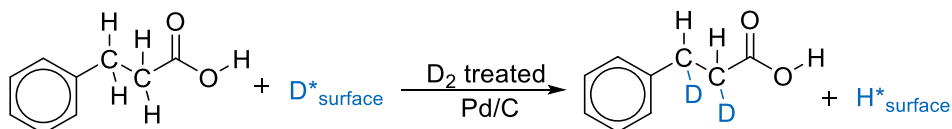
Figure 2-6. Decarboxylation rate of carboxylic acids as a function of the substituted D atom numbers at the α -C position.

(Reaction conditions: (1) For decarboxylation reaction: 100 mg of Pd/C catalyst dispersed in 80 mL of n-hexane and pretreated at 150 °C and 1 bar H₂ for 30 min, 5.3 mmol of carboxylic acid, reacted at 150 °C, 10 bar N₂. (2) For D₂ substitution: 100 mg of Pd/C catalyst dispersed in 80 mL of n-hexane and pretreated at 150 °C and 1 bar D₂ for 30 min, 80 mL of n-hexane as solvent, 0.53 mmol of carboxylic acid, reacted at 100 °C, 10 bar N₂ for 60 min.)

The fraction of D substituted on α -C linearly correlated with the decarboxylation rate (**Figure 2-6**). This positive correlation indicates that the dissociation of α -C–H bonds on PdH_x is an important step prior to the cleavage of the α -C–COO bond. This is further supported by the decarboxylation of 2-phenylpropionic acid, which has only one α -C–H group (**Figure A 2-8**). Its TOF was only 2.7 h⁻¹, which was one order of magnitude lower than that of 2-phenylacetic acid. This result suggests that carboxylic acids with fewer α -C–H groups available for activation will lead to lower decarboxylation rates under identical experimental conditions. However, the observed decrease exceeds the lower statistical availability of α -C–H, implying that the activity of the α -C*–COO* group positively correlates with the decarboxylation rate.

However, also C–H bonds in the arene ring were regioselectively converted into C–D bonds. Only the C–H bonds at meta positions of the arene ring of 2-phenylacetic acid and hydrocinnamic acid were substituted, whereas C–H bonds at ortho and para positions were not observed (**Table A 2-2**). This is attributed to the negative inductive effect of the carboxylic group, which makes meta-C more reactive than ortho- and para-C for the attack by sorbed H.

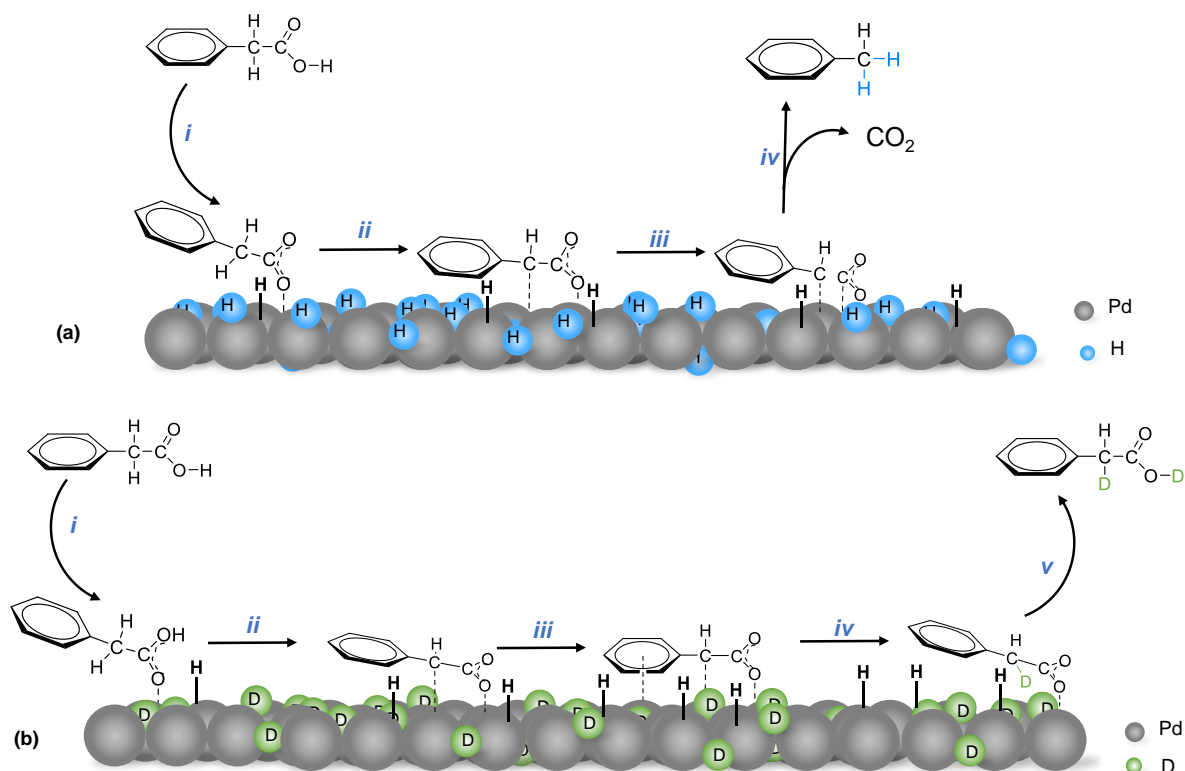
Combined, the observations lead to the hypothesis that the dissociation of α -C–H on Pd is an indispensable step for decarboxylation. The deuterium substitution reaction of carboxylic acids on D₂-pretreated Pd/C under mild conditions is presented in **Scheme 2-2**.



Scheme 2-2. Deuterium Substitution of C–H Groups on Hydrocinnamic Acid

Quantum chemical calculations also report that decarboxylation of arylaliphatic carboxylic acids on the Pd (111) surface involves dehydrogenation (C–H activation) at the α position prior to $-\text{CH}_x-\text{CO}_2$ bond scission, [15–17] which is consistent with our experimental observations. Thus, we propose the decarboxylation mechanism exemplified by 2-phenylacetic acid on the PdH_x/C catalyst in **Scheme 2-3a**. After 2-phenylacetic acid adsorption, the OH of the carboxylic group first binds to the Pd surface followed by facile O–H cleavage of the carboxylic acid group to form an Ar-CH₂-COO intermediate (step i). Then, the α -C–H bond adsorbs on the surface and dissociates to the Ar-CH-COO intermediate (step ii).

Afterward, it undergoes C–C bond cleavage to form a phenyl-alkyl intermediate (Ar-CH) and CO₂ (step iii). Finally, the Ar-CH species reacts with H on the Pd surface to form corresponding phenyl-alkane-toluene (Ar-CH₃) and desorbs (step iv), completing the catalytic cycle. However, the very low concentrations of H limit the rate of step iv, thus further limiting the overall decarboxylation rate. In contrast, PdH_x offer a H-rich (sub) surface, leading to a high rate for step iv; thus, in step iii, the C–C bond cleavage has a higher degree of rate control for the overall rate. When the Pd surface is pre-exposed with D, i.e., PdD_x, the Ar-CH-COO intermediate can react with D, forming Ar-CHD-COO, which leaves the surface as Ar-CHD-COOD (**Scheme 2-3b**).



Scheme 2-3. Proposed mechanisms of (a) Decarboxylation of arylaliphatic carboxylic acids on a H₂-pretreated Pd/C catalyst and (b) substitution of deuterium toward C-H and -COOH groups on 2-phenylacetic acid.

This path resembles a Mars–van Krevelen mechanism [39, 40] in which H on the Pd surface or incorporated in a subsurface position reacts with the Ar-CH intermediate and desorbs, while the consumed H is restored via dissociation of an α-C-H of another adsorbed carboxylic acid. On the metallic Pd, the lower concentration of H leads to a lower overall rate. Thus, the importance of H₂ pretreatment of Pd/C is interpreted to enable a higher concentration of surface H to promote the reaction with Ar-CH to Ar-CH₃ (toluene). Unpretreated Pd/C has a very low concentration of surface H that makes this step slower and reduces the overall decarboxylation rate.

2.4 Conclusion

This chapter shows that Pd/C catalyzes the decarboxylation of arylaliphatic carboxylic acids having an α-C-H group. Depending on the presence or absence of H₂, Pd/C exhibits bifunctional and competing catalytic activities for arylaliphatic carboxylic acids, i.e., arene ring hydrogenation in the presence of H₂ or decarboxylation in an inert atmosphere. The arene ring

hydrogenation product, 3-cyclohexyl-alkyl carboxylic acid, is one order of magnitude less reactive for decarboxylation.

H₂ pretreatment, increasing the steady-state concentration of H, was identified to be a critical procedure to promote the decarboxylation catalytic activity of Pd/C. The decarboxylation rate of H₂-pretreated Pd/C was 18 times higher than that of untreated Pd/C. The TPSR and in situ XANES showed that the H₂ pretreatment on Pd/C serves to generate sorbed H or subsurface H on α -PdH_x. This is an important surface species that facilitates the surface phenyl-alkyl group (Ar(CH₂)_n*) hydrogenation to phenyl-alkane (Ar(CH₂)_{n-1}CH₃). The low concentration of the H species on metallic Pd leads to a lower rate of reaction of the phenyl-alkyl group (Ar(CH₂)_n*) with H, limiting the overall decarboxylation rate.

Arylaliphatic carboxylic acids with different side-chain lengths (Ar(CH₂)_n-COOH) show different reaction rates depending on the number of methylene groups in the side chain. It was found that on D₂-pretreated Pd/C, the C–H bonds in the methylene groups were partly substituted with C–D bonds prior to decarboxylation. The decarboxylation rates show a positive correlation with the activation rate of α -C–H. Furthermore, we conclude that the dissociation of α -C–H is indispensable for the cleavage of the C–COO bond and its rate positively correlates with the decarboxylation rate. Furthermore, we conclude that the decarboxylation on H₂-pretreated Pd/C proceeds via an instantaneous cleavage of the O–H bond of the carboxylic group, forming an Ar-(CH₂)_n-COO* intermediate. Then, the α -C–H bond dissociates to the Ar-(CH₂)_{n-1}-CH*-COO* intermediate, followed by C–COO scission. Finally, the Ar-(CH₂)_{n-1}-CH* intermediate reacts with sorbed H to generate products Ar-(CH₂)_{n-1}-CH₃.

Overall, this chapter shows how Pd/C can be activated to catalyze decarboxylation under mild conditions with an onset temperature of 90 °C. The reaction mechanism and the structural requirements for the catalyst and substrate serve as a guide for further catalyst development for a broader set of substrates.

2.5 Appendix

Experiments related to the reaction mechanism, continuously collected XANES spectra, mass spectra for hydrocinnamic acid and ethylbenzene from D₂ substitution reaction, substituted D atoms on the arene ring, synchrotron facility for the in situ XANES measurements, N₂ adsorption–desorption, and H₂-chemisorption profile.

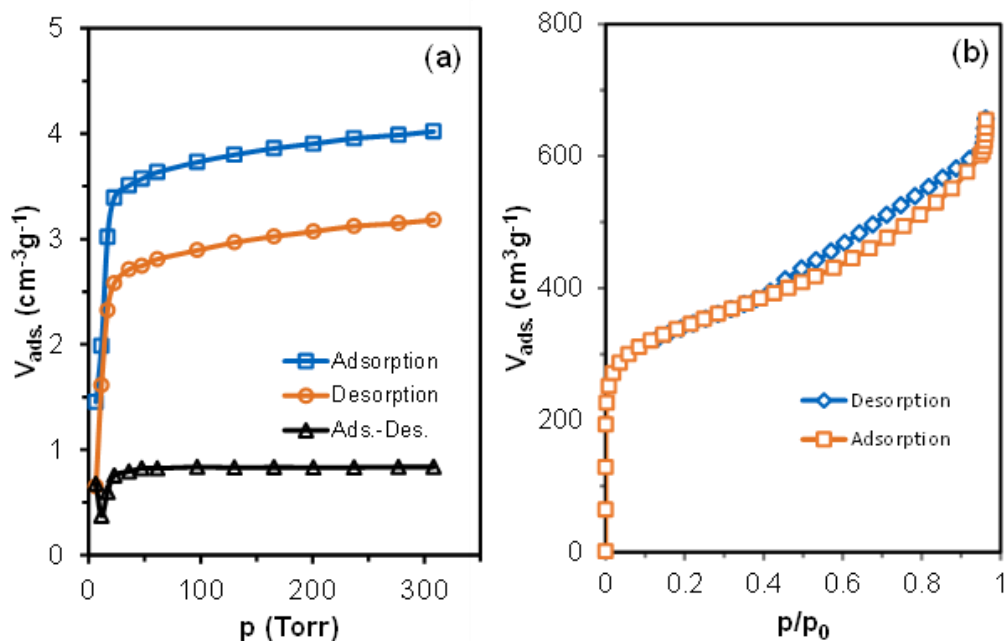


Figure A 2-1. (a) H₂ chemisorption and (b) N₂ adsorption-desorption profiles of Pd/C catalyst.

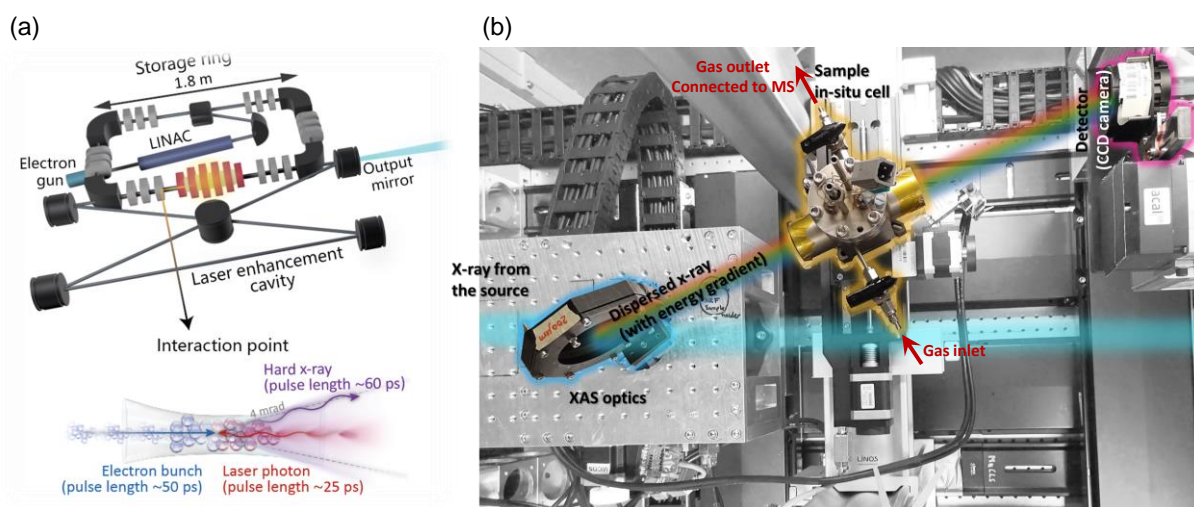


Figure A 2-2. (a) XANES measurement was conducted at a miniature synchrotron facility, the Munich Compact Light Source (MuCLS), which is based on inverse Compton scattering.

(Reproduced with permission from ref 2 Copyright 2020 Springer Nature) (b) In-situ XANES experimental setup from MuCLS.

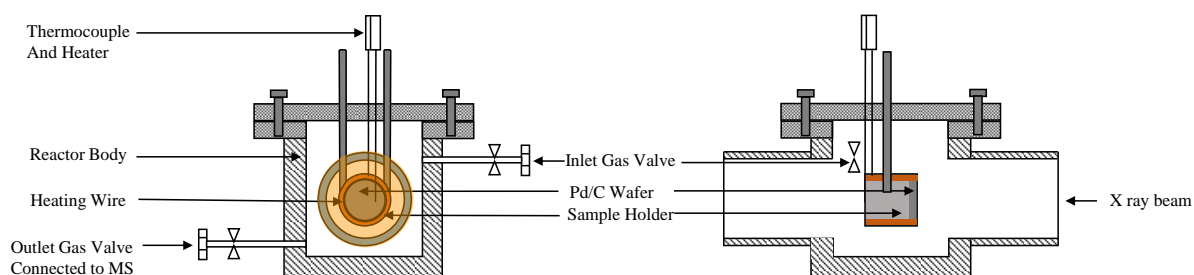


Figure A 2-3. Temperature programmed surface reaction cell with heating wire and gas flowing.

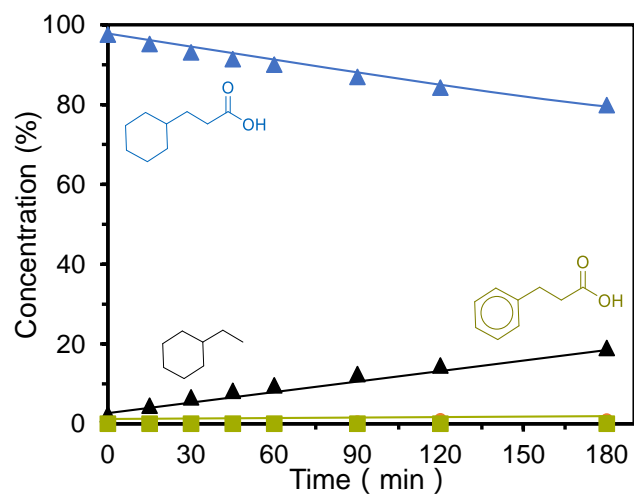


Figure A 2-4. Concentrations of products and reactant as a function of time in the reaction of 3-cyclohexylpropionic acid on Pd/C. Reaction conditions: 100 mg of Pd/C catalyst, 80 mL of n-dodecane as solvent, reacted at 300 °C and 20 bar H₂.

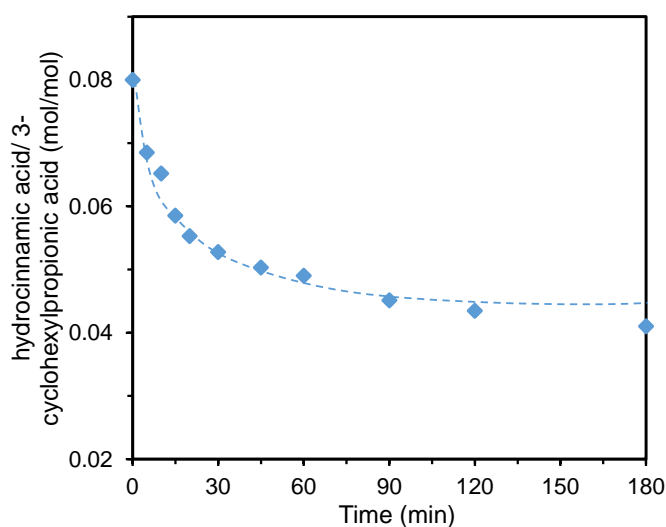


Figure A 2-5. The mol ratio between hydrocinnamic acid and 3-cyclohexylpropionic acid as a function of reaction time reacted under 300 °C 1 bar H₂ and 9 bar N₂ (100 mg of Pd/C catalyst, 80 mL of n-dodecane as solvent).

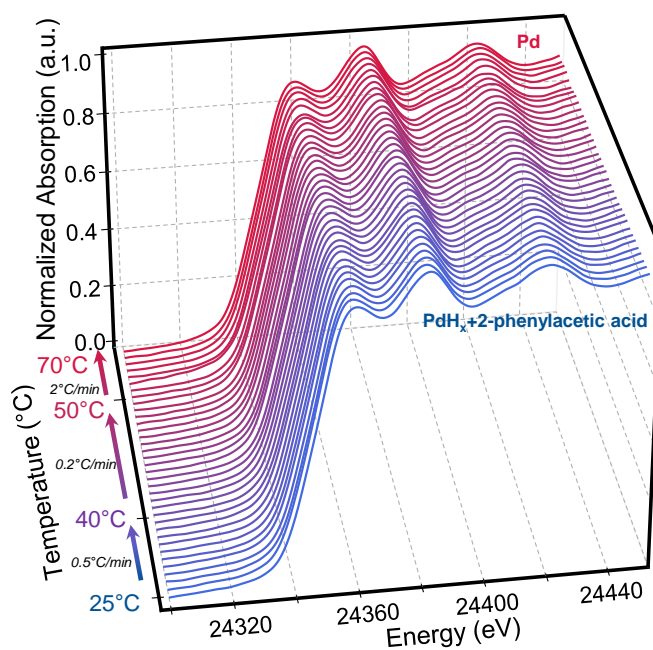


Figure A 2-6. Continuously collected Pd K-edge in-situ XANES spectra of the Pd species in a temperature programmed surface reaction (TPSR) process. Temperature of the TPSR was increased from 25 °C to 40 °C with rate of 0.5 °C /min, 40 °C to 50 °C with rate of 0.2 °C /min and from 50 °C to 70 °C with rate 2 °C /min (Reproduced with permission from Ref 1. Copyright 2021 Royal Society of Chemistry.)

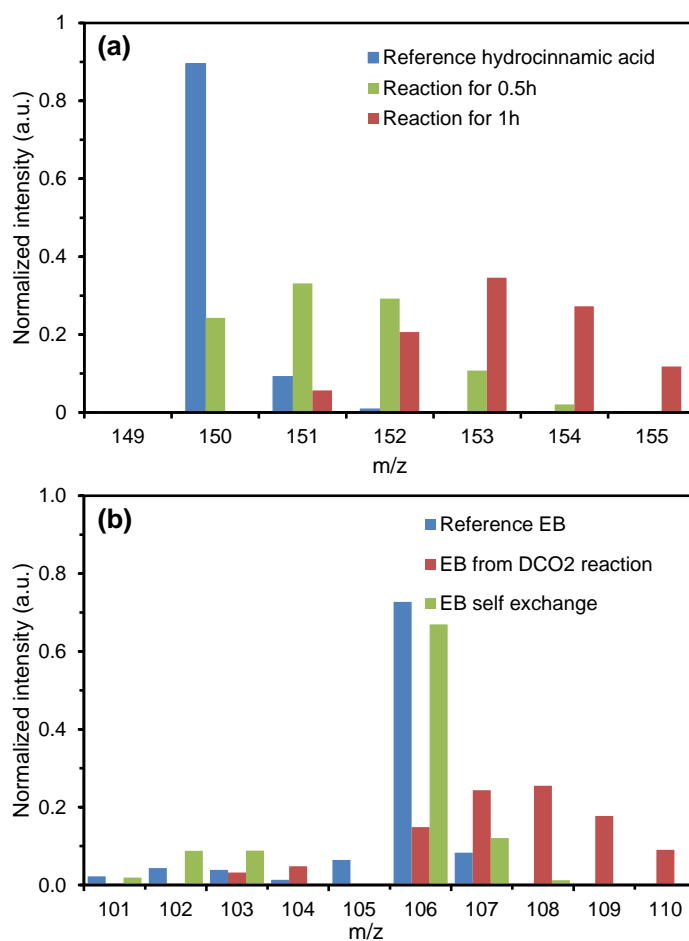


Figure A 2-7. (a) Mass spectra of hydrocinnamic acid after deuterium substitution for 0 h, 0.5 h and 1 h. Reaction condition: 100 mg of Pd/C catalyst was pretreated with 1 bar D₂ at 150 °C for 30 min. 0.53 mmol hydrocinnamic acid reacted at 100 °C 10 bar N₂. **(b)** Mass spectra of reference ethylbenzene (EB), EB generated from hydrocinnamic acid decarboxylation (DCO₂) and EB as substrate for self H-D exchange on the deuterium substitution pretreated Pd/C at 200 for 1 h. Reaction condition: 100mg Pd/C was pretreated with 1 bar D₂ at 150 °C for 30min. 0.53 mmol hydrocinnamic acid or 0.53 mmol ethylbenzene reacted at 200 °C 10 bar N₂ for 1 h.

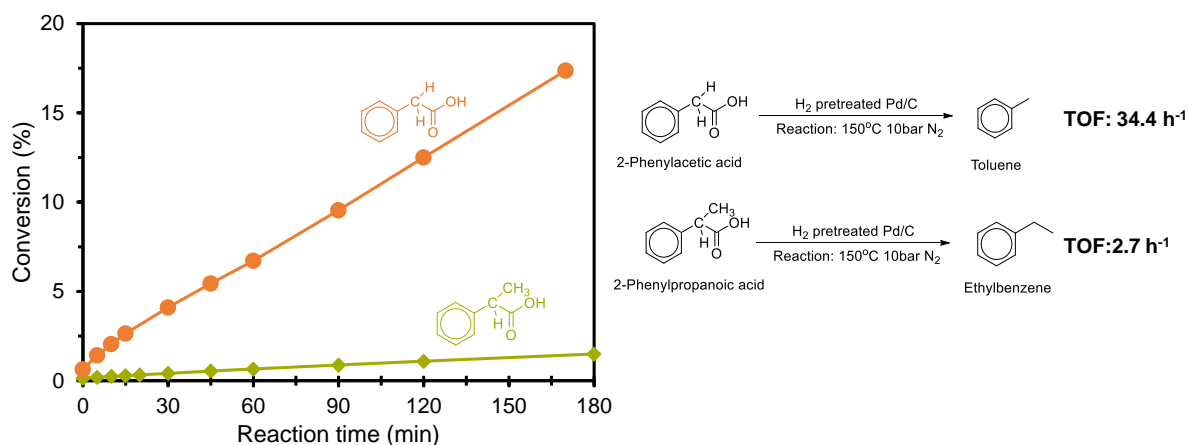


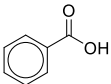
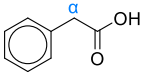
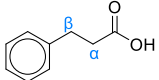
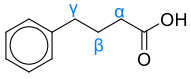
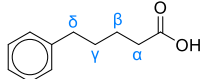
Figure A 2-8. Conversion of 2-phenylacetic acid and 2-phenylpropionic acid as a function of reaction time on H₂ pretreated Pd/C. reaction condition: 100 mg of Pd/C catalyst pretreated with 1 bar H₂ at 150°C for 30 min, n-dodecane as solvent, 5.3 mmol substrate carboxylic acid, reacted at 150 °C 10 bar N₂.

Table A 2-1. Catalysts and their decarboxylation performances of hydrocinnamic acid to ethylbenzene

Entry	Catalysts	Conv. (%)	TOF (h ⁻¹)
1	5 wt.% Pd/C	27.5	54
2	10 wt.% Pt/C	0.14	0.2
3	5 wt.% Rh/C	0.93	1.5
4	10wt.% Cu/C	0	0
5	10wt.% Ni/C	0	0

Reaction conditions: 80 mL n-dodecane as solvent, 0.1g catalyst (All the catalysts were pretreated with H₂ at 150 °C 10 bar H₂ for 1h before adding the reactant); 5.33mmol hydrocinnamic acid; Reaction temperature: 150 °C and 10 bar N₂.

Table A 2-2. Distribution of substituted D atoms in unconverted arylaliphatic carboxylic acids after reaction on D₂ pretreated Pd/C ^a

Entry	Substrate	Reaction time [min]	Substituted D atom numbers on arene ring ^[b]	
			Ortho & Para	Meta
1		60	0	0
2		60	0.04	0.14
3		60	0.06	0.33
4		60	0.03	0.02
5		60	0.01	0.01

^a Reaction condition: 100 mg of Pd/C catalyst pretreated at 150 °C and 1 bar D₂ for 30 min, 80 mL of n-hexane as solvent, 0.53 mmol carboxylic acid, reacted at 100 °C, 10 bar N₂ for 60 min. ^b Substituted D atom numbers were calculated from GC-MS and ¹H NMR results basing on Liu *et al.*'s research. [37]

2.6 Reference

- [1] L.J. Goossen, G.J. Deng, L.M. Levy, Synthesis of biaryls via catalytic decarboxylative coupling, *Science*, 313 (2006) 662-664.
- [2] A.J. Colussi, V.T. Amorebieta, M.A. Grela, Very low pressure pyrolysis of phenylacetic acid, *J. Chem. Soc. Faraday Trans.*, 88 (1992) 2125-2127.
- [3] L.J. Goossen, F. Manjolinho, B.A. Khan, N. Rodriguez, Microwave-Assisted Cu-Catalyzed Protodecarboxylation of Aromatic Carboxylic Acids, *J. Org. Chem.*, 74 (2009) 2620-2623.
- [4] S. Dupuy, F. Lazreg, A.M.Z. Slawin, C.S.J. Cazin, S.P. Nolan, Decarboxylation of aromatic carboxylic acids by gold(I)-N-heterocyclic carbene (NHC) complexes, *Chem. Commun.*, 47 (2011) 5455-5457.
- [5] P. Maki-Arvela, M. Snare, K. Eranen, J. Myllyoja, D.Y. Murzin, Continuous decarboxylation of lauric acid over Pd/C catalyst, *Fuel*, 87 (2008) 3543-3549.
- [6] I. Simakova, O. Simakova, P. Maki-Arvela, D.Y. Murzin, Decarboxylation of fatty acids over Pd supported on mesoporous carbon, *Catal. Today*, 150 (2010) 28-31.
- [7] J.H. Wu, J.J. Shi, J. Fu, J.A. Leidl, Z.Y. Hou, X.Y. Lu, Catalytic Decarboxylation of Fatty Acids to Aviation Fuels over Nickel Supported on Activated Carbon, *Sci. Rep.*, 6 (2016).
- [8] J. Fu, X.Y. Lu, P.E. Savage, Hydrothermal Decarboxylation and Hydrogenation of Fatty Acids over Pt/C, *Chemsuschem*, 4 (2011) 481-486.
- [9] X. Liu, M. Yang, Z.H. Deng, A. Dasgupta, Y. Guo, Hydrothermal hydrodeoxygenation of palmitic acid over Pt/C catalyst: Mechanism and kinetic modeling, *Chem. Eng. J.*, 407 (2021).
- [10] A.T. Madsen, E. Ahmed, C.H. Christensen, R. Fehrmann, A. Riisager, Hydrodeoxygenation of waste fat for diesel production: Study on model feed with Pt/alumina catalyst, *Fuel*, 90 (2011) 3433-3438.
- [11] J. Zhang, X.C. Huo, Y.L. Li, T.J. Strathmann, Catalytic Hydrothermal Decarboxylation and Cracking of Fatty Acids and Lipids over Ru/C, *ACS Sustain. Chem. Eng.*, 7 (2019) 14400-14410.
- [12] G.J.S. Dawes, E.L. Scott, J. Le Notre, J.P.M. Sanders, J.H. Bitter, Deoxygenation of biobased molecules by decarboxylation and decarbonylation - a review on the role of heterogeneous, homogeneous and bio-catalysis, *Green Chem.*, 17 (2015) 3231-3250.
- [13] J. Schwarz, B. Konig, Decarboxylative reactions with and without light - a comparison, *Green Chem.*, 20 (2018) 323-361.
- [14] T. Qin, J. Cornella, C. Li, L.R. Malins, J.T. Edwards, S. Kawamura, B.D. Maxwell, M.D. Eastgate, P.S. Baran, A general alkyl-alkyl cross-coupling enabled by redox-active esters and alkylzinc reagents, *Science*, 352 (2016) 801-805.
- [15] J.M. Lu, S. Behtash, A. Heyden, Theoretical Investigation of the Reaction Mechanism of the Decarboxylation and Decarbonylation of Propanoic Acid on Pd(111) Model Surfaces, *J. Phys. Chem. C*, 116 (2012) 14328-14341.

- [16] J.M. Lu, S. Behtash, M. Faheem, A. Heyden, Microkinetic modeling of the decarboxylation and decarbonylation of propanoic acid over Pd(111) model surfaces based on parameters obtained from first principles, *J. Catal.*, 305 (2013) 56-66.
- [17] H.H. Lamb, L. Sremaniak, J.L. Whitten, Reaction pathways for butanoic acid decarboxylation on the (111) surface of a Pd nanoparticle, *Surf. Sci.*, 607 (2013) 130-137.
- [18] M. Peroni, I. Lee, X. Huang, E. Barath, O.Y. Gutierrez, J.A. Lercher, Deoxygenation of Palmitic Acid on Unsupported Transition-Metal Phosphides, *Acs Catal.*, 7 (2017) 6331-6341.
- [19] C. Denk, S. Foraita, L. Kovarik, K. Stoerzinger, Y. Liu, E. Barath, J.A. Lercher, Rate enhancement by Cu in Ni_xCu_{1-x}/ZrO₂ bimetallic catalysts for hydrodeoxygenation of stearic acid, *Catal. Sci. Technol.*, 9 (2019) 2620-2629.
- [20] J.M. Lu, M. Faheem, S. Behtash, A. Heyden, Theoretical investigation of the decarboxylation and decarbonylation mechanism of propanoic acid over a Ru(0001) model surface, *J. Catal.*, 324 (2015) 14-24.
- [21] J.G. Immer, M.J. Kelly, H.H. Lamb, Catalytic reaction pathways in liquid-phase deoxygenation of C18 free fatty acids, *Appl. Catal. A: Gen.*, 375 (2010) 134-139.
- [22] I. Kubickova, M. Snare, K. Eranen, P. Maki-Arvela, D.Y. Murzin, Hydrocarbons for diesel fuel via decarboxylation of vegetable oils, *Catal. Today*, 106 (2005) 197-200.
- [23] W.F. Maier, W. Roth, I. Thies, P.V. Schleyer, Hydrogenolysis IV gas phase decarboxylation of carboxylic acids, *Chem. Ber. Recl.*, 115 (1982) 808-812.
- [24] M.F. Wagenhofer, E. Barath, O.Y. Gutierrez, J.A. Lercher, Carbon-Carbon Bond Scission Pathways in the Deoxygenation of Fatty Acids on Transition-Metal Sulfides, *Acs Catal.*, 7 (2017) 1068-1076.
- [25] B. Rozmyslowicz, A. Kirilin, A. Aho, H. Manyar, C. Hardacre, J. Warna, T. Salmi, D.Y. Murzin, Selective hydrogenation of fatty acids to alcohols over highly dispersed ReO_x/TiO₂ catalyst, *J. Catal.*, 328 (2015) 197-207.
- [26] N.K. Nag, A study on the formation of palladium hydride in a carbon-supported palladium catalyst, *J. Phys. Chem. B*, 105 (2001) 5945-5949.
- [27] J.E. Benson, H.S. Hwang, M. Boudart, Hydrogen-oxygen titration method for the measurement of supported palladium surface area, *J. Catal.*, 30 (1973) 146-153.
- [28] A. Baldi, T.C. Narayan, A.L. Koh, J.A. Dionne, In situ detection of hydrogen-induced phase transitions in individual palladium nanocrystals, *Nat. Mater.*, 13 (2014) 1143-1148.
- [29] V.A. Semikolenov, S.P. Lavrenko, V.I. Zaikovskii, A.I. Boronin, Pd/C catalysts deactivation and behavior of supported Pd particles upon heating, *React. Kinet. Catal. Lett.*, 51 (1993) 517-524.
- [30] V.A. Semikolenov, S.P. Lavrenko, V.I. Zaikovskii, Sintering of Pd particles on the surface of carbon supports in hydrogen, *React. Kinet. Catal. Lett.*, 51 (1993) 507-515.
- [31] Z.P. Huang, Z.T. Zhao, C.F. Zhang, J.M. Lu, H.F. Liu, N.C. Luo, J. Zhang, F. Wang, Enhanced photocatalytic alkane production from fatty acid decarboxylation via inhibition of radical oligomerization, *Nat. Catal.*, 3 (2020) 170-178.

- [32] A.L. Bugaev, A.A. Guda, K.A. Lomachenko, V.V. Srabionyan, L.A. Bugaev, A.V. Soldatov, C. Lamberti, V.P. Dmitriev, J.A. van Bokhoven, Temperature- and Pressure-Dependent Hydrogen Concentration in Supported PdH_x Nanoparticles by Pd K-Edge X-ray Absorption Spectroscopy, *J. Phys. Chem. C*, 118 (2014) 10416-10423.
- [33] A.L. Bugaev, O.A. Usoltsev, A.A. Guda, K.A. Lomachenko, I.A. Pankin, Y.V. Rusalev, H. Emerich, E. Groppo, R. Pellegrini, A.V. Soldatov, J.A. van Bokhoven, C. Lamberti, Palladium Carbide and Hydride Formation in the Bulk and at the Surface of Palladium Nanoparticles, *J. Phys. Chem. C*, 122 (2018) 12029-12037.
- [34] J. Huang, F. Deng, B. Günther, K. Achterhold, Y. Liu, A. Jentys, J.A. Lercher, M. Dierolf, F. Pfeiffer, Laboratory-Scale In-Situ X-Ray Absorption Spectroscopy of a Palladium Catalyst on a Compact Inverse-Compton Scattering X-Ray Beamline, *J. Anal. At. Spectrom.*, Accepted Manuscript (2021).
- [35] W.J. Shen, Y. Ichihashi, H. Ando, Y. Matsumura, M. Okumura, M. Haruta, Effect of reduction temperature on structural properties and CO/CO₂ hydrogenation characteristics of a Pd-CeO₂ catalyst, *Appl. Catal. A: Gen.*, 217 (2001) 231-239.
- [36] C.W. Lopes, J.L. Cerrillo, A.E. Palomares, F. Rey, G. Agostini, An in situ XAS study of the activation of precursor-dependent Pd nanoparticles, *PCCP*, 20 (2018) 12700-12709.
- [37] Y. Liu, F.M. Kirchberger, S. Müller, M. Eder, M. Tonigold, M. Sanchez-Sanchez, J.A. Lercher, Critical role of formaldehyde during methanol conversion to hydrocarbons, *Nat. Commun.*, 10 (2019) 1462.
- [38] T. Kurita, K. Hattori, S. Seki, M. Mizumoto, F. Aoki, Y. Yamada, K. Ikawa, T. Maegawa, Y. Monguchi, H. Sajiki, Efficient and convenient heterogeneous palladium-catalyzed regioselective deuteration at the benzylic position, *Chem. Eur. J.*, 14 (2008) 664-673.
- [39] A.V. Mironenko, D.G. Vlachos, Conjugation-Driven "Reverse Mars-van Krevelen"-Type Radical Mechanism for Low-Temperature C-O Bond Activation, *J. Am. Chem. Soc.*, 138 (2016) 8104-8113.
- [40] C.L. Wang, X.K. Gu, H. Yan, Y. Lin, J.J. Li, D.D. Liu, W.X. Li, J.L. Lu, Water-Mediated Mars-Van Krevelen Mechanism for CO Oxidation on Ceria-Supported Single-Atom Pt-1 Catalyst, *Acs Catal.*, 7 (2017) 887-891.
- [41] E. Eggl, M. Dierolf, K. Achterhold, C. Jud, B. Gunther, E. Braig, B. Gleich, F. Pfeiffer, The Munich Compact Light Source: initial performance measures, *J. Synchrotron Radiat.*, 23 (2016) 1137-1142.

Chapter 3. Promotion Effect of KHCO_3 on Palladium Hydride Catalyzed Decarboxylation of Aryl aliphatic Acid

Direct conversion of carboxylic acids into alkanes by decarboxylation reaction is an effective way to convert biomass derived chemicals to fuels. However, catalytic decarboxylation generally suffers from low activity and selectivity due to the high stability of the carboxyl group. Herein, we report the promotion effect of potassium bicarbonate (KHCO_3) to PdH_x/C catalyst for decarboxylation reaction. When introducing 1 wt. % KHCO_3 to PdH_x/C , the decarboxylation activity can be increased to more than one order of magnitude higher for various carboxylic acids. CO_2 -TPD and deuterium labeling results revealed that the modifier KHCO_3 increases surface basicity and induces dissociation of carboxyl group (COOH) to dissociatively adsorbed carboxylate anion, which is more active than the molecularly adsorbed carboxylic acid on the unmodified PdH_x/C , thereby greatly promoting the C-C bond cleavage. Thus, this chapter introduces a simple but efficient approach to promote the Pd-catalyzed decarboxylation of carboxylic acids.

3.1 Introduction

Upgrading biomass-derived feedstocks into hydrocarbon chemicals and fuels is promising alternative to current fossil-based production processes. Among the various oxygenic compounds in biomass, carboxylic acids can be converted to corresponding alkanes via hydrodeoxygenation, hydrodecarbonylation, and decarboxylation. Hydrodeoxygenation and hydrodecarbonylation approaches suffer from high energy consumption due to harsh reaction conditions (e.g. temperature ≥ 250 °C and H_2 pressures ≥ 2 MPa) [1–3]. Decarboxylation does not need high pressure of H_2 , but elevated temperature (≥ 300 °C) is still required and accompanied by low selectivity and deactivation of catalysts [3,4]. Therefore, it is important to develop new methods that convert the carboxylic acids into alkanes under low temperature and pressure.

We have reported in previous chapter that arylaliphatic carboxylic acids decarboxylate on carbon-supported alpha phase palladium hydride ($\alpha\text{-PdH}_x$) with 100% selectivity under relatively mild conditions (150 °C, 1 bar N_2). The palladium hydride phase generated from H_2 pretreatment creates an H-rich surface and greatly promotes decarboxylation [5,6]. The presence of a high concentration of H on the catalyst vastly increases the combination rate of H with H-deficient intermediates at surface to form the final hydrocarbon product [6–8].

Alkali and alkali earth metals are commonly used catalyst modifiers in a number of transition metal-catalyzed reactions. For example, K, Li modification on Cu-, Co-, Mo-, Pd-based catalysts promoted the alcohols selectivity in CO hydrogenation reactions [9–11]; Na, K, Ca modified Cu-, Fe- catalysts showed higher production of linear olefins in CO_2 hydrogenation reactions [12–15]; modification of Sr on Pd/MgO catalyst enhanced the rate of phenol hydrogenation [16]. These promotional effects have been attributed to, on the one hand, the modification of the surface acidity and basicity, and an increase of metal dispersion; and on the other hand, donation of electrons from alkali or alkali earth metals to the host-metal that increases their electron density [17] and stabilizes surface intermediates [18–20].

In this chapter, we aim to promote the decarboxylation activity of $\alpha\text{-PdH}_x$ by using potassium salts-based promoters (KOH, K_2CO_3 , KHCO_3 and KCl). In the decarboxylation reaction of arylaliphatic acid, 1wt. % KHCO_3 modified PdH_x/C catalysts exhibit the highest decarboxylate activity. We will show that the basicity of KHCO_3 promotes the dissociation of carboxylic acid to carboxylate, leading to a higher decarboxylation rate.

3.2 Experimental section

3.2.1 Catalyst preparation

3.2.1.1 Synthesis of Pd/C catalyst.

The 5wt. % Pd/C catalyst was synthesized by incipient wetness impregnation as follows: 0.1055 g $\text{Pd}(\text{OAc})_2$ were dissolved in 3 g acetone assisted by ultra-sonication and was impregnated with 1 g carbon support (Vulcan- XC-72 with the specific surface area of $218 \text{ m}^2\text{g}^{-1}$). After impregnation, the sample was dried at $60 \text{ }^\circ\text{C}$ overnight, and then calcinated in N_2 atmosphere (N_2 flow 50 mL/min) at $180 \text{ }^\circ\text{C}$ for 2 h, and further reduced at $250 \text{ }^\circ\text{C}$ for 2 h by H_2 (50 mL/min) with a heating rate of $5 \text{ }^\circ\text{C/min}$, the obtained catalyst was named as Pd/C.

3.2.1.2 Preparation of promoter(s) modified Pd/C catalysts

The promoter(s) modified Pd/C catalysts were prepared by simple wetness impregnation on the synthesized Pd/C catalysts. Corresponding promoter compounds (KHCO_3 , K_2CO_3 , KCl , etc.) was first fully dissolved in 20 mL water and then Pd/C catalyst powder was adding into the solution with continuous stirring for 6 hours. The solvent was removed via rotary evaporation at $60 \text{ }^\circ\text{C}$ and the obtained mixture was dried overnight in the oven. The obtained promoter-Pd/C catalyst was finely grinded before use. The weight percent of modifiers in catalysts was denoted by x wt. %, thus the promoted catalyst was denoted as x wt. % promoter-Pd/C.

3.2.1.3 Collection of used catalysts

Catalyst was collected after certain reaction, solvent was removed first by centrifuge, followed by washing with acetone for three times. The residual solid was dried overnight in the oven at $60 \text{ }^\circ\text{C}$.

3.2.2 Catalytic evaluation and kinetic measurements

3.2.2.1 Batch reaction

Catalytic conversions of hydrocinnamic carboxylic acids were performed in a high-pressure stainless-steel autoclave (300 mL) with a mechanical agitator. In a typical experiment, 100 mg catalyst, 80 mL alkane solvent (n-dodecane or n-hexane) and 2.66 mmol substrate were added into the autoclave and purged with N_2 for three times to completely remove air and afterwards a specific pressurized reaction gas (H_2 , N_2) was introduced into autoclave at room

temperature. The autoclave was then rapidly heated to desired temperature by a heating jacket. Samples of the liquid phase were continuously taken through a sampling tube with a filter at certain intervals in each experiment. The stirring rate was kept at 600 r/min during the reaction. When specifically mentioned, the prepared catalyst was first pretreated under 1 bar H_2 at 150 °C for 60min before adding substrate, the pretreatment processes were described as follow: 100 mg Pd/C catalyst was first dispersed in 80 mL solvent in the autoclave, then the reactor was purged with 1 bar H_2 and heated to 150 °C for 60min. After pretreatment, the reactor was cooled to room temperature and the reactant was added to the reactor and then purged with 10 bar N_2 and reacted at certain temperature.

Products in liquid phase was analyzed by gas chromatography (Shimadzu GC 2010) equipped with HP-5 Agilent column (30.0 m x 0.25 μm) and gas chromatography-mass spectrometry (Shimadzu, GC-MS 2010) equipped with HP-5 Agilent column (30.0 m x 0.25 μm). N-decane was used as an internal standard. Products in gas phase were collected by a gas bag and analyzed by a mass spectrometer (OmniStar Gas analysis system).

3.2.2.2 Deuterium Substitution Reaction.

The deuterium substitution reaction was also conducted in the high-pressure stainless-steel autoclave (300 mL). 100 mg catalyst was first dispersed in 80 mL of solvent (n-hexane) in the autoclave and pretreated with 1 bar deuterium (D_2) under 150 °C for 1 h. After the pretreatment, the mixture was cooled to room temperature and 0.13 mmol of hydrocinnamic acid or ethylbenzene was then added, purged and pressurized with N_2 to 10 bar at room temperature. Then, the autoclave was rapidly heated to 100 or 130 °C for the substitution reaction. Liquid samples were collected at a different time during the reaction and analyzed by GC-MS. After the reaction, the component in the solution was extracted with D_2O and characterized by the ^1H NMR spectroscopy.

3.2.2.3 Adsorption Isotherm Measurement

Adsorption of hydrocinnamic acid onto Pd/C and KHCO_3 -Pd/C in n-dodecane solution was carried out by measuring the hydrocinnamic acid concentration change in the solution before and after adsorption. Adsorption isotherms at certain temperatures (30 °C, 50 °C, 70 °C, 90 °C, and 100 °C) were obtained by immersing 200 mg of catalyst in an initial concentration 5 mM hydrocinnamic acid solution (30 mL) of in a batch reactor with continuous stirring. After adsorbing for at least 1 hour, a 1 mL sample was taken from the reactor through an installed filter in the batch reactor. The concentration of samples was determined by GC with n-decane

as the internal standard. The residual mixture was supplemented with 1 mL n-dodecane and a certain amount of hydrocinnamic acid to the next desired concentration. The maximum concentration was 300-400 mM. The uptake (q) is calculated by $q = V (c_0 - c_e)/m$. c_0 is the initial bulk concentration, c_e is the bulk concentration after equilibrium, V is the volume of solution, m is the mass of catalyst.

3.2.3 Catalyst characterization

3.2.3.1 H_2 -Chemisorption

The dispersion of the Pd was determined by H_2 chemisorption. The Pd/C was pretreated under vacuum at 588 K for 1 h and then cooled to 313 K. The first hydrogen adsorption isotherm was measured at 1–40 kPa H_2 . Afterwards the sample were outgassed at 313 K for 1 h and a second set of isotherms was measured. The concentrations of chemisorbed H_2 on the metal were determined by extrapolating the difference isotherm of the two to zero hydrogen pressure. The dispersion of the Pd was estimated from the concentration of chemisorbed H_2 assuming a stoichiometry of 1:1 metal to hydrogen atoms.

3.2.3.2 CO-TPD

The dispersion of Pd was also determined by temperature programmed desorption (TPD) of CO. For typical experiments, ~50 mg catalyst sample were pre-reduced at 150 °C (10 °C/min ramping rate) in H_2 for 1h to reduce the partial oxidized Pd. Then, the samples were outgassed by vacuum to 10^{-3} mbar for 1h to remove surface adsorbed H_2 . After cooling to 30 °C, CO was absorbed with partial pressure of 5 mbar for 1 h. Subsequently, samples were outgassed for 1 h again to remove all physisorbed CO molecules. Then all samples were subsequently heated from 30 °C to 700 °C to desorb CO. An attached mass spectrometer (Balzers QME 200) was used for the surface properties analysis. The amount of desorbed CO was determined by the integration of the MS signal calibrated to a standard material (Pd/C was used as the reference).

3.2.3.3 AAS

The contents of Pd and promoters on synthesized catalyst were measured by atomic absorption spectroscopy (AAS) on a UNICAM 939 AA-Spectrometer.

3.2.3.4 XRD

X-ray diffraction patterns were collected using a Philips X'Pert Pro System, with Cu- $\text{K}\alpha$ radiation source operating at 45 kV and 40 mA. The sample was measured with a scanning rate

of $0.02^\circ \text{ s}^{-1}$ in the $10\text{-}70^\circ 2\theta$ -range. The partial size of the Pd was calculated according to Scherrer equation: $D=K\lambda/\beta\cos\theta$.

3.2.3.5 CO_2 -TPD

The nature and the concentration of surface basic site was analyzed by temperature programmed desorption (TPD) of CO_2 . For typical experiments, ~ 50 mg catalyst sample were pre-reduced at 150° C ($10^\circ \text{ C}/\text{min}$ ramping rate) in H_2 for 1h to reduce the partial oxidized Pd. Then, the samples were outgassed by vacuum to 10^{-3} mbar for 1h to remove surface adsorbed H_2 . After cooling to 80° C , CO_2 was absorbed with partial pressure of 5 mbar for 1 h. Subsequently, samples were outgassed for 1 h to remove all physisorbed CO_2 molecules. Then all samples were subsequently heated from 80° C to 770° C to desorb CO_2 . An attached mass spectrometer (Balzers QME 200) was used for the surface properties analysis. The amount of desorbed CO_2 was determined by the integration of the MS signal calibrated to a standard material (KHCO_3 decomposition was employed in this study).

3.3 Results and Discussion

3.3.1 Decarboxylation reaction of hydrocinnamic acid on $\alpha\text{-PdH}_x/\text{C}$

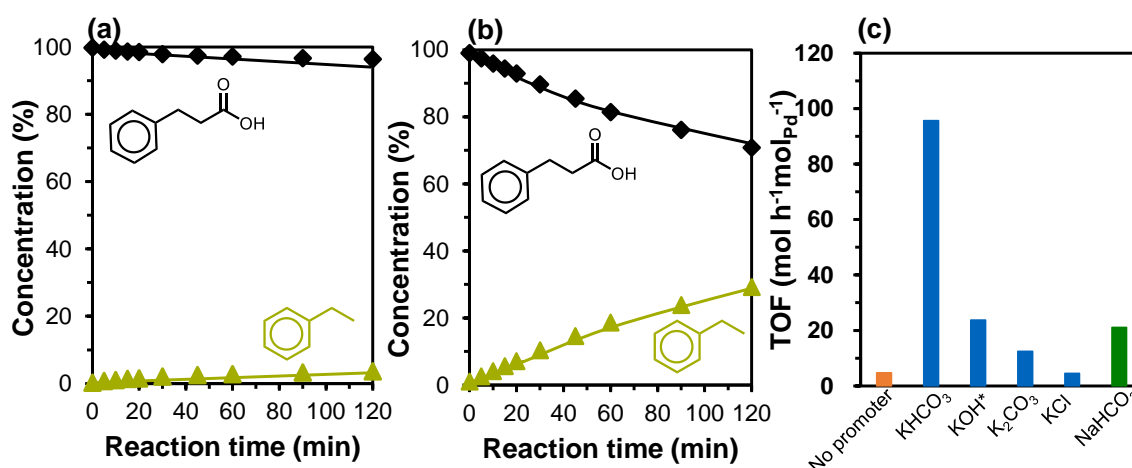


Figure 3-1. Concentrations of reactant and product as a function of time in the reaction of hydrocinnamic acid decarboxylation on (a) PdH_x/C and (b) $1\text{wt. \% KHCO}_3\text{-PdH}_x/\text{C}$; (c) Decarboxylation rate of hydrocinnamic acid on PdH_x/C with and without alkali metal salt with 1wt. \% loadings (*: 0.5wt. \% loading for KOH).

(Reaction conditions: 50 mg catalyst dispersed in 80 mL n-dodecane and pretreated with 1bar H_2 at 150° C for 1 h, 2.66 mmol hydrocinnamic acid and reacted at 10 bar N_2 150° C)

The reaction of hydrocinnamic acid decarboxylation was first carried out at $150\text{ }^\circ\text{C}$ and 10 bar N_2 on Pd/C , but no conversion of hydrocinnamic acid was observed in 2 h. After pretreating Pd/C with 1 bar H_2 at $150\text{ }^\circ\text{C}$ for 1 h to obtain PdH_x/C , an ethylbenzene yield of 2.5% was observed after 2 h reaction with a decarboxylation rate of $2.6\text{ }\mu\text{mol g}_{\text{Pd}}^{-1}\text{ s}^{-1}$, corresponding to a turnover frequency (TOF) of 5 h^{-1} (**Figure 3-1a**). It demonstrates the critical role of PdH_x from the H_2 pretreatment to obtain high decarboxylation activity on Pd catalysts, in accordance with our previous report [6]. Further, with 1 wt. % KHCO_3 on PdH_x/C , the decarboxylation TOF was greatly promoted by over one order of magnitude to 96 h^{-1} (**Figure 3-1b and Figure 3-1c**). Besides KHCO_3 , several other alkali-metal compounds were also chosen as additives to PdH_x/C to investigate the influence of different modifiers. **Figure 3-1c** showed other potassium-based modifiers including K_2CO_3 , KOH also promoted the decarboxylation rates to 10 h^{-1} and 26 h^{-1} , but less effective than KHCO_3 . In contrast, neutral KCl doped catalyst $\text{KCl-PdH}_x/\text{C}$ had no promotion effect on the PdH_x/C as the rate of $\text{KCl-PdH}_x/\text{C}$ (TOF of 5 h^{-1}) is identical with PdH_x/C . These results indicate that basicity of promoters is critical for the rate enhancement. Since KHCO_3 has the highest promotion effect than KOH , K_2CO_3 but less basic, it seems that promoter with weak basicity can elevate the decarboxylation activity of PdH_x/C to the largest extent.

The promotion effect of KHCO_3 also applied for decarboxylation of various types of carboxylic acids including aromatic acids (benzoic acids), aryl-substituted aliphatic carboxylic acid ($\text{Ar-C}_n\text{H}_{2n}\text{-COOH}$, $n \geq 1$), and aliphatic acid (palmitic acid). Results were compiled in **Table A 3-1**. All tested carboxylic acids were converted to corresponding C_{n-1} hydrocarbons with 100% selectivity on both modified and unmodified PdH_x/C catalysts. The KHCO_3 modified PdH_x/C showed one order of magnitude higher activity than unmodified catalyst. To understand such promotion effect, KHCO_3 modified PdH_x/C catalyst for hydrocinnamic acid decarboxylation was investigate in detail next.

3.3.2 Influence of K Content on Catalytic Performance

The influence of modifier KHCO_3 loading on PdH_x/C in the decarboxylation of hydrocinnamic acid was studied. As shown in **Figure 3-2**, unmodified PdH_x/C had a poor decarboxylation activity with a TOF of only 5 h^{-1} . The addition of 0.5 wt. % KHCO_3 to PdH_x/C increased the TOF by over 10 folds, to 55 h^{-1} . Then increasing KHCO_3 loading from 0.5 to 1.0 wt. % (**Figure 3-2**), doubled the TOF to 96 h^{-1} . However, when further increasing the KHCO_3

loading, the decarboxylation TOFs gradually declined from 37 h^{-1} at 2 wt. % KHCO_3 to only 10 h^{-1} at 8 wt. % KHCO_3 . The volcano-type trend between KHCO_3 loading and decarboxylation rate is similar to other studies relating to the noble metal- alkali combination catalysts [17,21–23].

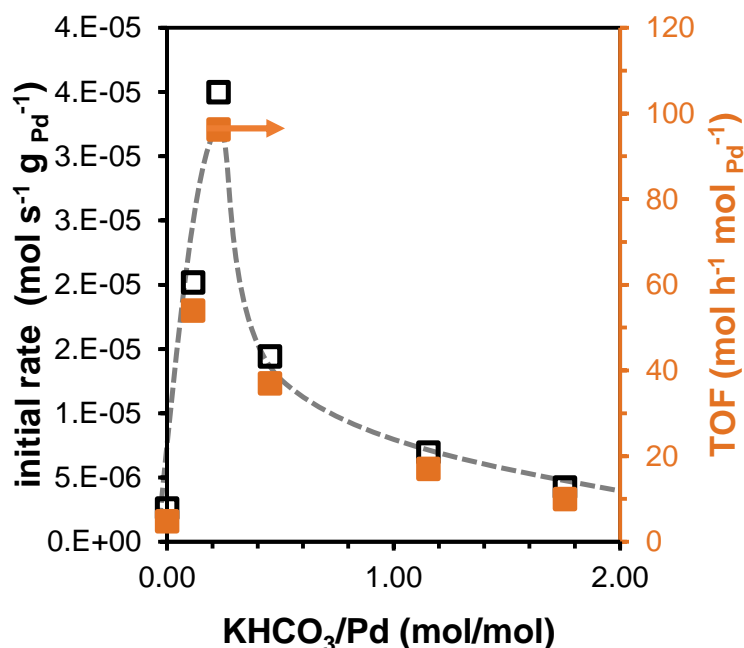


Figure 3-2. Initial reaction rate and TOF of hydrocinnamic acid decarboxylation as a function of K and Pd ratio on PdH_x/C .

Reaction conditions: 50 mg catalyst dispersed in 80 mL n-dodecane and pretreated with 1 bar H_2 at $150 \text{ }^\circ\text{C}$ for 1 h, 2.66 mmol hydrocinnamic acid and reacted at 10 bar N_2 $150 \text{ }^\circ\text{C}$.

3.3.3 Physical and Chemical Properties of Catalysts

Table 3-1. Basic physicochemical properties of the Pd/C and KHCO_3 promoted- Pd/C catalysts.

Catalyst	Pd loading ^a (wt. %)	KHCO_3 ^a (wt. %)	Pd diameter ^b (nm)	Pd Dispersion ^c (%)	Pd Dispersion ^d (%)
5wt.%Pd/C	4.8	0.06	4.7	21	21
0.5wt.% KHCO_3 -Pd/C	4.6	0.6	4.9	14	14
1wt.% KHCO_3 -Pd/C	4.7	1.0	4.9	14	13
2wt.% KHCO_3 -Pd/C	4.7	2.0	4.7	15	15
5wt.% KHCO_3 -Pd/C	4.6	4.4	4.5	16	14
8wt.% KHCO_3 -Pd/C	4.8	7.6	4.8	16	13

^a Determined by AAS. ^b Determined by Scherrer equation from XRD patterns, ^c Determined by H_2 -Chemisorption, ^d Determined by CO-chemisorption.

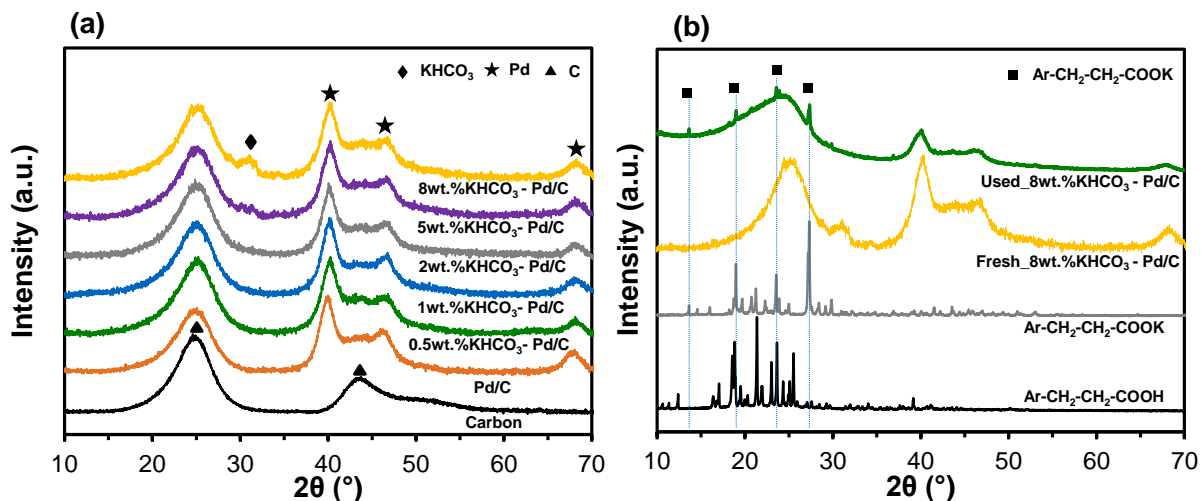


Figure 3-3. XRD patterns of (a) activated carbon, Pd/C and KHCO_3 -Pd/C catalysts with different KHCO_3 loadings, (b) Comparison among fresh and used 8wt. % KHCO_3 -Pd/C, hydrocinnamic acid ($\text{Ar-CH}_2\text{-CH}_2\text{-COOH}$) and potassium hydrocinnamate ($\text{Ar-CH}_2\text{-CH}_2\text{-COOH}$).

To investigate how KHCO_3 promotes the activity of PdH_x/C , physicochemical properties of KHCO_3 -Pd/C catalysts were characterized and compared. **Table 3-1** summarizes the practical loading of Pd and KHCO_3 on these catalysts. For parent Pd/C, the Pd loading was 4.8 wt. %. It is worth noting that about 0.06 wt. % of KHCO_3 was detected on Pd/C, which may be carried over from the impurities in the carbon support. All KHCO_3 -Pd/C catalysts were prepared from the same parent Pd/C. For the KHCO_3 -promoted catalysts, even after reacting at 150 °C for 1h (i.e., used-8wt. % KHCO_3 -Pd/C), the practical Pd loadings were almost identical on all these samples. The practical KHCO_3 loadings were also in good agreement with the nominal values of the fresh KHCO_3 -modified catalysts, and the minor difference could be caused by experimental errors during the synthesis procedures.

The results of the CO- and H_2 - chemisorption showed decreased Pd dispersion compared to parent Pd/C, which indicate partial blockage of Pd by KHCO_3 promoters. At high loadings, KHCO_3 aggregation was observed by the specific diffraction peaks (JCPDS 70-0095) [24–26] on 5wt. % and 8 wt. % KHCO_3 -Pd/C XRD profiles in **Figure 3-3a**. Diffraction peaks at 2θ values of 40.2°, 46.7°, and 68.2° are observed on all samples which are assigned to the (111), (200), and (220) lattice planes of Pd. Applying Scherrer equation, the crystallite sizes of Pd

were calculated to be identical of 4.7 ± 0.2 nm (**Table 3-1**). Moreover, after reacting at 150°C for 1h, the used 8wt. % KHCO_3 -Pd/C showed obvious changes in its XRD patterns (**Figure 3-3b**). Diffraction peaks of KHCO_3 disappeared and a set of new peaks of potassium hydrocinnamate ($\text{Ar-CH}_2\text{-CH}_2\text{-COOK}$) appeared. Thus, the identification of potassium hydrocinnamate reveals that hydrocinnamic acid reacts with the KHCO_3 modifier to hydrocinnamate.

Previous studies on the promotion effect of the alkali metals such as K, Na, etc., to the host active metals including Pt, Cu, and Fe have found that alkali metals can modulate the surrounding chemical environment of host metals by forming new type of sites at the their perimeters, resulting in adjusting the surface acid-base property and the electron states [13,15,27–31]. So next, we investigate whether the surface chemical properties variation causes our observed promotion effect of KHCO_3 in the Pd-catalyzed decarboxylation reaction.

3.3.4 Temperature-Programmed Surface Reaction (TPSR) in Combination with Operando XANES

To verify whether modifier KHCO_3 influences the electronic structure of Pd, Pd/C and KHCO_3 -Pd/C were investigated by temperature-programmed surface reaction (TPSR) of 2-phenylacetic acid decarboxylation with *in situ* X-Ray absorption near-edge structure (XANES). In batch reactions, the 2-phenylacetic acid exhibited a similar decarboxylation rate with the hydrocinnamic acid on the KHCO_3 -PdH_x/C catalysts (Shown in **Figure A 3-1**). In TPSR, 2-phenylacetic acid was pre-adsorbed on PdH_x/C or KHCO_3 -PdH_x/C, then under a linear increasing temperature the electronic state of Pd was monitored on XANES and the reaction product was detected online with a mass spectrometer. The results (**Figure 3-4a**) show that both of the unmodified PdH_x/C and 1wt. % KHCO_3 -PdH_x/C catalysts have decarboxylation activities in the solvent-free condition. Toluene, the decarboxylation product from 2-phenylacetic acid, appeared at above 100°C on PdH_x/C, while on KHCO_3 -PdH_x/C it appeared at around 80°C , which is 20°C lower than the PdH_x/C. In situ XANES (**Figure 3-4b**) shows Pd K-edge XANES spectra of Pd/C and KHCO_3 -Pd/C after sequential treatment with H_2 and N_2 at 150°C for 1 h, with the XANES spectrum of a Pd foil as a reference. Both spectra of Pd/C and KHCO_3 -Pd/C exhibit 2 characteristic peaks at 24360 eV and 24383 eV, the position and intensity of which are identical to the reference spectrum of Pd foil [32–34], suggesting that Pd atoms are in metallic state in these two catalysts at this condition. XANES result indicates that there is no

obvious electron transfer from the KHCO_3 to Pd atoms. Therefore, the promoting effect of KHCO_3 on Pd/C is not caused by modification of electronic structure of Pd.

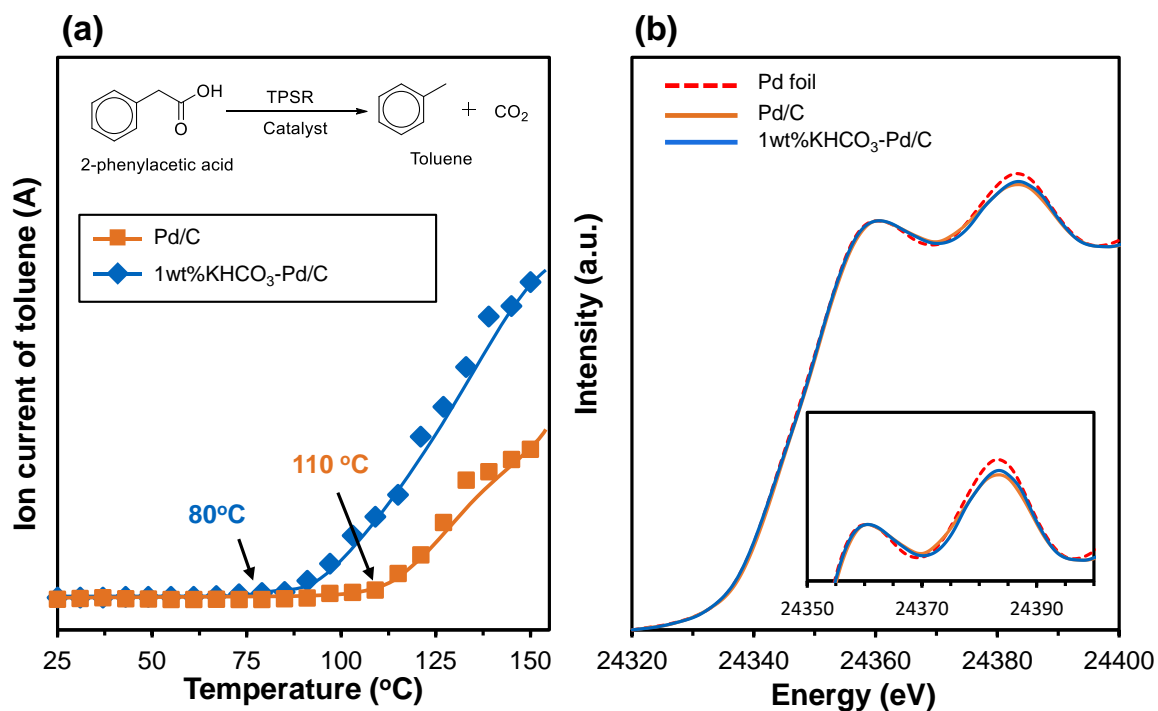


Figure 3-4. (a) Rate of toluene formation in the decarboxylation of pre-adsorbed 2-phenylacetic acid on PdH_x/C and $\text{KHCO}_3\text{-PdH}_x/\text{C}$ in the temperature programmed surface reaction (TPSR). Catalysts wafer were pretreated at 150 °C for 30 min in the H_2 flow (30 mL/min) and cooled down to the room temperature. After pretreatment, 2-phenylacetic acid pre-adsorption was conducted in the glove box. And TPSR was measured in the N_2 flow (30 mL/min). (Temperature ramping rate for TPSR reaction: 5 °C /min from 25 to 150 °C and holding at 150 °C for 1 h); (b) Normalized Pd K-edge XANES spectra of Pd foil, Pd/C and $\text{KHCO}_3\text{-Pd/C}$ catalysts. Pd/C and $\text{KHCO}_3\text{-Pd/C}$ samples were first pretreated in H_2 flow at 150 °C for 1h and switched to N_2 flow for another 1h pretreatment, then cool down to room temperature in N_2 atmosphere. Spectra were collected at room temperature, and the maximum value of spectra was normalized to 1. (The inset shows the enlarged spectra from 24350 eV to 24400 eV)

3.3.5 Temperature Programmed Desorption of CO_2 (CO_2 -TPD) of the Catalysts

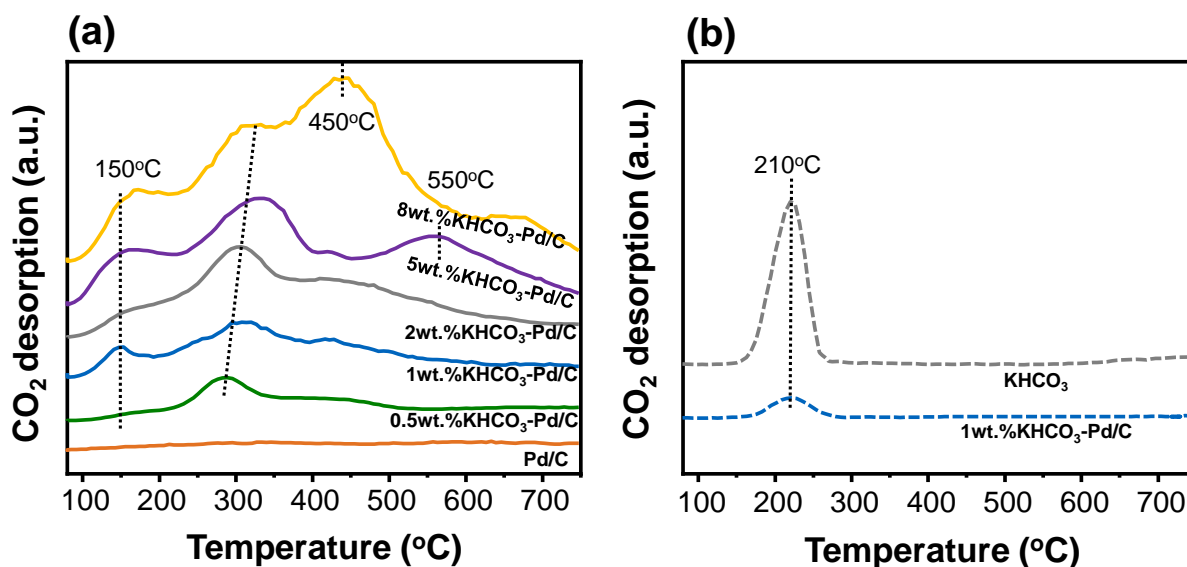


Figure 3-5. CO_2 -TPD profiles of the (a) Pd/C and KHCO_3 -Pd/C catalysts with KHCO_3 loading varies from 0.5 to 8wt. %, and (b) decomposition profiles of 1wt. % KHCO_3 -Pd/C and pure KHCO_3 .

CO_2 -TPD measurements were applied to determine the basicity of Pd/C. CO_2 -TPD profile of unmodified Pd/C in **Figure 3-5a** shows no obvious peak suggesting no basic sites on its surface (**Figure 3-5a**). All the KHCO_3 modified Pd/C exhibit at least two CO_2 desorption peaks at 100 – 180 °C and 230 – 380 °C referring to the weak and medium Lewis basic sites, respectively. One additional broad peak from 380 to 450 °C exists on samples with high KHCO_3 loadings (≥ 5 wt. %), corresponds to strong Lewis basic sites. For reference, the decomposition profiles of KHCO_3 and 1wt. % KHCO_3 -Pd/C in **Figure 3-5b** shows a peak at 150 – 250 °C which is not overlapped with any peaks in CO_2 -TPD profiles of KHCO_3 -Pd/C catalysts, indicating that all these three basic sites were created by the interaction between promoter KHCO_3 and Pd/C. Meanwhile, the percentage of strong basic sites in total sites increases with the KHCO_3 loading, indicating that higher loadings of KHCO_3 lead to stronger basicity on the Pd/C (**Table A 3-2**).

Therefore, we could reasonably hypothesize that the basicity of the KHCO_3 -Pd/C catalyst may alternate the chemisorption state of hydrocinnamic acid, i.e., inducing the deprotonation of $-\text{COOH}$ to generate carboxylate intermediate. In the decarboxylation activity results in **Figure 3-2a**, catalysts with low KHCO_3 loadings (i.e. 0.5wt. % and 1wt. % KHCO_3 -Pd/C) had weaker basicity but higher catalytic activities than 5 wt. % KHCO_3 -Pd/C, 8 wt. % KHCO_3 -

Pd/C that had stronger basic sites. The lower promotion effect of stronger base (K_2CO_3 and KOH) compared to KHCO_3 also substantiates the critical role of weak basicity of the promoter. Thus, weak surface basicity is the main cause for the promotion effect of KHCO_3 to PdH_x/C .

3.3.6 Effect of KHCO_3 on on Reaction Kinetics for Hydrocinnamic Acid Decarboxylation

To further explore the promotion effect of KHCO_3 to PdH_x/C catalyst in the hydrocinnamic acid decarboxylation, we carried out kinetic study for the reaction. The TOF for hydrocinnamic acid conversion in PdH_x/C and $\text{KHCO}_3\text{-PdH}_x/\text{C}$ catalysts are compared in **Table 3-2** and **Figure A 3-2**. The TOFs for hydrocinnamic acid decarboxylation was much higher on $\text{KHCO}_3\text{-PdH}_x/\text{C}$ than on the PdH_x/C .

The measured reaction orders for hydrocinnamic acid are 0th order on all catalysts, indicating that all the catalyst surfaces are saturated with adsorbed hydrocinnamic acid. (**Figure A 3-2**). The activation energy (E_a) for hydrocinnamic acid decarboxylation was determined by measuring the temperature-dependence of reaction rate and using Arrhenius plot (**Figure A 3-2c**). The E_a value is 97 kJ mol^{-1} on unmodified PdH_x/C . The 1 wt. % $\text{KHCO}_3\text{-PdH}_x/\text{C}$ has the highest decarboxylate rate (TOF of 96 h^{-1}) and the highest E_a of 151 kJ mol^{-1} . In contrast, in higher loading of KHCO_3 promoted catalysts, both the activity (19 h^{-1} and 13 h^{-1}) and activation energy (120 kJ mol^{-1}) are lower.

The pre-exponential factors (A) also illustrate a same trend as the E_a on these catalysts: It is over 3 orders of magnitude higher on $\text{KHCO}_3\text{-PdH}_x/\text{C}$ than that on unmodified PdH_x/C (**Table 3-2**). The identical 0th reaction order of hydrocinnamic acid on all catalysts excludes the influence of promoter on the adsorption and coverage of hydrocinnamic acid, which was also substantiated by the similar adsorption enthalpies and entropies on the unmodified PdH_x/C and 1wt. % KHCO_3 modified catalysts (see **Supplementary Note 1, Figure A 3-3** and **Table A 3-3** for details). Thus, the variation in reactivity, activation energy and pre-exponential factor (A) by the KHCO_3 modification originates from its influence on surface reaction steps on Pd.

Table 3-2. Summary of reaction rates, reaction orders, Arrhenius equation derived apparent activation energy for the decarboxylation of hydrocinnamic acid.

Catalyst	TOF _{423K} ^a	Reaction Order	Ea ^b	A ^b
	h^{-1}		kJ mol^{-1}	

Pd/C	5	0	97	2.3×10^6
0.5wt.%KHCO₃-Pd/C	57	0	136	9.9×10^{11}
1wt.%KHCO₃-Pd/C	96	0	151	8.2×10^{13}
2wt.%KHCO₃-Pd/C	38	0	136	9.5×10^{11}
5wt.%KHCO₃-Pd/C	19	0	120	4.4×10^9
8wt.%KHCO₃-Pd/C	13	0	120	3.2×10^9

^a Initial TOF at 150 °C and 10 bar N_2 with initial hydrocinnamic acid concentration of 33 mM. ^b Apparent activation energy and pre-exponential factor obtained from the Arrhenius equation.

From the kinetic results, we hypothesize that besides molecularly adsorbed hydrocinnamic acid on Pd, there is another form of hydrocinnamic acid activated by KHCO_3 . Since $\text{Ar-CH}_2\text{-CH}_2\text{-COOK}$ was observed in the reaction of decarboxylation of hydrocinnamic acid on 8wt. % $\text{KHCO}_3\text{-PdH}_x/\text{C}$ (**Figure 3-3b**), it is reasonable to conclude that on all the KHCO_3 modified PdH_x/C catalysts, the basic KHCO_3 abstracts the carboxylic proton from hydrocinnamic acid, generating a hydrocinnamate anion on Pd surface. Based on Glein and Verhoek *et al.*'s [90–93] reports that the deprotonated carboxylate anions possess higher decarboxylation activity than the original carboxylic acids (2-phenylacetic acid, acetic acid, and trichloroacetic acid etc.,) in thermal reactions in aqueous phase. Therefore, the hydrocinnamate anion is the precursor to trigger the decarboxylation reaction.

3.3.7 Adsorption States of Hydrocinnamic Acid on PdH_x/C and $\text{KHCO}_3\text{-PdH}_x/\text{C}$ catalysts

To investigate how KHCO_3 influenced the adsorption state of arylaliphatic acid, i.e., hydrocinnamic acid before the surface reaction, deuterium (D_2) substitution reaction was applied and the exchanged D position on the substrate molecular was also traced.

The D_2 substitution reactions were first carried out at 100 °C which is relatively lower than the decarboxylation temperature (150 °C) in order to avoid decarboxylation and probe only the adsorbed species. After reaction for 5 h at 100 °C, no decarboxylation product (i.e., ethylbenzene) was observed, however, D-substituted hydrocinnamic acid was detected. The MS patterns (**Figure A 3-4a**) of hydrocinnamic acid after the reaction exhibit an increase in the mean m/z of molecular ion from 149.96 to 151.27 and 153.28 on PdD_x/C and 1wt. % $\text{KHCO}_3\text{-PdD}_x/\text{C}$, respectively. Their ^1H NMR spectra (**Figure A 3-5**) showed that ratios of H atoms in the arene ring and $\alpha\text{-C-H}$ and $\beta\text{-C-H}$ of the hydrocinnamic acid changed from 1:0.40:0.40 to

1:0.34:0.34 and 1:0.25:0.25 on PdD_x/C and $\text{KHCO}_3\text{-PdD}_x/\text{C}$, respectively. By combination of the mass spectra and $^1\text{H-NMR}$ results, the distribution of substituted deuterium on hydrocinnamic acid was determined (detailed calculations were presented in **Supplementary Note 2**). Overall, a higher degree of D-substitution of hydrocinnamic acid was observed on 1wt. % $\text{KHCO}_3\text{-PdD}_x/\text{C}$ (30%) than on PdD_x/C (13%). In specific, 0.42 out of 2 of the α - and β -C–H groups and 0.33 out of 5 of aromatic C–H bonds were substituted to C–D on the D_2 pretreated PdH_x/C (**Table 3-3**). On $\text{KHCO}_3\text{-PdD}_x/\text{C}$, 0.92 out of 2 of the α - and β -C–H groups, and 0.75 out of 5 of arene ring C–H bonds was converted to C–D. The higher α -C–H substitution on $\text{KHCO}_3\text{-PdD}_x/\text{C}$ is in agreement with our previous results that the decarboxylation activity was positively related with the activation of α -C–H bonds [6]. Moreover, 73% of –COOH was substituted by deuterium into –COOD on KHCO_3 promoted PdH_x/C catalyst, which is 5-folds higher than that on the unmodified PdD_x/C catalyst (only 14% D atoms substituted). The identification of D-labeled hydrocinnamic acid verifies the reversibility of the proton abstraction of COOH. The 5-fold higher degree of D substitution of the carboxyl group on KHCO_3 -modified PdD_x/C catalyst than unmodified PdD_x/C indicates a more efficient proton abstraction by KHCO_3 , namely surface KHCO_3 reacted with the proton (H) of the COOH group, generating a carboxylate anion (COO^-). The carboxylate anion intermediate is prone to decarboxylation.

Table 3-3. Distribution of Substituted D Atoms in Hydrocinnamic Acid after Reaction on D_2 -Pretreated Pd catalysts ^a

Catalyst	Substituted D Atom numbers ^b				
	Hydrocinnamic acid	Arene ring	β	α	–COOH ^c
Pd/C	1.31	0.33	0.42	0.42	0.14
1wt.% $\text{KHCO}_3\text{-Pd/C}$	3.32	0.75	0.92	0.92	0.73

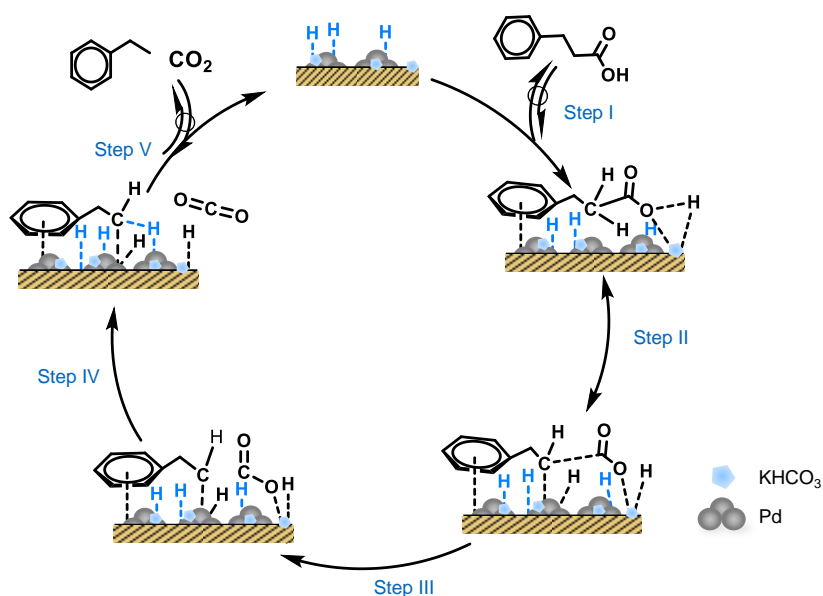
^a: Reaction conditions: 100 mg of Pd/C catalyst pretreated at 150 °C and 1 bar D_2 for 5h, 80 mL of n-hexane as the solvent, 0.13 mmol of carboxylic acid, reacted at 100 °C, 10 bar N_2 for 5h; ^b: Substituted D atom numbers on the whole hydrocinnamic acid is from the GC-MS results; the distribution of substituted D was obtained from GC-MS patterns and $^1\text{H NMR}$ results. ^c: Substituted D atoms on –COOH group obtained from the difference between hydrocinnamic acid molecule and arene ring+ β + α positions. Detailed calculation process can be found in **Supplementary Note 2**.

When increasing the D_2 substitution reaction temperature to 150°C, D-substituted ethylbenzene was produced. MS results (**Figure A 3-4b**) show that 2.87 D atoms of ethylbenzene were substituted on $\text{KHCO}_3\text{-PdD}_x/\text{C}$, which is much higher than that on PdD_x/C (1.12 D atoms). Thus, after the activation of C-H bonds on hydrocinnamic acid, the activated

adsorbed carboxylic acid undergoes C-COO cleavage and then recombines with a H to produce the final ethylbenzene product.

3.3.8 Mechanism of Hydrocinnamic Acid Decarboxylation on Pd-Elementary Steps and their Reversibility

To interpret the marked differences in the kinetic properties on PdH_x/C and KHCO_3 promoted catalysts, we next discuss the general mechanism of the decarboxylation reaction on Pd-based catalysts. The decarboxylation mechanisms on PdH_x/C and $\text{KHCO}_3\text{-PdH}_x/\text{C}$ catalysts are regarded as identical based on D_2 substitution results. According to our previous reports [6], this decarboxylation mechanism follows a Mars-van Krevelen type mechanism (**Scheme 3-1**). First of all, the H_2 pretreated Pd has a small amount of surface and subsurface H atoms, as PdH_x species. The catalytic sequence starts with the adsorption of arene ring and $-\text{COOH}$ of hydrocinnamic acid ($\text{R-CH}_2\text{-COOH}$) on Pd surface, forming molecularly chemisorbed $\text{R-CH}_2\text{-COOH}^*$ species (Step I). Then, the adsorbed $-\text{COOH}^*$ and $\alpha\text{-C-H}$ bonds dissociate to H_{ads} adatoms and dissociatively adsorbed carboxylate group R-CH-COO^* intermediate (Step II). In the next step (Step III) C-C bond of adsorbed R-CH-COO^* breaks, generating surface-bounded R-CH^* and CO_2 species, and CO_2 was regarded to desorb from the active sites immediately. Afterwards, a H atom attacks the R-CH^* intermediates forming saturated R-CH_3^* (Step IV). The catalytic cycle completes with the quasi-equilibrated desorption of ethylbenzene (R-CH_3) from active sites (Step V).



Scheme 3-1. Schematic illustration of hydrocinnamic acid decarboxylation pathways on KHCO_3 -modified Pd catalyst.

In general, the adsorption and desorption steps (Step I, V) occur much faster than the surface reaction, thus, they are considered to be quasi-equilibrated. Hydrocinnamic acid dissociative step (Step II) generally is much faster than C-C bond cleavage step (Step III) because it is observed that the H atoms of α -C-H bond and -COOH group were rapidly substituted by D without decarboxylation under relatively mild conditions (100 °C), thus is also considered to be quasi-equilibrated. However, according to the D_2 substitution results, rate of dissociation step largely depends on surface basicity: the appropriate surface basicity on the KHCO_3 -modified catalyst promotes the COOH dissociation, but on the neutral surface of PdH_x/C the COOH dissociation is rather slow. Furthermore, according to our previous reports [6] and D_2 substitution results at the α -C-H position under mild conditions in this study, the H addition of R-CH^* - intermediates (Step IV) is fast and does not control the overall reaction rate. Therefore C-C bond cleavage step (Step III) is concluded to be the rate-determining step.

The general apparent rate equation (**Eq. 3-1**) for the decarboxylation of hydrocinnamic acid (HDCA) is:

$$r = -\frac{dC_{\text{HDCA}}}{dt} = k_{\text{eff}} C_{\text{RCOOH}}^n \quad \text{Eq. 3-1}$$

k_{eff} is the lumped rate constant, which involves the equilibrium and rate constants of adsorption and surface reaction elementary steps; n is the apparent reaction order of the hydrocinnamic acid and C_{RCOOH} is the initial concentration of hydrocinnamic acid. Then according to the reaction pathway illustrated in **Scheme 3-1** and C-C bond cleavage step as the rate-determining step, a more detailed expression of reaction rate (r , **Eq. 3-2**) and the reaction order (n , **Eq. 3-3**) is then derived by applying the steady state approximation for surface intermediates (see derivation in **Supplementary Note 3**).

$$r_3 = -\frac{dC_{\text{RCOOH}}}{dt} = \frac{k_3 K_2 K_a C_{\text{RCOOH}}/C_H}{1 + K_a C_{\text{RCOOH}} + K_a K_2 C_{\text{RCOOH}}/C_H} \quad \text{Eq. 3-2}$$

$$n = \frac{\partial \ln r}{\partial \ln C_{\text{RCOOH}}} = \theta_* \quad \text{Eq. 3-3}$$

k_3 is the rate constant of the C-C bond scission step; K_a and K_2 are the equilibrium constants of the hydrocinnamic acid adsorption and -COOH dissociation steps; C_H donates the concentration of surface and subsurface H; θ_* is the coverage of empty sites on the surface.

The derived expression of the reaction order (**Eq. 3-3**) is a function of only the concentration of the empty sites (θ_*). Since the reaction order of hydrocinnamic acid on all catalysts are 0th order, θ_* should also be 0, indicating that Pd surface is saturated by hydrocinnamic acid. Under 0th order reaction, the rate **Eq. 3-2** can be simplified to **Eq. 3-4** (see derivation in **Supplementary Note 4**):

$$r_{0\text{th}} = \frac{k_3 K_2}{C_H + K_2} \quad \text{Eq. 3-4}$$

Then the measured activation energy under 0th order ($Ea^{0\text{th}}$) (**Eq. 3-5**) was derived by the Arrhenius equation,

$$Ea^{0\text{th}} = -\frac{\partial \ln k_{\text{meas.}}}{\partial \left(\frac{1}{RT}\right)} = -\frac{\partial \ln r_{0\text{th}}}{\partial \left(\frac{1}{RT}\right)} = Ea_3 + \Delta H_2^0 \cdot \theta_{\text{RCOOH}} \quad \text{Eq. 3-5}$$

Ea_3 in **Eq. 3-5** is the activation energy of C-C bond cleavage in Step III; ΔH_2^0 is the enthalpy change of COO-H dissociation to COO* and H* in Step II; θ_{RCOOH} is the coverage of molecularly hydrocinnamic acid on the catalytic surface, which adds up to 1 with the coverage of the dissociated acid ($\theta_{\text{RCOOH}} + \theta_{\text{RCOO}} = 1$).

We have shown in the D-substitution experiment that the dissociation of COOH on the unmodified PdD_x/C catalyst is weak, indicating that the catalyst surface is dominated by the molecularly adsorbed hydrocinnamic acid. On the contrary, the large amount of substituted D of -COOH on the KHCO_3 -modified PdD_x/C demonstrates that dissociated hydrocinnamic acid occupied most of the active sites. Therefore, the PdH_x/C surface has higher θ_{RCOOH} and lower θ_{RCOO} compared to KHCO_3 -modified PdH_x/C , leading to a reformulation of **Eq. 3-5** to **Eq. 3-6** and **Eq. 3-7**:

On PdH_x/C :

$$\lim_{\theta_{\text{RCOOH}} \rightarrow 1} Ea^{0\text{th}}(\theta_{\text{RCOOH}}) = \lim_{\theta_{\text{RCOOH}} \rightarrow 1} (Ea_3 + \Delta H_2^0 \cdot \theta_{\text{RCOOH}}) \approx Ea_3 + \Delta H_2^0 \quad \text{Eq. 3-6}$$

And on $\text{KHCO}_3\text{-PdH}_x/\text{C}$:

$$\lim_{\theta_{\text{RCOOH}} \rightarrow 0} Ea^{0\text{th}}(\theta_{\text{RCOOH}}) = \lim_{\theta_{\text{RCOOH}} \rightarrow 1} (Ea_3 + \Delta H_2^0 \cdot \theta_{\text{RCOOH}}) \approx Ea_3 \quad \text{Eq. 3-7}$$

Thus, from **Eq. 3-6** and **Eq. 3-7**, the measured activation energy ($Ea^{0\text{th}}$) on the unmodified PdH_x/C catalyst equals to the sum of activation energy (Ea_3) of the C-C bond scission (Step III) and enthalpy change of -COOH dissociation (Step II). However, on $\text{KHCO}_3\text{-PdH}_x/\text{C}$ catalyst, the measured activation energy ($Ea^{0\text{th}}$) only equals the activation energy of C-C bond cleavage in Step III (Ea_3).

Therefore, the energy diagram of this decarboxylation reaction on PdH_x/C and KHCO_3 -modified PdH_x/C catalysts could be summarized in **Figure 3-6**. Carboxylic acid initially

adsorbed on the surface in a molecular form (Adsorbed State, **Ad.S.**), followed by the dissociation of the H on the COOH group to the dissociation state (**Di.S.**). The KHCO_3 modifier promotes COOH dissociation to carboxylate anion by reversibly abstracts the proton from COOH, which makes the carboxylate anion as the most abundant surface species. Thus, the overall activation energy for KHCO_3 -modified PdH_x/C is from the dissociated state to the transition state 1 (**T.S.I**) in **Figure 3-6**. However, the overall activation energy for PdH_x/C needs to additionally include the dissociation enthalpy (ΔH^0_2), because the neutral surface of the unmodified PdH_x/C catalyst is less effective to dissociate COOH. After the C-C bond cleavage step, intermediates CO_2 and Ar-CH^* were formed. After hydrogen addition, the phenyl-alkane (here is ethylbenzene) was finally generated.

Thus, it is reasonable to explain the difference in activation energies (**Table 3-2**) between unmodified PdH_x/C and KHCO_3 -modified PdH_x/C . On PdH_x/C , the low E_a (96 kJ mol^{-1}) was a sum of the COOH dissociation enthalpy (ΔH^0_2) and activation energy from the dissociated state to the transition state (E_{a3}). In contrast, the rapid dissociation of COOH on the KHCO_3 -modified surface makes the dissociation enthalpy kinetically inconsequential, resulting in the E_a^{Oth} on KHCO_3 - PdH_x/C equal to E_{a3} , which is overall higher than that on PdH_x/C . Moreover, KHCO_3 - PdH_x/C with different KHCO_3 modifier loadings exhibited quite different activation energies: insufficient basic sites on 0.5wt. % KHCO_3 - PdH_x/C limit the dissociation of COOH attributing to a relatively lower activation energy of 136 kJ mol^{-1} . Catalysts with stronger basicity (i.e., 5wt. % and 8wt. % KHCO_3 - PdH_x/C) undergo an irreversible acid-base neutralization reaction with COOH to form H_2O and strongly adsorbed potassium carboxylate (RCOOK), which was verified by the XRD results in **Figure 3-3b**, blocking the basic sites on the catalyst resulting in relatively low rate and activation energy ($\sim 120 \text{ kJ mol}^{-1}$). Furthermore, activation energy on $\text{KOH-PdH}_x/\text{C}$ ($E_a^{\text{Oth}} = 122 \text{ kJ mol}^{-1}$) is comparable with E_a^{Oth} on 5wt. % and 8wt. % KHCO_3 - PdH_x/C (120 kJ mol^{-1}), which could also be attributed to the strong surface basicity caused by KOH.

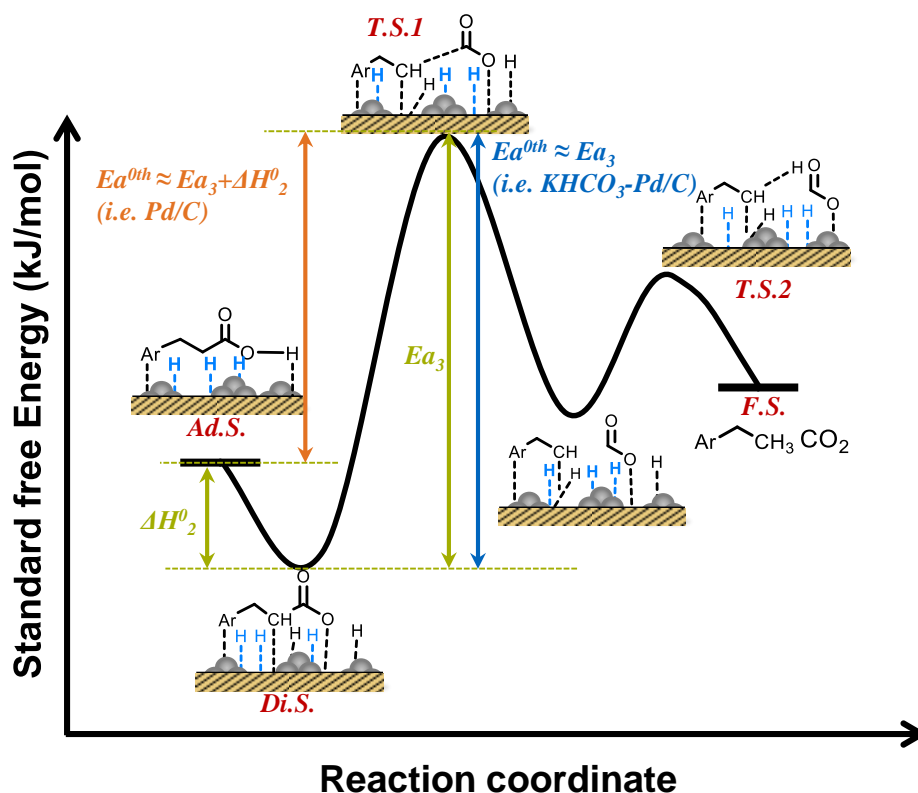


Figure 3-6. Standard free energy profile of the hydrocinnamic acid decarboxylation on Pd-based catalysts. *Ad.S.* refers to adsorption state; *Di.S.* refers to dissociation state; *T.S.* refers to transition state and *F.S.* refers to final state.

3.4 Conclusion

Alkali metals salts promotes the reaction rates of the PdH_x/C -catalyzed decarboxylation of aryl aliphatic acids. Modifiers with weak basicity, i.e., KHCO_3 , can increase the decarboxylation rate to a maximum TOF of 96 h^{-1} , which is more than one order of magnitude higher than the unmodified PdH_x/C ($\sim 5 \text{ h}^{-1}$). Stronger basis, e.g. K_2CO_3 , KOH , and KHCO_3 with high loadings ($> 5 \text{ wt. } \%$) also promoted the reaction, but to a less extent.

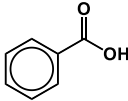
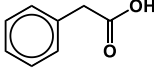
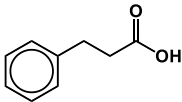
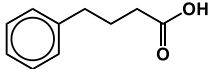
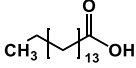
The KHCO_3 modification did not change the crystallite sizes or oxidation states of Pd, as verified by XRD and operando XANES. CO_2 -TPD showed that surface basic sites were introduced by the addition of KHCO_3 , which was active to abstract the proton (H) from the carboxyl group (COOH) of molecularly adsorbed substrates, driving the dissociation of the carboxylic acid to the corresponding carboxylate. This higher dissociation was shown by the 73% of $-\text{COOH}$ of hydrocinnamic acid substituted by deuterium into $-\text{COOD}$ on KHCO_3 -promoted PdD_x/C catalyst, while the substitution degree was only 14% on the unmodified

PdD_x/C catalyst. The carboxylate was the precursor to break the C-COO bond, which has an activation energy of 151 kJ/mol.

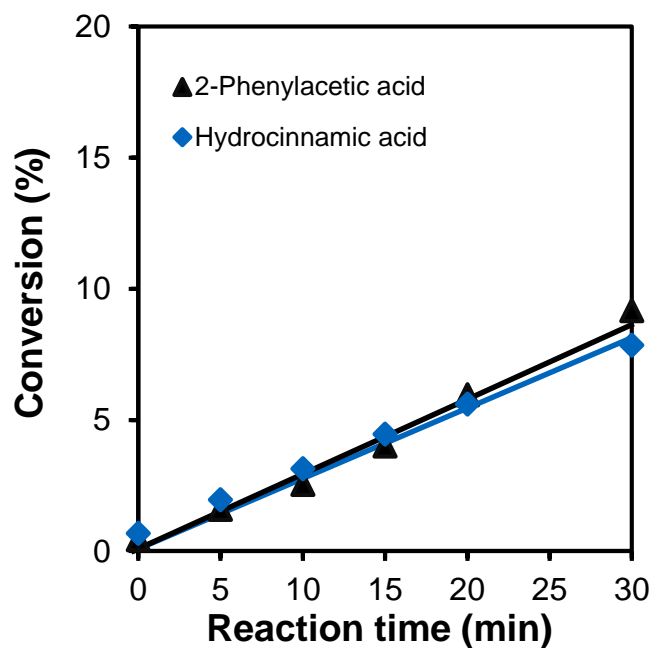
Overall, this research chapter represents a simple but efficient approach to promote the Pd-catalyzed decarboxylation of carboxylic acids. The revealing of the mechanism of promotion effect of alkali metal points to a potential to further carry out the reaction at milder conditions.

3.5 Appendix

Table A 3-1. Decarboxylation of various carboxylic acids on Pd/C and KHCO_3 -modified Pd/C ^a.

Entry	Carboxylic acid	Product	TOF (h^{-1})	
			Pd/C	1wt.% KHCO_3 -Pd/C
1		Benzene	1	6
2		Toluene	13	130
3		Ethylbenzene	5	96
4		Propylbenzene	3	58
5 ^b		n-Pentadecane	1	106

^a Reaction conditions: 100 mg catalyst dispersed in 80 mL n-dodecane and pretreated with 1 bar H_2 at 150 °C for 1 h, 2.66 mmol substrate carboxylic acid and reacted at 10 bar N_2 150 °C. ^b palmitic acid was reacted at 10 bar N_2 300 °C.

**Figure A 3-1.** Conversion of hydrocinnamic acid and 2-phenylacetic acid decarboxylation as a function of reaction time.

(Reaction conditions: 50 mg 1wt. % KHCO_3 -Pd/C catalyst dispersed in 80 mL n-dodecane with H_2 pretreatment at 150 °C for 1 h and reacted in 10 bar N_2 and 150°C with an initial carboxylic acid concentration of 33 mM;)

Table A 3-2. Distribution of the strength of Basicity on Pd/C and KHCO_3 modified catalysts

Catalyst	Basic strength distribution ($\mu\text{mol CO}_2/\text{g cata.}$)			Total basicity ($\mu\text{mol CO}_2/\text{g cata.}$)
	weak (80–200°C)	medium (200–400°C)	strong (>400 °C)	
Pd/C	0	0	0	0
0.5wt. % KHCO_3 -Pd/C	14	43	40	97
1wt. % KHCO_3 -Pd/C	17	48	30	95
2wt. % KHCO_3 -Pd/C	30	116	75	221
5wt. % KHCO_3 -Pd/C	48	115	119	282
8wt. % KHCO_3 -Pd/C	35	79	147	261

^a Results were obtained by CO_2 -TPD

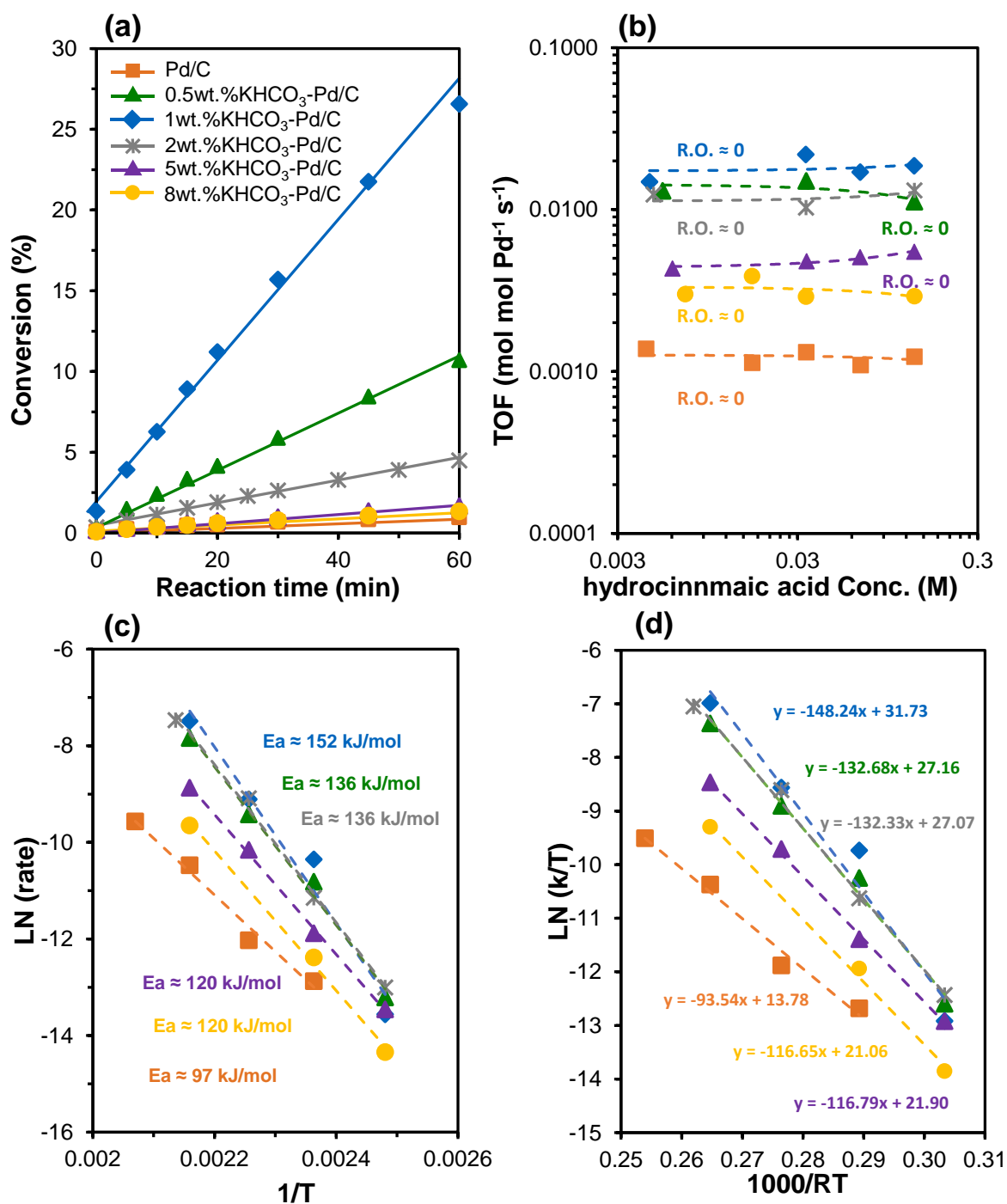


Figure A 3-2. (a) Conversion of hydrocinnamic acid as a function of reaction time at 10 bar N_2 and 150 °C with an initial hydrocinnamic acid concentration of 33 mM; (b) Initial reaction rate as a function of hydrocinnamic acid concentration varying from 3 mM to 166 mM and reacted at 150 °C 10 bar N_2 ; (c) Initial reaction rate as a function of reaction temperature varying from 130 °C to 210 °C with an initial hydrocinnamic acid concentration of 33 mM; (Reaction conditions: 50 mg catalyst dispersed in 80 mL n-dodecane with H_2 pretreatment at 150 °C for 1 h and reacted in 10 bar N_2); (d) Eyring plots for the decarboxylation of hydrocinnamic acid on Pd/C and KHCO_3 -Pd/C.

3.5.1 Supplementary Note 1: Adsorption isotherms of hydrocinnamic acid

The adsorption isotherms of hydrocinnamic acid on Pd/C and 1 wt. % KHCO_3 -Pd/C were measured. **Figure A 3-3** illustrated the adsorption isotherms of at 30 °C, 50 °C, 70 °C, 90 °C, and 110 °C. Both of these two sets of isotherms have similar characteristics, el., have a linear part in the low concentration regime and reached a constant uptake value beyond 150 mM hydrocinnamic acid. With increasing the adsorption temperature, both the initial slope and the saturation uptake amount decreased, manifesting weaker adsorption and lower adsorption capacity. By regression of the isotherms with Langmuir adsorption model, (fitting lines are dash line in **Figure A 3-3**), the adsorption constants ($K^o_{ads.}$) and saturation uptakes ($Q_{sat.}$) were obtained and compiled in **Table A 3-3**. The adsorption constants of both of the catalysts show a decrease trend when increasing the adsorption temperature following an exothermic adsorption trend. Based on these adsorption constants, the adsorption enthalpy ($\Delta H^o_{ads.}$), entropy ($\Delta S^o_{ads.}$), and free energy ($\Delta G^o_{ads.}$), which were listed in **Table A 3-3**, were obtained by Van't Hoff equation. The adsorption enthalpy and entropy of hydrocinnamic acid adsorption on bare Pd/C and KHCO_3 -Pd/C are almost the same, which are $-8.9 \pm 0.6 \text{ kJ mol}^{-1}$, $1.6 \pm 1.6 \text{ J mol}^{-1} \text{ K}^{-1}$ and $-10.3 \pm 0.7 \text{ kJ mol}^{-1}$, $2.3 \pm 2.3 \text{ J mol}^{-1} \text{ K}^{-1}$, respectively. These calculated adsorption parameters, together with the reaction orders on both of these catalysts, indicate the high coverage of hydrocinnamic acid on catalysts' surfaces, and further confirm the previous kinetic analysis that the dissociative adsorption step does not control the overall rate.

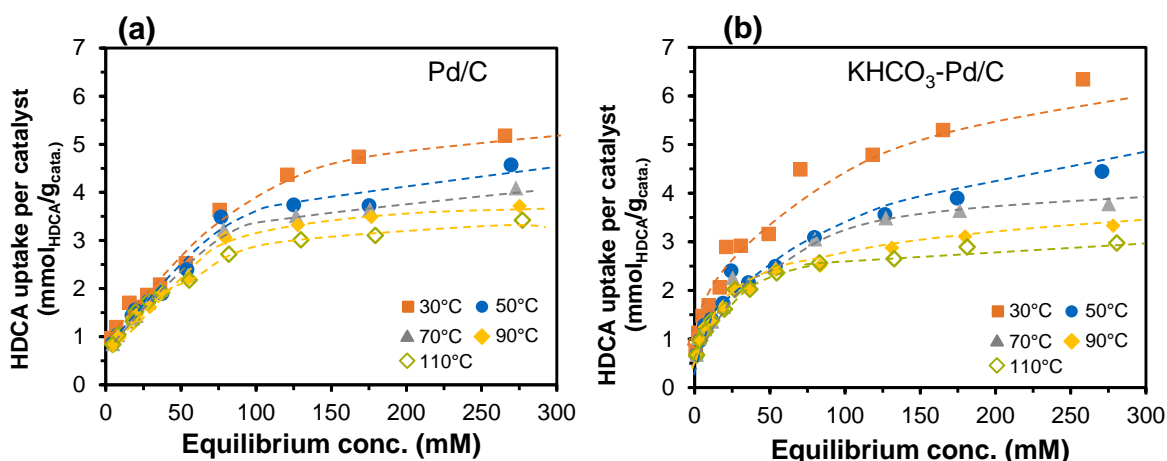


Figure A 3-3. Adsorption isotherms of hydrocinnamic acid on (a) Pd/C and (b) 1 wt.% KHCO_3 -Pd/C catalysts in organic phase at 30 °C, 50 °C, 70 °C, 90 °C, and 110 °C.

Table A 3-3. Adsorption properties of hydrocinnamic acid on Pd/C and 1wt. % KHCO_3 -Pd/C catalysts at different temperatures.

T °C	Pd/C					1wt. % KHCO_3 -Pd/C				
	$Q_{\text{sat}}^{\text{a}}$	$K^{\circ}_{\text{ads.}}^{\text{b}}$	$\Delta G^{\circ}_{\text{ads.}}$	$\Delta H^{\circ}_{\text{ads.}}$	$\Delta S^{\circ}_{\text{ads.}}$	$Q_{\text{sat}}^{\text{a}}$	$K^{\circ}_{\text{ads.}}^{\text{b}}$	$\Delta G^{\circ}_{\text{ads.}}$	$\Delta H^{\circ}_{\text{ads.}}$	$\Delta S^{\circ}_{\text{ads.}}$
	mmol/g		$\text{kJ}\cdot\text{mol}^{-1}$	$\text{kJ}\cdot\text{mol}^{-1}$	$\text{J}\cdot\text{K}^{-1}\text{mol}^{-1}$	mmol/g		$\text{kJ}\cdot\text{mol}^{-1}$	$\text{kJ}\cdot\text{mol}^{-1}$	$\text{J}\cdot\text{K}^{-1}\text{mol}^{-1}$
30	5.18	42.82	-9.47			5.29	80.10	-11.05		
50	4.57	32.64	-9.36			4.51	60.95	-11.04		
70	4.08	27.88	-9.45	-8.9 ± 0.6	1.6 ± 1.6	4.10	44.85	-10.86	-10.3 ± 0.7	2.3 ± 2.3
90	3.71	23.61	-9.55			3.78	40.07	-11.14		
110	3.42	-	-			3.56	34.44	-11.27		

^a Obtained by the maxima in adsorption isotherm. ^b Obtained by fitting adsorption isotherm with Langmuir adsorption model.

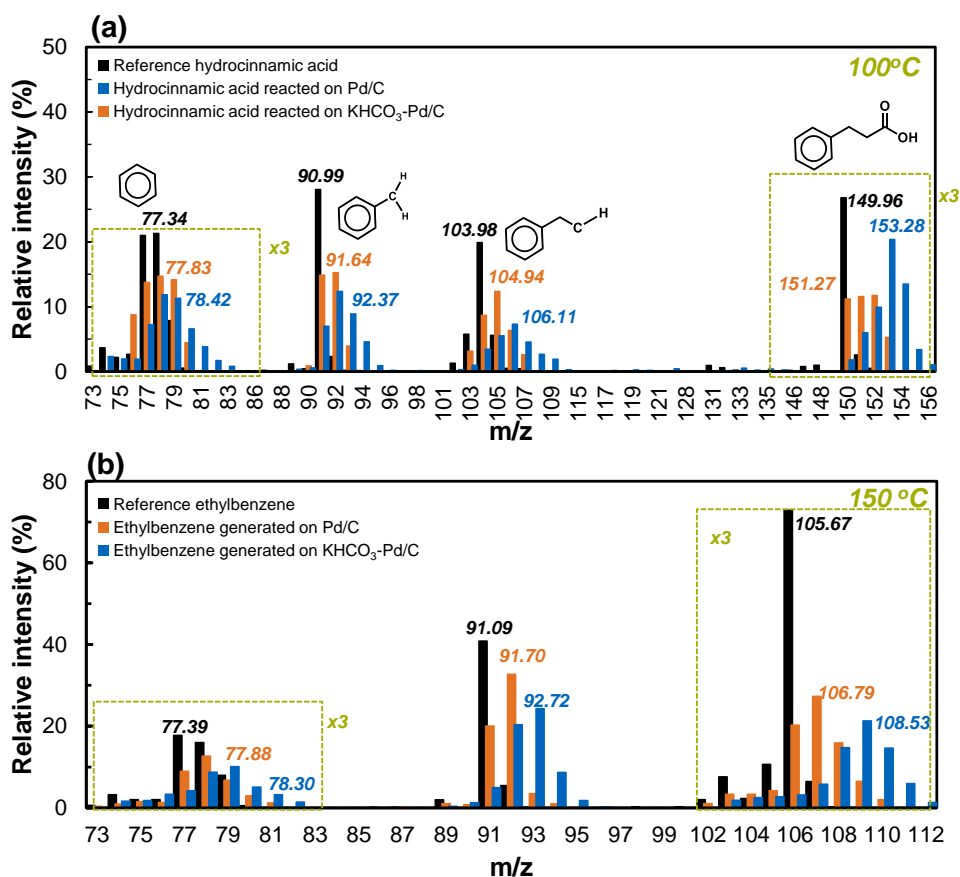


Figure A 3-4. (a) Mass spectra of hydrocinnamic acid after deuterium substitution on D_2 pretreated Pd/C and KHCO_3 -Pd/C at 100 °C for 5 h. (b) Mass spectra of ethylbenzene generating from hydrocinnamic acid decarboxylation on D_2 pretreated Pd/C and KHCO_3 -Pd/C at 150 °C for 1 h.

(**Reaction condition:** 100 mg catalyst was pretreated with 1 bar D_2 at 150 °C for 1 h. 0.13 mmol hydrocinnamic acid reacted at 100°C 10 bar N_2 for 5h or 150 °C 10 bar N_2 for 1 h; The fragments in the dashed box are the result of three times the original intensity.)

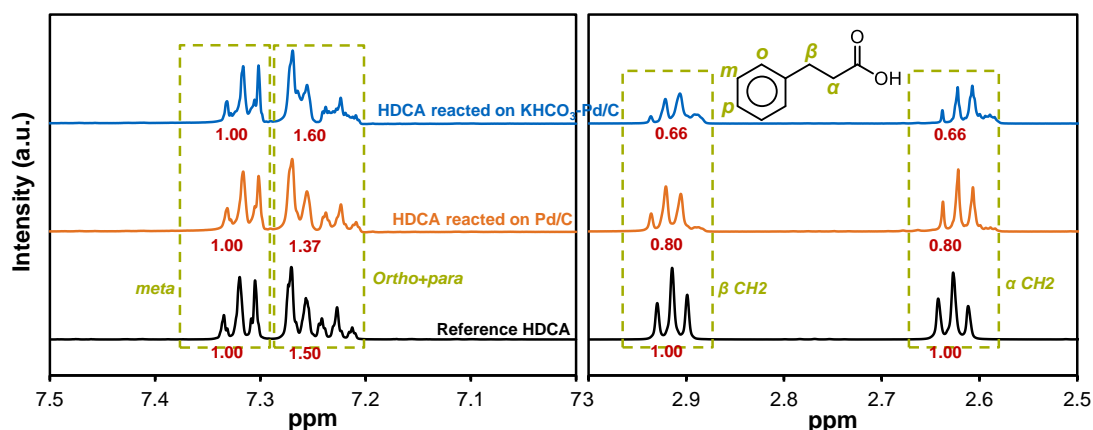


Figure A 3-5. ^1H NMR spectra of the reference hydrocinnamic acid (HDCA), and HDCA after D_2 substitution reaction on the D_2 pretreated Pd/C and 1wt. % KHCO_3 -Pd/C.

3.5.2 Supplementary Note 2: Derivation of the substituted deuterium distribution results

Take the substituted deuterium of hydrocinnamic acid from the bare Pd/C as example:

From the GC-MS results in **Figure A 3-4A**, the substituted D atoms on the hydrocinnamic acid molecule ($\text{C}_6\text{H}_5\text{-CH}_2\text{-CH}_2\text{-COOH}$) is equals to the $151.27-149.96=1.31$, and that on the $\text{C}_6\text{H}_5\text{-CH}_2\text{-CH}$ part is $104.94-103.98=0.96$.

We assume that the remaining H atoms numbers on the $\text{C}_6\text{H}_5\text{-CH}_2\text{-CH}$ part after deuterium substitution is x , by combining with the ^1H NMR results (**Figure A 3-5**) after substitution, we can obtain that:

$$2.37x + 0.8x + 0.8x = 9 - 0.96 - \frac{2 - 0.8x}{2}$$

To solve this equation, we can get

$$x = 1.97$$

Thus, remaining H atoms on arene ring, $\beta\text{-C-H}$ and $\alpha\text{-C-H}$ can be obtained as follows:

$$2.37 \times 1.97 : 0.8 \times 1.97 : 0.8 \times 1.97 = 4.67 : 1.58 : 1.58$$

And the substituted D atoms can be obtained:

$$(5 - 4.67) : (2 - 1.58) : (2 - 1.58) = \mathbf{0.33 : 0.42 : 0.42}$$

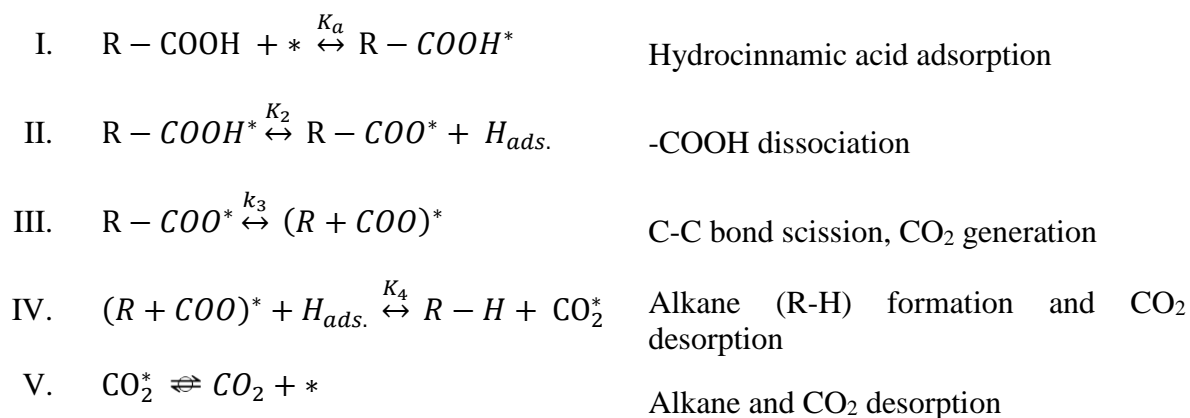
Therefore,

Since the total substitution on the hydrocinnamic acid molecule is 1.31, and the substituted D on the $\text{C}_6\text{H}_5\text{-CH}_2\text{-CH}$ is equal to the sum of arene ring, $\beta\text{-C-H}$ and $\alpha\text{-C-H}$ which is 1.17, indicating the substituted D atoms on the -COOH group is **0.14**.

For the substituted D of hydrocinnamic acid on the $\text{KHCO}_3\text{-Pd/C}$ catalysts, the same calculation method was applied as above.

3.5.3 Supplementary Note 3: Derivation of the rate equation and reaction order:

Hypothesis, adsorption and dissociation are separated to 2 steps.



We assume the C-COO scission is the rate-determining step and the adsorbed H from the -COOH dissociation is non-competitive adsorption with the -COO^* . Therefore, the rate equation of the rate-determining step is derived from the following derivations:

$$r_3 = k_3 \theta_{RCOO}$$

$$\theta_{RCOOH} + \theta_{RCOO} + \theta_H + \theta_* + \theta_R + \theta_{CO_2} + \theta_{RH} = 1$$

We regarded the dissociated H from the -COOH is non-competitive adsorption with the -COO^* , so $\theta_H \approx 0$.

Besides, since Step III is the rate-determining step,

$$\theta_R, \theta_{CO_2}, \theta_{RH} \approx 0$$

Therefore,

$$\theta_{RCOOH} + \theta_{RCOO} + \theta_* \approx 1$$

And

$$K_a = \frac{\theta_{\text{RCOOH}}}{C_{\text{RCOOH}}\theta_*}$$

$$K_2 = \frac{\theta_{\text{RCOO}}C_H}{\theta_{\text{RCOOH}}}$$

So,

$$\theta_* = \frac{1}{1 + K_a C_{\text{RCOOH}} + K_a K_2 C_{\text{RCOOH}}/C_H}$$

$$\theta_{\text{RCOOH}} = K_a C_{\text{RCOOH}} \theta_* = \frac{K_a C_{\text{RCOOH}}}{1 + K_a C_{\text{RCOOH}} + K_a K_2 C_{\text{RCOOH}}/C_H}$$

$$\theta_{\text{RCOO}} = \frac{K_2 \theta_{\text{RCOOH}}}{C_H} = \frac{K_2}{C_H} \times \frac{K_a C_{\text{RCOOH}}}{1 + K_a C_{\text{RCOOH}} + \frac{K_a K_2 C_{\text{RCOOH}}}{C_H}}$$

$$r_3 = k_3 \theta_{\text{RCOO}} = \frac{k_3 K_2}{C_H} \times \frac{K_a C_{\text{RCOOH}}}{1 + K_a C_{\text{RCOOH}} + K_a K_2 C_{\text{RCOOH}}/C_H}$$

Reaction order with respect to carboxylic acid:

$$n = \frac{\partial \ln r}{\partial \ln C_{\text{RCOOH}}} = \frac{\partial C_{\text{RCOOH}}}{\partial \ln C_{\text{RCOOH}}} \times \frac{\partial \ln r}{\partial C_{\text{RCOOH}}} = C_{\text{RCOOH}} \times \frac{\partial \ln r}{\partial C_{\text{RCOOH}}}$$

$$= C_{\text{RCOOH}} \times \frac{\partial}{\partial C_{\text{RCOOH}}} \left\{ \ln(k_3 K_a K_2 C_{\text{RCOOH}}/C_H) - \ln[1 + K_a C_{\text{RCOOH}} + K_a K_2 C_{\text{RCOOH}}/C_H] \right\}$$

$$= C_{\text{RCOOH}} \times \left[\frac{1}{C_{\text{RCOOH}}} - \frac{K_a + K_a C_{\text{RCOOH}}}{1 + K_a C_{\text{RCOOH}} + K_a K_2 C_{\text{RCOOH}}/C_H} \right]$$

$$= \frac{1}{1 + K_a C_{\text{RCOOH}} + K_a K_2 C_{\text{RCOOH}}/C_H} = \theta_*$$

Reaction order w.r.t. to carboxylic acid: $n = \theta_*$

3.5.4 Supplementary Note 4: Derivation of the measured activation energy

Since the reaction order on both of Pd/C and KHCO_3 -Pd/C catalysts are zero orders, indicating the hydrocinnamic acid has very high coverage. Thus the $\theta_* \approx 0$.

Therefore,

Under extremely high hydrocinnamic acid concentration:

$$r_{\text{0th}} = \lim_{C_{\text{RCOOH}} \rightarrow \infty} r_3 = \frac{k_3 K_2}{C_H} \times \frac{K_a}{K_a + K_a K_2/C_H} = \frac{k_3 K_2}{C_H + K_2}$$

And

$$\theta_{\text{RCOOH}} = \frac{K_a C_{\text{RCOOH}}}{1 + K_a C_{\text{RCOOH}} + K_a K_2 C_{\text{RCOOH}}/C_H} \xrightarrow{C_{\text{RCOOH}} \rightarrow \infty} = \frac{C_H}{C_H + K_2}$$

$$\theta_{\text{RCOO}} = \frac{K_2}{C_H} \times \frac{K_a C_{\text{RCOOH}}}{1 + K_a C_{\text{RCOOH}} + \frac{K_a K_2 C_{\text{RCOOH}}}{C_H}} \xrightarrow{C_{\text{RCOOH}} \rightarrow \infty} = \frac{K_2}{C_H + K_2}$$

According to Arrhenius equation,

$$k_3 = A_3 e^{-\frac{Ea_3}{RT}}$$

$$K_2 = A_2 e^{-\frac{\Delta H_2^0}{RT}}$$

Where A_3 and A_2 are the pre-exponential factors of different steps, Ea_3 and ΔH_2^0 are the activation energy of Step II and reaction enthalpy of Step II.

Therefore, under the conditions of reaction orders are 0th,

$$Ea^{0th} = -\frac{\partial \ln k_{meas.}}{\partial \left(\frac{1}{RT}\right)} = -\frac{\partial \ln r_3}{\partial \left(\frac{1}{RT}\right)} = -\frac{\partial \ln \left(\frac{k_3 K_2}{C_H + K_2}\right)}{\partial \left(\frac{1}{RT}\right)}$$

$$= -\frac{\partial}{\partial \left(\frac{1}{RT}\right)} [\ln k_3 + \ln K_2 - \ln(C_H + K_2)]$$

$$= -\frac{\partial \ln k_3}{\partial \left(\frac{1}{RT}\right)} - \frac{\partial \ln K_2}{\partial \left(\frac{1}{RT}\right)} + \frac{\partial \ln(C_H + K_2)}{\partial \left(\frac{1}{RT}\right)} = Ea_3 + \Delta H_2^0 - \frac{\partial \ln \left[\frac{1}{(C_H + K_2)}\right]}{\partial \left(\frac{1}{RT}\right)}$$

$$= Ea_3 + \Delta H_2^0 - \frac{1}{(C_H + K_2)} \times \frac{\partial K_2}{\partial \left(\frac{1}{RT}\right)} = Ea_3 + \Delta H_2^0 - \frac{K_2}{(C_H + K_2)} \times \frac{\partial \ln K_2}{\partial \left(\frac{1}{RT}\right)}$$

$$= Ea_3 + \Delta H_2^0 - \theta_{\text{RCOO}} \times \Delta H_2^0 = Ea_3 + \Delta H_2^0 - (1 - \theta_{\text{RCOOH}}) \times \Delta H_2^0$$

$$= Ea_3 + \Delta H_2^0 \theta_{\text{RCOOH}}$$

Thus:

$$Ea^{0th} = Ea_3 + \Delta H_2^0 \theta_{\text{RCOOH}}$$

3.6 Reference

- [1] S. Lestari, P. Mäki-Arvela, J. Beltramini, G.Q.M. Lu, D.Y. Murzin, Transforming triglycerides and fatty acids into biofuels, *ChemSusChem*. 2 (2009) 1109–1119.
- [2] J. Zhang, C. Zhao, Development of a Bimetallic Pd-Ni/HZSM-5 Catalyst for the Tandem Limonene Dehydrogenation and Fatty Acid Deoxygenation to Alkanes and Arenes for Use as Biojet Fuel, *ACS Catal.* 6 (2016) 4512–4525.
- [3] R.W. Gosselink, S.A.W. Hollak, S.W. Chang, J. Van Haveren, K.P. De Jong, J.H. Bitter, D.S. Van Es, Reaction pathways for the deoxygenation of vegetable oils and related model compounds, *ChemSusChem*. 6 (2013) 1576–1594.
- [4] B. Peng, X. Yuan, C. Zhao, J.A. Lercher, Stabilizing catalytic pathways via redundancy: Selective reduction of microalgae oil to alkanes, *J. Am. Chem. Soc.* 134 (2012) 9400–9405.
- [5] Z. Huang, Z. Zhao, C. Zhang, J. Lu, H. Liu, N. Luo, J. Zhang, F. Wang, Enhanced photocatalytic alkane production from fatty acid decarboxylation via inhibition of radical oligomerization, *Nat. Catal.* 3 (2020) 170–178.
- [6] F. Deng, J. Huang, E.E. Ember, K. Achterhold, M. Dierolf, A. Jentys, Y. Liu, F. Pfeiffer, J.A. Lercher, On the Mechanism of Catalytic Decarboxylation of Carboxylic Acids on Carbon-Supported Palladium Hydride, *ACS Catal.* (2021) 14625–14634.
- [7] H.H. Lamb, L. Sremaniak, J.L. Whitten, Reaction pathways for butanoic acid decarboxylation on the (111) surface of a Pd nanoparticle, *Surf. Sci.* 607 (2013) 130–137.
- [8] J. Lu, S. Behtash, M. Faheem, A. Heyden, Microkinetic modeling of the decarboxylation and decarbonylation of propanoic acid over Pd(1 1 1) model surfaces based on parameters obtained from first principles, *J. Catal.* 305 (2013) 56–66.
- [9] V.P. Santos, B. Van Der Linden, A. Chojecki, G. Budroni, S. Corthals, H. Shibata, G.R. Meima, F. Kapteijn, M. Makkee, J. Gascon, Mechanistic Insight into the Synthesis of Higher Alcohols from Syngas: The Role of K Promotion on MoS_2 Catalysts, (2013).
- [10] E. Heracleous, E.T. Liakakou, A.A. Lappas, A.A. Lemonidou, Investigation of K-promoted Cu-Zn-Al, Cu-X-Al and Cu-Zn-X (X = Cr, Mn) catalysts for carbon monoxide hydrogenation to higher alcohols, *Appl. Catal. A Gen.* 455 (2013) 145–154.
- [11] A.F. Gusovius, R. Prins, Alloy formation in Li-promoted Pd/SiO₂ catalysts for the synthesis of methanol, *J. Catal.* 211 (2002) 273–277.
- [12] J. Wei, J. Sun, Z. Wen, C. Fang, Q. Ge, H. Xu, New insights into the effect of sodium on Fe₃O₄- based nanocatalysts for CO₂ hydrogenation to light olefins, *Catal. Sci. Technol.* 6 (2016) 4786–4793.
- [13] Y. Han, C. Fang, X. Ji, J. Wei, Q. Ge, J. Sun, Interfacing with Carbonaceous Potassium Promoters Boosts Catalytic CO₂ Hydrogenation of Iron, *ACS Catal.* 10 (2020) 12098–12108.
- [14] L. Guo, J. Sun, X. Ji, J. Wei, Z. Wen, R. Yao, H. Xu, Q. Ge, Directly converting carbon dioxide to linear α -olefins on bio-promoted catalysts, *Commun. Chem.* 1 (2018) 1–8.
- [15] P. Zhai, C. Xu, R. Gao, X. Liu, M. Li, W. Li, X. Fu, C. Jia, J. Xie, M. Zhao, X. Wang, Y.-W. Li, Q. Zhang, X.-D. Wen, D. Ma, Highly Tunable Selectivity for Syngas-Derived

- Alkenes over Zinc and Sodium-Modulated Fe_5C_2 Catalyst, *Angew. Chemie.* 128 (2016) 10056–10061.
- [16] U.R. Pillai, E. Sahle-Demessie, Strontium as an efficient promoter for supported palladium hydrogenation catalysts, *Appl. Catal. A Gen.* 281 (2005) 31–38.
- [17] P. Panagiotopoulou, D.I. Kondarides, Effects of alkali promotion of TiO_2 on the chemisorptive properties and water-gas shift activity of supported noble metal catalysts, *J. Catal.* 267 (2009) 57–66.
- [18] S. Zhang, X. Liu, Z. Shao, H. Wang, Y. Sun, Direct CO_2 hydrogenation to ethanol over supported Co_2C catalysts: Studies on support effects and mechanism, *J. Catal.* 382 (2020) 86–96.
- [19] Y. Cheng, J. Lin, K. Xu, H. Wang, X. Yao, Y. Pei, S. Yan, M. Qiao, B. Zong, Fischer-Tropsch Synthesis to Lower Olefins over Potassium-Promoted Reduced Graphene Oxide Supported Iron Catalysts, *ACS Catal.* 6 (2016) 389–399.
- [20] L. Ding, T. Shi, J. Gu, Y. Cui, Z. Zhang, C. Yang, T. Chen, M. Lin, P. Wang, N. Xue, L. Peng, X. Guo, Y. Zhu, Z. Chen, W. Ding, CO_2 Hydrogenation to Ethanol over Cu@Na-Beta , *Chem.* 6 (2020) 2673–2689.
- [21] C.P. Huang, J.T. Richardson, Alkali Promotion of Nickel Catalysts, *J. Catal.* 8 (1978) 1–8.
- [22] I. V. Yentekakis, R.M. Lambert, M.S. Tikhov, M. Konsolakis, V. Kioussis, Promotion by sodium in emission control catalysis: A kinetic and spectroscopic study of the Pd-catalyzed reduction of NO by propene, *J. Catal.* 176 (1998) 82–92.
- [23] A.M. Kazi, B. Chen, J.G. Goodwin, G. Marcelin, N. Rodriguez, T.K. Baker, Li^+ promotion of Pd/ SiO_2 : The effect on hydrogenation, hydrogenolysis, and methanol synthesis, *J. Catal.* 157 (1995) 1–13.
- [24] Q. Ye, X. Wang, Y. Lu, Kinetic behavior of potassium bicarbonate crystallization in a carbonate-based CO_2 absorption process, *Chem. Eng. Res. Des.* 93 (2015) 136–147.
- [25] S. Toan, Q. Lai, W. O'Dell, Z. Sun, H. Song, Y. Zhao, M. Radosz, H. Adidharma, C. Russell, H. Yao, Y. Wang, W. Fei, M. Fan, Green, safe, fast, and inexpensive removal of CO_2 from aqueous KHCO_3 solutions using a nanostructured catalyst $\text{TiO}(\text{OH})_2$: A milestone toward truly low-cost CO_2 capture that can ease implementation of the Paris Agreement, *Nano Energy.* 53 (2018) 508–512.
- [26] S. Abouelhassan, F. Salman, M. Elmansy, E. Sheha, Characterization of KHCO_3 Single Crystals, 11 (2004) 83–86.
- [27] M.D. Porosoff, J.W. Baldwin, X. Peng, G. Mpourmpakis, H.D. Willauer, Potassium-Promoted Molybdenum Carbide as a Highly Active and Selective Catalyst for CO_2 Conversion to CO, (n.d.).
- [28] J. Li, J. Zhang, S. Wang, G. Xu, H. Wang, D.G. Vlachos, Chemoselective Hydrodeoxygenation of Carboxylic Acids to Hydrocarbons over Nitrogen-Doped Carbon–Alumina Hybrid Supported Iron Catalysts, (2019).
- [29] D. Xu, M. Ding, X. Hong, G. Liu, Mechanistic Aspects of the Role of K Promotion on Cu-Fe-Based Catalysts for Higher Alcohol Synthesis from CO_2 Hydrogenation, *ACS Catal.* (2020) 14516–14526.

- [30] H. Ma, L. Zeng, H. Tian, D. Li, X. Wang, X. Li, J. Gong, Efficient hydrogen production from ethanol steam reforming over La-modified ordered mesoporous Ni-based catalysts, *Appl. Catal. B Environ.* 181 (2016) 321–331.
- [31] P. Panagiotopoulou, D.I. Kondarides, Effects of promotion of TiO_2 with alkaline earth metals on the chemisorptive properties and water-gas shift activity of supported platinum catalysts, *Appl. Catal. B Environ.* 101 (2011) 738–746.
- [32] M. Selinsek, B.J. Deschner, D.E. Doronkin, T.L. Sheppard, J.D. Grunwaldt, R. Dittmeyer, Revealing the Structure and Mechanism of Palladium during Direct Synthesis of Hydrogen Peroxide in Continuous Flow Using Operando Spectroscopy, *ACS Catal.* (2018).
- [33] A.L. Bugaev, O.A. Usoltsev, A.A. Guda, K.A. Lomachenko, I.A. Pankin, Y. V. Rusalev, H. Emerich, E. Groppo, R. Pellegrini, A. V. Soldatov, J.A. Van Bokhoven, C. Lamberti, Palladium Carbide and Hydride Formation in the Bulk and at the Surface of Palladium Nanoparticles, *J. Phys. Chem. C.* 122 (2018) 12029–12037.
- [34] A.L. Bugaev, A.A. Guda, K.A. Lomachenko, V. V. Srabionyan, L.A. Bugaev, A. V. Soldatov, C. Lamberti, V.P. Dmitriev, J.A. Van Bokhoven, Temperature- and pressure-dependent hydrogen concentration in supported PdH_x nanoparticles by Pd K-edge X-ray absorption spectroscopy, *J. Phys. Chem. C.* 118 (2014) 10416–10423.
- [35] C.R. Glein, I.R. Gould, E.D. Lorange, H.E. Hartnett, E.L. Shock, Mechanisms of decarboxylation of phenylacetic acids and their sodium salts in water at high temperature and pressure, *Geochim. Cosmochim. Acta.* 269 (2020) 597–621.
- [36] G.C.Q. Da Silva, T.M. Cardozo, G.W. Amarante, C.R.A. Abreu, B.A.C. Horta, Solvent effects on the decarboxylation of trichloroacetic acid: Insights from: Ab initio molecular dynamics simulations, *Phys. Chem. Chem. Phys.* 20 (2018) 21988–21998.
- [37] F.H. Verhoek, The Kinetics of the Decomposition of Trichloroacetates in Ethyl Alcohol, *J. Am. Chem. Soc.* 67 (1945) 1062–1064.
- [38] F.H. Verhoek, The Kinetics of the Decomposition of the Trichloroacetates in Various Solvents, *J. Am. Chem. Soc.* 56 (1934) 571–577.

Chapter 4. Summary

The motivation of this dissertation is to figure out the intrinsic catalytic mechanism in the Pd-catalyzed hydrodeoxygenation of carboxylic acids, including the identification of hydrodeoxygenation pathways and active species, explanation of the promotion effect of the alkali-metal compounds on Pd catalysts for the decarboxylation reaction. The successful conversions of carboxylic acids were carried out in a heterogeneous liquid-solid catalytic system under relatively mild operation conditions. The properties of catalysts, intermediates together with reaction rates, reaction orders as well as product selectivity are comprehensively investigated as they are key influential parameters to reaction mechanisms.

An aryl-substituted aliphatic carboxylic acid (hydrocinnamic acid) was chosen as the model molecule to study the Pd-catalyzed hydrodeoxygenation reaction mechanism. Following the activity measurement under different H₂ pressures, it is found that Pd/C exhibits bifunctional and competing catalytic activities for arylaliphatic carboxylic acids, i.e., arene ring hydrogenation in the presence of H₂ or decarboxylation in an inert atmosphere. The arene ring hydrogenation product, 3-cyclohexyl-alkyl carboxylic acid is one order of magnitude less reactive than the unsaturated hydrocinnamic acid for decarboxylation, or even prefers the indirect decarboxylation reaction pathway namely first dehydrogenation to hydrocinnamic acid with subsequent decarboxylation to the ethylbenzene product.

Palladium hydride (PdH_x) which forms during the H₂ pretreatment was identified more active than the metallic Pd for the decarboxylation of carboxylic acids in both the solvent and solvent-free conditions. Dissociation of α -C-H is indispensable for the cleavage of the C-COO bond, and the activation rate of α -C-H, verified by the proportional correlation of substituted C-D bonds on α -C position with the decarboxylation rate. Thus the decarboxylation mechanism on PdH_x was proposed to start via an instantaneous cleavage of the O-H bond of the carboxylic group, forming an Ar-(CH₂)_n-COO* intermediate. Then, the α -C-H bond dissociates to the Ar-(CH₂)_{n-1}-CH*-COO* intermediate, followed by C-COO scission. Finally, the Ar-(CH₂)_{n-1}-CH* intermediate reacts with sorbed H to generate products Ar-(CH₂)_{n-1}-CH₃. Presence of hydride in the Pd lattice increases the steady-state concentration of H on the surface which promotes the hydrogenation step in the decarboxylation mechanism. The rate-determining step of the proposed mechanism is ascribed to the C-COO cleavage.

Decarboxylation performance of PdH_x catalysts can be greatly influenced by the surface properties including basicity and acidity. Weak surface basicity was verified with relatively

higher promotion effect. The modification of surface basicity can be facilely achieved by loading proper type and concentration of alkali-metal compounds to PdH_x/C surface. Among tested samples modified with KHCO₃, K₂CO₃, KOH and KCl, 1wt. % KHCO₃ modified PdH_x/C catalysts promote the decarboxylation activity to almost 20 times higher than the original PdH_x/C catalyst. XANES excluded electronic structure differences caused by the KHCO₃. CO₂-TPD and XRD disclosed the variation of surface basicity caused by KHCO₃, and XRD results further verified that the basic KHCO₃ abstracted the proton from COO-H, resulting a carboxylate intermediate on the surface. Kinetic analysis revealed the variation of surface basicity has no influence on the adsorption of hydrocinnamic acid as the reaction order on all catalysts are zero order, but activation energy has significant difference due to the basicity change. 1wt.% KHCO₃-Pd/C, which exhibits a weak basicity, can fully activates the H bonds in reactant molecular especially the carboxyl group to dissociated carboxylate intermediate by reversible deprotonation. In contrast, strong basicity on the surface induces irreversible neutralization of carboxylic acid group with alkali-metal compounds and generating H₂O and strong adsorbed carboxylate, while neutral surface are insufficient to fully activate the carboxylic acid reactant.

From the mechanistic perspective, decarboxylation mechanism on PdH_x/C and KHCO₃-PdH_x/C follows the same mechanism proposed in **Chapter 2** with the C-C bond cleavage as the rate-determining step. Weak basic surface (i.e., 1wt. %KHCO₃-Pd/C) induces the dissociation of the carboxyl group, making the dissociatively adsorbed deprotonated carboxylate dominating the active sites. In comparison, molecularly adsorbed carboxylic acid occupies the catalytic surface of PdH_x/C. The dissociatively adsorbed intermediate are more prone to C-C bond scission than the molecularly adsorbed carboxylic acid, thus, leading to the higher decarboxylation activity.

Curriculum Vitae

Fuli Deng

Born on 10.10.1993 in Sichuan, China

- 9/2018 – 02/2023** Ph.D. at Lehrstuhl für Technische Chemie II (*Prof. Dr. Johannes A. Lercher*)
School of Natural Sciences, Department of Chemistry
Technical University of Munich
Topic: *Reaction Mechanism for Pd-Catalyzed Decarboxylation of Carboxylic Acid*
Research Area: Heterogeneous catalysis; Biomass utilization; Electrocatalysis.
- 09/2015 – 06/2018** M.Sc. in Chemical Engineering, (*Prof. Dr. Hairong Yue*)
Department of Chemical Engineering
Sichuan University
Topic: *Research on Tuning the Active Sites of Novel Copper Based Catalysts for Catalytic Hydrogenation of Ethylene Carbonate*
Research Area: Heterogeneous catalysis; Energy and Environmental Catalysis
- 09/2011 – 06/2015** B.Sc. in Chemical Engineering (*Prof. Dr. Daijun Liu*)
Department of Chemical Engineering
Sichuan University